Master's Thesis

A lower limit for the lightest RHN mass from wash-in Leptogenesis

Dominik Wilken

Münster, March 14, 2025

First Examiner: Junior-Prof. Dr. Kai Schmitz
Second Examiner: Prof. Dr. Michael Klasen

Contents

Chapter 1

Introduction

One of the fundamental questions in modern physics and cosmology is the observed dominance of matter over antimatter in the universe. The Standard Model (SM) of particle physics, in its current form, does not provide a mechanism to generate this asymmetry. To explain this discrepancy, extensions of the SM introduce mechanisms such as baryogenesis and, more specifically, leptogenesis, which can dynamically generate a baryon asymmetry during the evolution of the early universe.

To set the stage for leptogenesis, I first review the necessary theoretical frameworks. In Section, I provide an overview of the Standard Model, with a focus on the lepton sector and spontaneous symmetry breaking. Next, I discuss the Standard Model of cosmology (ΛCDM) and the history of the early universe, emphasizing key events such as inflation, baryogenesis, and electroweak symmetry breaking. Finally I present the observational evidence for a baryon asymmetry, quantify its magnitude, and discuss why conventional models struggle to explain it.

Building on this, Chapter 2 goes into the mechanisms of baryogenesis and leptogenesis. In Chapter 3, I introduce the concept of wash-in leptogenesis, a novel approach that allows for significantly lower heavy neutrino masses compared to traditional thermal leptogenesis. Finally, in Chapter 4, I explore how wash-in leptogenesis can be extended to temperatures below 100 TeV, determining the theoretical lower limits of this process.

The standard model of particle physics

The Standard Model (SM) is our best current framework for understanding fundamental particles and their interactions. It describes matter as spin-$\frac{1}{2}$ fermions and their interactions through spin-1 vector bosons, along with the Higgs field, a spin-0 scalar responsible for mass generation.

The SM is built upon the gauge symmetry $SU(3)_C \times SU(2)_L \times U(1)_Y$, which breaks at low energies to $SU(3)_C \times U(1)_{EM}$. This symmetry structure dictates the behaviour of quarks, leptons, and force carriers. This gap in the SM strongly suggests the presence of new physics, such as the see-saw mechanism, which I explore in Section 2.2.1.

A key element of the SM relevant for leptogenesis is spontaneous symmetry breaking via the Higgs mechanism. The Higgs doublet field ϕ develops a vacuum expectation value (vev), breaking electroweak symmetry and giving mass to particles through Yukawa interactions. The Higgs part of the lagrangian takes the form:

$$\mathcal{L}_\phi = (D^\mu \phi)^\dagger D_\mu \phi + \underbrace{\mu^2 \phi^\dagger \phi - \lambda(\phi^\dagger \phi)^2}_{=V(\phi)} \tag{1.1}$$

where $\mu^2 > 0$ leads to spontaneous breaking of the symmetry, shifting the Higgs field to a nonzero vev,

$$\langle \phi \rangle = \frac{1}{\sqrt{2}} \begin{pmatrix} 0 & v \end{pmatrix}, \tag{1.2}$$

where $v \approx 246$ GeV. This results in the breaking of $SU(2)_L \times U(1)Y$ down to $U(1)_{EM}$, giving mass to the weak gauge bosons and, through Yukawa couplings, to the fermions.

For the left handed lepton doublet $\ell_\alpha = \begin{pmatrix} \nu_\alpha \\ \alpha_L \end{pmatrix}$ and the corresponding right handed singlet α_R , the Yukawa interaction is given by:

$$\mathcal{L}_\ell = -h^\ell \bar{\ell_\alpha} \phi \alpha_R + h.c. \tag{1.3}$$

which, after electroweak symmetry breaking, leads to mass terms:

$$\mathcal{L}_\ell^M = m_\alpha (\bar{\alpha}_L \alpha_R + \bar{\alpha}_R \alpha_L) + h.c. \tag{1.4}$$

where $m_\alpha = h^\ell v/\sqrt{2}$. This mechanism successfully explains the masses of charged leptons but does not generate neutrino masses, necessitating extensions such as the see-saw mechanism, which I discuss in Section 2.2.1.

Overview of the history of the early Universe

The Standard Model of Cosmology (ΛCDM) combines general relativity with the SM to describe the evolution of the universe. It includes the cosmological constant (Λ), which drives the observed accelerated expansion, and cold dark matter (CDM), an unknown form of matter that constitutes about 25% of the universe's energy density.

The early universe underwent several key phases that are relevant for baryogenesis. Immediately after the Big Bang, a period of rapid inflation smoothed out density fluctuations and set the stage for structure formation. Following inflation, the universe reheated, filling space with a hot plasma of particles.

Baryogenesis must have occurred after inflation but before the onset of Big Bang Nucleosynthesis (BBN). As the universe cooled, the electroweak phase transition took place around 150 GeV, breaking electroweak symmetry. Neutrino decoupling and BBN followed, leading to the formation of the first atomic nuclei. Approximately 370,000 years later, photons decoupled from matter, leaving behind the cosmic microwave background (CMB), a crucial observational probe of the early universe.

The Baryon asymmetry of the Universe (BAU)

Naively one would expect that during the big bang an equal amount of matter and antimatter would have been created and the ratio between the two to remain equal, as one would not expect them to behave exactly the same with opposite charge(s). Due to annihilation between matter and antimatter it would then be expected that the density of baryons n_B to be the same as that of anti baryons $n_{\bar{B}}$, thereby producing a large number of photons, leading to [1]

$$\frac{n_B}{n_\gamma} = \frac{n_{\bar{B}}}{n_\gamma} = 10^{-18} \tag{1.5}$$

Located on the Mountain, in a large tree east of the entrance of the Railroad, and west of Linus' tent. It is only available after reaching 6 hearts of friendship with Leo.

This is in contrast to what we observe, namely that we primarily detect matter and next to none (primordial) antimatter. The difference between the baryon and and anti baryon density is measured to be [2]

$$\eta_B = \frac{n_B - n_{\bar{B}}}{n_\gamma} \simeq 6.12 \times 10^{-10} \tag{1.6}$$

One could think that it's just because the antimatter is just concentrated in other regions due to random chance, but if that were the case we would expect characteristic γ-ray emissions from $\bar{p}p$ annihilations leading to the production of neutral pions, which then lead to an excess of electromagnetic radiation at 100 MeV. From this one can get the constraint that at least all other galaxies within about 10 Mpc mainly consist out of matter. [3]

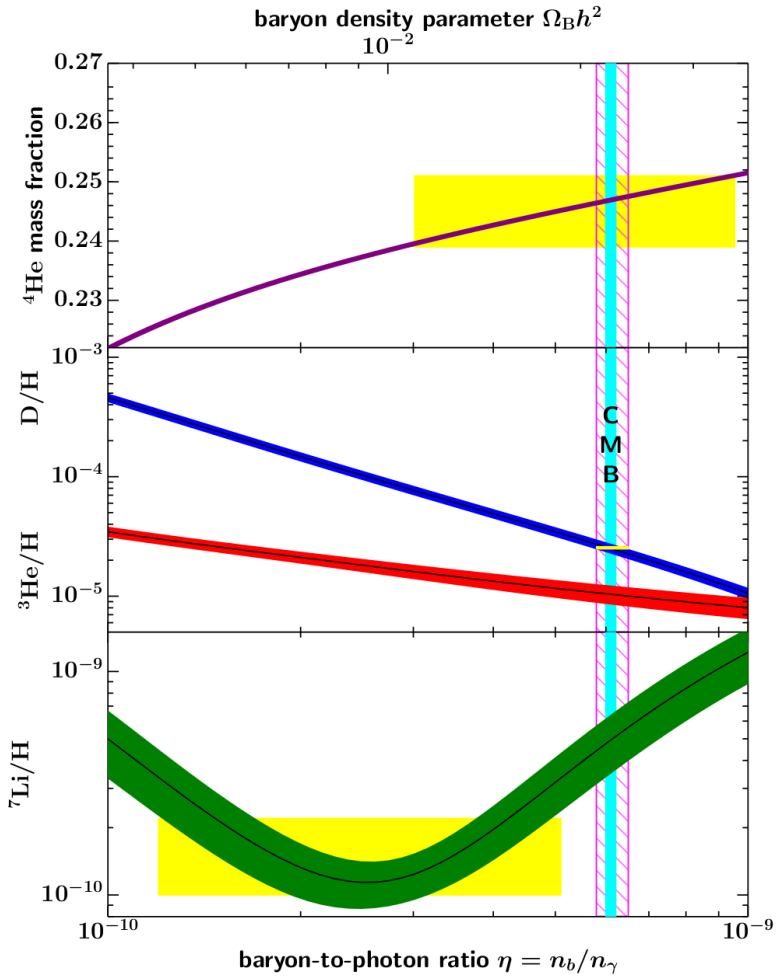

Figure 1.1: Measurements of the baryon number density from different methods [2]

The most stringent bounds on the amount of antimatter in the universe come from the measurement of light element abundances, especially the fraction of Deuterium, in comparison with BBN predictions. This along with angular fluctuations in the CMB provide the best evidence of a lack of primordial antimatter in the universe.

Mechanisms to dynamically produce this asymmetry have been thought of for many decades now, collectively called baryogenesis. A main flaw of early baryogenesis models was that they require new particles of very high masses, which are both very difficult for us to find, and the process of creating the asymmetry often can be washed out again easily. I will discuss the basics of baryogenesis in Section 2.1 A new development was the invention of leptogenesis, using a detour through the lepton sector instead of directly creating a baryon asymmetry, which allows for the masses of the new particles to be orders of magnitudes lower, yet still too high to be detectable any considerable future, and also brings with it it's own washout problems. I give an overview over the general mechanism in Section 2.2

A novel process to further develop the ideas of classical leptogenesis, called wash-in leptogenesis has been proposed recently and allows for significantly lower heavy particle masses. In this work we want to study the exactly lower limits this process allows. How this process works I will explain in Chapter3 and to explore the lower mass bound this allows for in Chapter 4

Chapter 2

Dynamically creating a baryon asymmetry

2.1 Baryogenesis

In order to successfully construct a mechanism that dynamically creates a baryon asymmetry, baryogenesis for short, Andrei Sakharov early on formulated three criteria that should be fulfilled[4]. These criteria since are known as *Sakharov principles*, and they are

1. Violation of Baryon number ($\not{B}$)
2. Violation of C and CP symmetry ($\not{C}, \not{CP}$)
3. Interactions out of thermal equilibrium

The first one, **Baryon number violation**, is rather self-explanatory as to get an asymmetry in the number of baryons at some point there has to be a deviation from the (assumed) symmetry of particles and antiparticles being created in the big bang. As a matter of fact baryon number violation is already realised in the standard model in the electroweak sector, through the chiral anomaly and so called sphaleron processes, which both have a strong theoretical foundation, though have not yet been observed directly.

Beyond the standard model baryon number seems to be quite naturally violated in many grand unified theories (GUTs) with new - heavy - gauge bosons facilitating baryon lepton number violating interactions. These theories also need to finite lifetime of the proton, which current measurements put lower bounds on as $\tau_p \gtrsim 10^{33}$ years, which translates to a very high mass scale for those new gauge bosons at $M_{\mathrm{GUT}} \sim 10^{15-16}\,\mathrm{GeV}$. In most GUTs Baryon number violation coincides with lepton number violation, leaving the difference between those $(B - L)$ conserved, but hence violating $B + L$.

Next up is **C *and* CP violation**, which means there have to be interactions which differ under charge conjugation (C) and the combination of charge conjugation with parity (CP). In practice this means there has to be some difference in how particles and their antiparticle equivalent behave. If this were not the case even with $\not{B}$ processes they would just lead to a symmetric production of baryons and antibaryons, which would still lead to no asymmetry.

This is once again fulfilled in the SM already, again in the electroweak sector, in which C and P are violated maximally. And as could be observed in an experimental setting there is CP violation in the decay of neutral Kaons. Therefore it is easily imaginable for other instances of $\not{CP}$ to occur at higher energies as well.

At last the **Interactions outside of thermal equilibrium** point is the most interesting condition, as it is not already fulfilled in the standard model (of particle physics). It can be easily achieved through the expansion of the universe though, leading to the entire universe cooling down, and therefore the production of heavy particles being stopped after some time.

This is because as long as the temperature of the universe is way above the mass of some (heavy) particle X: $T \gg m_X$ it will lead to a thermal population of X particles and the rates of X decay and inverse decay are the same. As the universe cools down now it will at some point reach a temperature

$T \lesssim m_X$ and new X particles will no longer be produced. As long as now the decay rate Γ_X of the X particles cannot compete with the expansion of the universe: $\Gamma_X \lesssim H$ a deviation from the equilibrium distribution is achieved and our particles can calmly decay without having to worry about any back reaction washing out the potentially achieved asymmetry.

It is also possible to create baryogenesis mechanisms which do not require all of these conditions, though some more complicated and exotic physics would be required for that.

2.1.1 Models of Baryogenesis

In the following I want to give a short overview of some models of baryogenesis, such as the vanilla scenario already alluded to, which could be realised in a $SU(5)$ GUT, or electroweak baryogenesis, which relies on type-I phase transition in the electroweak sector and some models which might also be adapted for a more general *chargegenesis* mechanism which I will come back to later in Chapter 3.4

2.1.1.1 Direct Baryogenesis

As has already shone through in the discussion of the Sakharov principles, the general idea for most models of baryogenesis consists of having heavy particles, maybe gauge bosons belonging to some GUT, decaying outside of thermal equilibrium, both into baryons and antibaryons, while slightly favouring the decay into baryons due to CP violation in the decay.

As previously mentioned $SU(5)$ is good candidate for a GUT and naturally offers a candidate particle to facilitate baryogenesis in a direct way. It predicts the existence of so called leptoquarks, X- and Y-bosons carrying a $B - L$ charge of $\pm\frac{2}{3}$.

To get an asymmetry in the decay modes we have to take into account the interference terms between the tree level processes and the 1-loop corrections. It is important to note that it is necessary for another, different heavy particle to be present in those loops (here the Y boson) as otherwise the asymmetry would be cancelled out.

An obvious "flaw" here is that the created asymmetry still conserves $B - L$ and so the produced baryon asymmetry is susceptible to be washed out by so called sphaleron processes. To illustrate this I show in Figure 2.1 how vanilla baryogenesis only creates an asymmetry that is $B-L$ conserving and so is only able to move on the indicated diagonal. The same is true for the electroweak sphaleron processes, which are only capable of moving the asymmetries along this diagonal, and draws the asymmetries back to the origin at $B = L = 0$, therefore washing out the previously created asymmetry.

2.1.1.2 Electroweak Baryogenesis

As already stated the SM provides the necessary requirements for baryogenesis, with the crucial deviation from thermal equilibrium here being given in form of the electroweak phase transition. Because in the case of a first order phase transition the spontaneous breaking of the electroweak symmetry could lead to regions in the universe in which the phase is already broken, while in other regions the unbroken phase remains.[5]

So bubbles would be created in the plasma in which the phase is broken, and these bubbles would expand into the plasma with the unbroken phase, until the entire universe is covered in the broken phase. Fermions would still be massless in the symmetric phase and only acquire their mass through the Higgs vev inside the bubbles with the broken phase, leading to the bubble wall acting as a potential barrier for the fermions, so they can scatter of it [6]. Due to $\not{C}\not{P}$ these wall collisions could lead to differential treatment of particles and their antiparticles. So quarks could be more likely to pass through the wall than antiquarks, leading to an antiquark abundance in the symmetric phase, and a quark abundance in the broken phase, overall still balancing each other out. Yet in the symmetric phase sphaleron processes are still very efficient and washing out the asymmetry outside the bubble, while inside the bubble those processes are inefficient leading to the created asymmetry in there there to freeze in.

As the bubbles of the broken Higgs phase would continue to expand and cover the entire universe one would get arrive at a net baryon asymmetry this way. Problems with this mechanism are that it

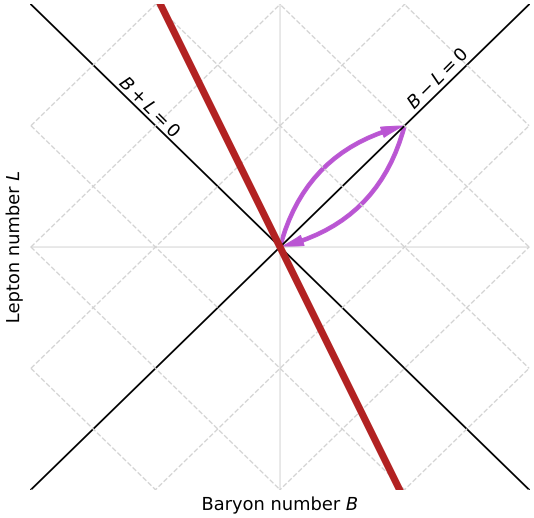

Figure 2.1: Schematic view of the evolution of baryon number B and lepton number L in the early universe. First creating a $B-L$ conserving asymmetry which is consequently washed out by electroweak sphalerons.
The red line indicated the attractor solution the sphalerons facilitate.

requires the EWPT to be a first order phase transition, in order for the nucleation bubbles to exist. A condition for this to work though is that the Higgs mass is light enough $m_\phi \lesssim 90\,\text{GeV}$, which at the latest since the detection of the Higgs at a mass of $m_\phi \approx 125\,\text{GeV}$ we know is not the case.

Though there are modifications to still make a first order phase transition and therefore electroweak Baryogenesis still viable, for example in [7].

2.1.1.3 Primordial Black Holes

As another source for the baryon asymmetry one might use primordial black holes (PBHs)[8]. So black holes not produced through the collapse of dying stars, but black holes formed through overdensities shortly after the big bang due to quantum fluctuations, which would have comparatively light masses in contrast to stellar mass black holes. These smaller sized black holes would also evaporate a lot quicker than their much heavier counterparts.

We get Baryon number violation, along with a violation of all other charges that don't have long range effects (like electric charge), as even a black hole formed entirely out of baryons would emit baryons and antibaryons (roughly) equally, irregardless of the baryon number previously poured into its creation. How would we now get PBHs predominantly formed out of baryons or antibaryons? This is where the CP violation comes into play, in that one could imagine due to said $\not{C}\not{P}$ (and $\not{C}$) antibaryons being able to move more freely in the primordial plasma, which could potentially lead to antibaryons being disproportionately captured by PBHs.

Otherwise the asymmetry might be created via some high mass particle which exhibits $\not{C}\not{P}$ in its decay and by that create the baryon asymmetry directly, very similar to the "vanilla" baryogenesis scenario. The difference here being that instead of producing the heavy particles out of the thermal bath now they are produced by the PBHs, which allows for heavier particles, as black holes will produce the entire particle spectrum. Depending on the time for the black holes to evaporate this might even happen late enough so that sphalerons wouldn't wash out the created asymmetry.

2.1.1.4 Axion inflation induced Baryogenesis

It is known that axion inflation can produce a bunch of fermions and helical (hyper-)magnetic fields. [9]

But first what is axion inflation? Standard inflation mechanisms propose a scalar field φ in a shallow potential, slowly rolling down that potential. During that rolling process it facilitates the exponential inflation phase in the early universe. Axions meanwhile were invented to solve the strong CP problem, which involves the question why there seems to be no $\not{C}\not{P}$ in QCD, even though the Lagrangian explicitly allows for such a term, which can be parametrised through a parameter θ

$$\mathcal{L}^{\Theta}_{\mathrm{QCD}} = \bar{\theta}\frac{g_s^2}{16\pi^2}G^{\mathrm{a}}_{\mu\nu}\tilde{G}^{\mathrm{a}\mu\nu} \tag{2.1}$$

$$\bar{\theta} = \theta + \arg\det M_q \tag{2.2}$$

where here G is the gluon field strength tensor, $\tilde{G}^{\mathrm{a}\mu\nu} = -\varepsilon^{\mu\nu\rho\sigma}G^{\mathrm{a}}_{\rho\sigma}/2$, and M_q being the quark mass matrix. Measurements of the neutron dipole momentum constrain the $\bar{\Theta} < 10^{-10}$ (from $d_N < 1.8\times10^{-26}\mathrm{e}\cdot\mathrm{cm}$ [2]), which is unnaturally small. In order to give an explanation for the weirdly small Θ one can introduce an axion φ as the (Pseudo-)Nambu-Goldstone Boson of a spontaneously broken $U(1)_{PQ}$ symmetry, with small mass of order $\frac{\Lambda^2_{QCD}}{f_{PQ}}$ [10, 11] which couples due to a chiral anomaly in $U(1)_{PQ}$ to the QCD Lagrangian via a term like

$$\mathcal{L}^{\varphi}_{QCD} = C_{\varphi}\frac{\varphi}{f_{PQ}}\frac{g_s^2}{16\pi^2}G^{\mathrm{a}}_{\mu\nu}\tilde{G}^{\mathrm{a}\mu\nu} \tag{2.3}$$

With the θ term from before one get's an axion potential which is minimal for $v_{\varphi} = -\frac{\bar{\Theta}f_{PQ}}{C_a}$, so expanding around v_{φ} leads to a cancellation of the $G\bar{G}$ term in the Lagrangian and therefore explains the missing observation.

This axion can now also be identified with the pseudo scalar inflaton field, responsible for the phase of exponential inflation in the early universe. Hence the name axion-inflation. And as has been studied in further detail in [9] axion inflation can lead to the production of gauge fields and through those also fermions, through a similar coupling of the axion field to the hypercharge gauge field of the form

$$\mathcal{L}^{\varphi}_{Y} = \frac{\alpha_Y}{4\pi}\frac{\varphi}{f_{\varphi}}F_{\mu\nu}\tilde{F}^{\mu\nu} \tag{2.4}$$

leading to the exponentially amplified production of helical hypermagnetic fields. This amplified gauge field production can lead to a competing scenario for baryogenesis and could in combination easily lead to an overproduction of the baryon asymmetry compared to what is actually observed. [12, 13]

$$\partial_\mu j^\mu_i = -\varepsilon_i g_i Y_i^2\frac{\alpha_Y}{4\pi}F_{\mu\nu}\tilde{F^{\mu\nu}} + \dots \tag{2.5}$$

2.2 Leptogenesis

A wider review to leptogenesis than I can give here can be found in in[14, 15, 1]. The basic idea of leptogenesis, or in full *baryogenesis via leptogenesis* [16], is to create a lepton asymmetry first which is converted into a baryon asymmetry via the aforementioned sphaleron precesses. This naturally leads to the question how to produce this lepton asymmetry. The common way to achieve this is very similar to the classical baryogenesis scenario in that we take heavy particles decaying asymmetrically into leptons and anti leptons.

A favoured choice for such a particle are right handed neutrinos, which are already introduced in the so called see-saw mechanism, which also gives rise to neutrino masses.

Again to illustrate the goal of leptogenesis is illustrated in Figure 2.2

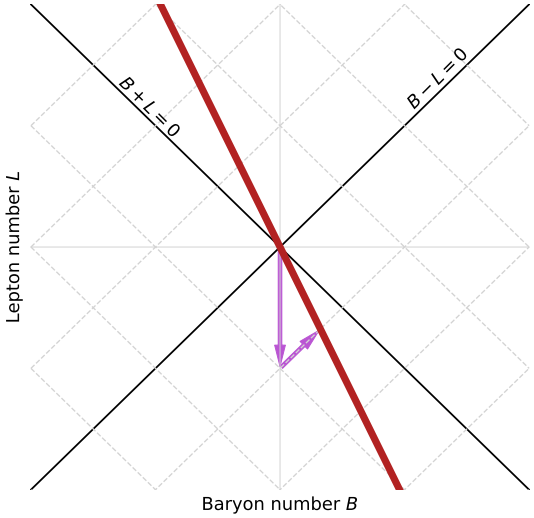

Figure 2.2: Evolution of baryon number B and lepton number L in the case of leptogenesis. The decay of heavy particles first produces an asymmetry in only L thereby changing $B-L$, which is then transferred by $B-L$ conserving sphalerons into a baryon asymmetry as well.

2.2.1 See-saw mechanism and neutrino properties

In the standard model only left-handed neutrinos (and right-handed anti-neutrinos) exist, which is equivalent to say that neutrinos are massless in the standard model, as the lack of the other chirality state prohibits the inclusion of an Dirac mass term, as is found for any other fermion, in the Lagrangian. Yet through the observation of neutrino flavour oscillations, which arise through a misalignment of the mass eigenstates and flavour eigenstates of the neutrinos, it was shown that at least two neutrino mass eigenstates must have a mass greater than zero. While neutrino oscillations (from solar and atmospheric neutrinos) let us measure the mass *differences* between the neutrino mass eigenstates, they do not tell us about the absolute mass scale of the neutrinos. Curiously enough the sign of the mass difference obtained from atmospheric neutrinos also cannot be determined which leads to two different mass orderings for the neutrino, referred to as either "Normal Ordering"(NO): $m_1 < m_2 < m_3$ and "Inverted Ordering"(IO): $m_3 < m_1 < m_2$.

Attempts are being made to determine the absolute mass scale of the neutrinos, for one through cosmological and model dependent analyses, most recent of which are DESI results that constrain the sum of neutrino masses to $\sum_\nu m_\nu < 0.072\,\text{eV}$, leaving for the lightest neutrino mass $m_{\text{lightest}} < 0.0086\,\text{eV}$. [17] Model independent measurements of the neutrino mass, through the very precise measurement of the β-decay spectrum of tritium is performed by the KATRIN experiment, currently constraining the mass of the electron (anti-)neutrino to $m_e < 0.45\,\text{eV}$ [18].

To generally allow for a neutrino mass it is quite simple to just add right handed neutrinos (RHNs) to the standard model, and thereby having a Yukawa term in the Lagrangian like we have for other fermions, as the only reason to not have included it in the first place is that neutrinos seemed massless (as demonstrated that we still don't know exactly how small the neutrino mass actually is) and that right handed neutrinos would be singlets under all standard model gauge interactions, i.e. completely uncharged and not interacting with any other standard model particles, making a direct detection impossible.

Yet the measurement of non-zero neutrino mass would be enough motivation to now add the

relevant Yukawa term to the Lagrangian, denoting RHNs as N_i, with i denoting the generation:

$$\mathcal{L}_\nu^{\text{Yukawa}} = -\sum_i^{N_R} \sum_{\alpha=e,\mu,\tau} h_{\alpha i}^\nu \bar{N}_i \phi \ell_\alpha + h.c. \tag{2.6}$$

where N_R is the total number of RHNs, ℓ_α the left-handed lepton doublet of flavour α and ϕ the standard model Higgs field. $h_{i\alpha}^\nu$ denotes the Yukawa coupling matrix for the neutrinos. Through the process of electroweak symmetry breaking the Higgs field acquires a vacuum expectation value $v = 246\,\text{GeV}$ resulting in the generation of a Dirac mass term for the neutrinos:

$$\mathcal{L}_\nu^{\text{Dirac}} \sum_i^{N_R} \sum_{\alpha=e,\mu,\tau} -\frac{1}{2}(m_D)_{i\alpha} N_i \nu_\alpha \tag{2.7}$$

where the Dirac mass matrix is given as $m_D = h_{i\alpha}^\nu \frac{v}{\sqrt{2}}$. In order to account for such small neutrino masses (less than a millionth that of the lightest not-neutrino particle in the SM, the electron) an almost unreasonably small Yukawa coupling would be required, leaving us to explain the huge hierarchy between the Yukawa couplings of the different particles.

A way out of requiring such small Yukawa couplings is now to recognise that RHNs are completely uncharged in the SM, which allows them to be their own anti particle. These types of fermions are called Majorana fermions, and it it allows us to write an additional mass term in the Lagrangian:

$$\mathcal{L}_\nu^{\text{Majorana}} = -\frac{1}{2} \sum_{i,j}^{n_R} \bar{N}_i^C M_{ij} N_j \tag{2.8}$$

where M now is the Majorana mass matrix, which let's us combine the two neutrino mass terms into one like:

$$\mathcal{L}_\nu^{\text{Mass}} = \begin{pmatrix} \bar{\nu} & \bar{N}^C \end{pmatrix} \begin{pmatrix} 0 & m_D \\ m_D^T & M \end{pmatrix} \begin{pmatrix} \nu \\ N \end{pmatrix} \tag{2.9}$$

To now arrive at the neutrino masses we observe from that one has to diagonalise this mass matrix. If we assume that the eigenvalues of the Majorana mass matrix are significantly larger than the eigenvalues of the Dirac mass matrix, written as $M \gg m_D$, which is called the see-saw condition, we get a mass spectrum consisting of three light neutrino masses and three very heavy neutrino masses roughly corresponding to the eigenvalues of M. The three light masses are the ones for which the see-saw picture comes into play as they turn out to be

$$m_\nu = -m_D^T M^{-1} m_D = -\frac{m_D^T m_D}{M} \tag{2.10}$$

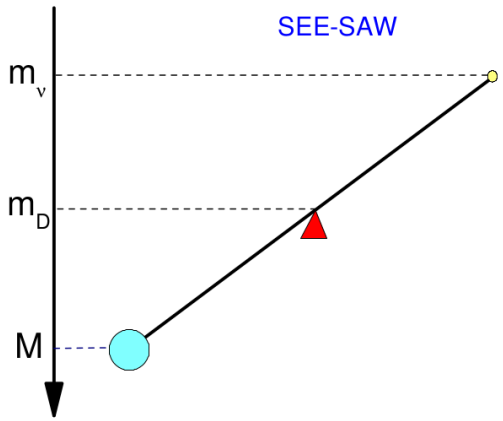

Figure 2.3: Illustration of the see-saw mechanism (taken from [14])

What this means is that the heavy Majorana masses lead to observed neutrino masses orders of magnitude smaller than the Dirac mass, like on a see-saw when a heavier person simply lifts up a person who is a lot lighter, though lifing up in the neutrino's case means ending up lighter.

A way to parametrise the neutrino Yukawa matrix is the so called Casas-Ibarra parametrisation [19, 20].

$$h_{i\alpha}^\nu = \frac{i}{v/\sqrt{2}} \sqrt{M_i} R_{ia} \sqrt{m_a} U_{i\alpha}^\dagger \tag{2.11}$$

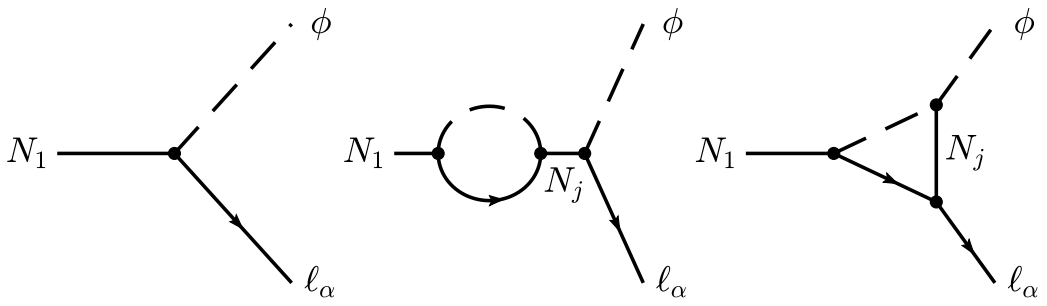

Figure 2.4: Diagrams relevant for successful leptogenesis

$M_i = (M_1, M_2, M_3)$ the eigenvalues of the Majorana mass matrix, and $m_a = (m_1, m_2, m_3)$ the light neutrino mass eigenstates, of which so far we are able to measure the mass differences $\Delta m^2_{12} = m^2_2 - m^2_1$ and $\Delta m^2_{13} = m^2_3 - m^2_1$, while the absolute neutrino scale m_1 remains undetermined (potentially even massless), though strongly constrained. U refers to the neutrino mixing, or PMNS, matrix

$$U = \begin{pmatrix} c_{12}c_{13} & s_{12}c_{13} & s_{13}e^{-i\delta} \\ -s_{12}c_{23} - c_{12}s_{13}s_{23}e^{i\delta} & c_{12}c_{23} - s_{12}s_{13}s_{23}e^{i\delta} & s_{23}c_{13} \\ s_{12}s_{23} - c_{12}s_{13}c_{23}e^{i\delta} & -c_{12}s_{23} - s_{12}s_{13}c_{23}e^{i\delta} & c_{23}c_{13} \end{pmatrix} \begin{pmatrix} 1 & 0 & 0 \\ 0 & e^{i\sigma_1} & 0 \\ 0 & 0 & e^{i\sigma_2} \end{pmatrix} \tag{2.12}$$

Here $c_{ij} = \cos\theta_{ij}$ and $s_{ij} = \sin\theta_{ij}$. σ_1 and σ_2 are two undetermined Majorana phases, and $\sigma_i \in [0, 2\pi)$

And R a rotation matrix:

$$R = S \cdot R_x \cdot R_y \cdot R_z \tag{2.13}$$

$$= \begin{pmatrix} s_1 & 0 & 0 \\ 0 & s_2 & 0 \\ 0 & 0 & s_3 \end{pmatrix} \begin{pmatrix} 1 & 0 & 0 \\ 0 & \cos r_x & \sin r_x \\ 0 & -\sin r_x & \cos r_x \end{pmatrix} \begin{pmatrix} \cos r_y & \sin r_y & 0 \\ -\sin r_y & \cos r_y & 0 \\ 0 & 0 & 1 \end{pmatrix} \begin{pmatrix} \cos r_z & 0 & \sin r_z \\ 0 & 1 & 0 \\ -\sin r_z & 0 & \cos r_z \end{pmatrix} \tag{2.14}$$

for which $s_i \in [-1, 1]$, $x, y, z \in \mathbb{C}$ with $|r_x|, |r_y|, |r_z| \leq 1$

This gives us now 3 real and 3 complex degrees of freedom, so in total 9 real d.o.f. Along with the 2 Majorana phases, the 3 Majorana masses and the unknown absolute mass scale of the light neutrinos, we get in total 12 free parameters (15 real degrees of freedom) one can choose here.

The parameters for the PMNS matrix (except the potential Majorana phases) and the differences between the light neutrino states can be measured and are shown in Table 2.1.

θ_{12}	$33.68°$	δ	$212°$
θ_{13}	$43.3°$	Δm^2_{21}	$7.49 \times 10^{-5}\,\mathrm{eV}^2$
θ_{23}	$8.56°$	Δm^2_{13}	$2.513 \times 10^{-3}\,\mathrm{eV}^2$

Table 2.1: Measured neutrino parameters [21]

2.2.2 "Vanilla" leptogenesis

Important for leptogenesis to work is that that there are more than one type of particles running in the loop, so the interference term leads to the possibility of CP violation in the first place. This requires therefore at least two generations of right handed neutrinos.

The this interference then leads to the asymmetry parameter

$$\varepsilon_i = \frac{3}{16\pi} \sum_{i \neq j} \frac{\Im\left[\left(h^{\nu\,\dagger} h^{\nu}\right)^2_{ij}\right]}{\left(h^{\nu\,\dagger} h^{\nu}\right)_{ii}} \frac{\xi\left(a_j/a_i\right)}{\sqrt{a_j/a_i}} \tag{2.15}$$

$$\xi(x) = \frac{2}{3} x \left[(1+x)\ln\frac{1+x}{x} - \frac{2-x}{1-x}\right] \tag{2.16}$$

By comparing the total decay rate of the heavy neutrinos $\Gamma_i = \sum_\alpha \Gamma(N_i \longrightarrow \ell_\alpha \phi) + \Gamma(N_i \longrightarrow \ell^\dagger_\alpha \phi^*)$ to the expansion rate of the universe when the temperature arrives at the mass of said heavy neutrino, i.e. the temperature at which the RHN stop being relativistic, we arrive at the so called decay parameter K_i which describes the strength of the wash out of the asymmetry, or the strength how much the number density of RHNs is pushed towards the equilibrium:

$$K_i = \frac{\Gamma_i}{H(T = M_i)} \tag{2.17}$$

This means that for $K \ll 1$ the life time $\tau_i = \Gamma_i^{-1}$of the neutrinos will be (much) larger than the lifetime of the universe at that point, as $H \approx 1/(2t)$ during the phase of radiation domination. As a consequence the equilibrium density of the neutrinos $N^{eq}_{N_i}$ starts dropping off a lot quicker than N_{N_i} will decrease, therefore leading to the out of equilibrium situation.

When $K_i \gg 1$ the RHN will decay and inverse decay a lot more frequently leading to equilibrium being restored far more easily and therefore washing out any asymmetry that may have been produced before.

For a quantitative look at the evolution of the heavy neutrino particle densities one uses so called Boltzmann equations(more on that in section 2.3). For the RHNs it can be written as [14, 15]:

$$\frac{dN_{N_i}}{dz} = -D_i\left(N_{N_i} - N^{eq}_{N_i}\right) \tag{2.18}$$

where $z = \frac{M_1}{T}$, and N_{N_i} is the number density in a comoving (one might as well use $\eta_{N_i} = n_{N_i}/n_\gamma$ or $Y_{N_i} = n_{N_i}/s$) volume and the Decay factor D_i which is given through

$$D_i = K_i a_i z \frac{K_1(z)}{K_2(z)} \tag{2.19}$$

with modified Bessel functions of the second type K_1, K_2, and $a_i = \dfrac{M_i^2}{M_1^2}$ and D_i therefore only differentiating between the heavy neutrino species based on K_i.

In the end we only care about the contributions of the lightest RHN, as the asymmetries produced by the heavier RHNs would get washed out by the inverse decays of N_1 later on as $T > M_1$ for quite some time after $T < M_2, M_3$.

The total asymmetry is then described by a Boltzmann equation encompassing the total $B - L$ asymmetry

$$\frac{dN_{B-L}}{dz} = \sum_i \varepsilon_i D_i \left(N_{N_i} - N^{eq}_{N_i}\right) - N_{B-L} \sum_i W_i(z) \tag{2.20}$$

Where the $W_i(z)$ is the wash out factor composed of the reaction rates of inverse decays and $\Delta L = 2$ violating processes being mediated by N_i

To get the total created asymmetry $B - L$ one now has to solve these differential equations until $z \gg 1$, i.e. until the wash out through any processes involving any N_i is not efficient any more and N_{B-L} doesn't get affected by this anymore. While $B-L$ cannot be affected any more there are still the aforementioned sphalerons which conserve $B - L$ yet violate $B + L$, leading to that part of the lepton asymmetry gets converted into a baryon asymmetry. This can be described by a simple conversion factor which turns out to be $a_{sph} = \frac{28}{79}$

Aside from the elegance of explaining neutrino masses and the BAU all in one fell swoop, for leptogenesis to work out successfully there are of course some constraints. For one the washout cannot be large otherwise any produced asymmetry will be washed out again to quickly. Another point is that the asymmetry needs to be sufficiently large to produce an asymmetry large enough to explain the observed value of the baryon asymmetry. This leads to the famous Davidson-Ibarra bound on how high the RHN masses have to be [22, 23]:

$$M_i \gtrsim 10^9\,\mathrm{GeV} \tag{2.21}$$

Simultaneously heavy neutrino masses above $M_i \gtrsim 10^7\,\mathrm{GeV}$ lead to questions about naturalness as they would introduce strong corrections to the Higgs mass and one needs to include a lot of fine tuning in the theory to make it work out. On the other hand lower heavy neutrino masses of course lead to larger Yukawa couplings in order to achieve the small neutrino masses we observe, which further leads to strong washout of the asymmetry.

2.2.3 Modifications

To tackle these problems there have been many many models suggested that also use right handed neutrinos to create a lepton asymmetry - to be converted into a baryon asymmetry by sphalerons - both via the same thermal mechanism as well as through non thermal means.

2.2.3.1 Resonant Leptogenesis

One way to get below the high mass requirements is to make use of resonant enhancement of RHN production by having RHN masses which are nearly degenerate, in a scenario called *Resonant Leptogenesis* [24, 25, 26].

Here

$$M_1 \approx M_2 < M_3 \quad \text{or} \quad M_1 \approx M_2 \approx M_3 \tag{2.22}$$

Through these almost degenerate RHN masses the the potentially created asymmetry can be enhanced and allows for heavy neutrino masses around the electroweak scale in the case of two almost degenerate RHN, or even below 100 GeV for three quasi-degenerate RHN.

2.2.3.2 ARS Leptogenesis

Another way to allow for right handed neutrinos to account for the BAU while having significantly lower masses is achieved through oscillations of the RHNs. Hence this mechanism is called Baryogenesis via neutrino oscillations , or as it is commonly referred to ARS leptogenesis, after Akhmedov, Rubakov and Smirnov who first described it [27].

Very different from the previous resonant case, which required RHN masses to be nearly degenerate to produce resonant enhancement, for the oscillation scenario to work out we need a strong mass hierarchy so that the lightest RHN has a mass **below** the electroweak phase transition, when sphalerons are virtually non existent any more, while at least one of the RHN needs a mass above the EWPT.

The way this mechanism works is that flavour oscillations in the RHN give rise to CP violation, while still conserving total lepton number

$$L^{\mathrm{tot}} = L + L_1 + L_2 + L_3 \tag{2.23}$$

where L is the SM lepton number, and L_i lepton number associated with the individual RHN. Oscillations can then lead from a starting point at which $L^{\mathrm{tot}} = 0 = L_i$ to a state in which $L^{\mathrm{tot}} = 0 \neq L_i$, i.e. an uneven distribution of the lepton number across the different flavours. Through their Yukawa couplings they can transfer that flavour asymmetry into the left handed neutrinos, at which point it becomes important that at least one heavy neutrino (N_1) has a mass below $T_{\mathrm{EW}} \sim 100\,\mathrm{TeV}$, so that it

cannot fully equilibrate before the EWPT. This means some amount of the asymmetry can be stored in L_1 while the other flavour asymmetries will be converted into a baryon asymmetry through sphalerons. As the sphalerons become inactive after EWPT the parts of the asymmetry that get produced then cannot be converted anymore.

With this mechanisms a lightest RHN mass of $M_1 \sim 1\,\mathrm{GeV}$ (and $M_1 \ll 100\,\mathrm{GeV}$) can be achieved.

It can further be noted that it exhibits some similarities to the scenario of *Dirac Leptogenesis*[28], in which neutrinos are assumed to have a Dirac nature (i.e. no Majorana masses), which can facilitate leptogenesis by similarly "storing" the asymmetry in right handed electrons to protect it from washout.

2.3 Boltzmann equations

In order to describe the evolution of particle densities we want to make use of so called Boltzmann equations. These are derived from the evolution of the phase space density $f(\vec{x}, \vec{p}, t)$ for a classical ideal gas in an enclosed volume. [29]

Generally this process can be expressed as

$$\hat{L}[f] = C[f] \tag{2.24}$$

With $\hat{L}$ being the Liouville operator, acting on the phase space density, and C the so called collision operator which encompasses the collisions the particles are involved in.

The Liouville operator is arrived at by considering the evolution of a number of particles within an phase space volume element $d^3x\, d^3p$ around $(\vec{x}, \vec{p})$. In the presence of an external force $\vec{F}$, but no collisions, the particles will move into the new volume $d^3x'\, d^3p'$ around $(\vec{x} + \vec{v}\delta t, \vec{p} + \vec{F}\delta t)$. For a conserved number of particles (i.e. no collisions) this leads to

$$f(\vec{x} + \vec{v}\delta t, \vec{p} + \vec{F}\delta t, t + \delta t) d^3x'\, d^3p' = f(\vec{x}, \vec{p}, t) d^3x\, d^3p \tag{2.25}$$

As long as the force $\vec{F}$ does not depend on time $d^3x'\, d^3p' = d^3x\, d^3p$ and therefore

$$f(\vec{x} + \vec{v}\delta t, \vec{p} + \vec{F}\delta t, t + \delta t) = f(\vec{x}, \vec{p}, t) \tag{2.26}$$

By taking $\delta t \to 0$ we can expand this to first order in δt giving us the common expression for the Liouville operator

$$f(\vec{x} + \vec{v}\delta t, \vec{p} + \vec{F}\delta t, t + \delta t) - f(\vec{x}, \vec{p}, t) = 0 \tag{2.27}$$

$$f(\vec{x}, \vec{p}, t) + \left[\vec{v} \cdot \nabla_x f + \vec{F} \cdot \nabla_p f + \frac{\partial f}{\partial t}\right] \delta t - f(\vec{x}, \vec{p}, t) = 0 \tag{2.28}$$

$$\hat{L}[f] = \left(\frac{\partial}{\partial t} + \frac{\vec{p}}{m} \cdot \nabla_x + \vec{F} \cdot \nabla_p\right) f(\vec{x}, \vec{p}, t) = 0 \tag{2.29}$$

The equality $\hat{L}[f] = 0$ of course only holds as long as there are no collisions occurring, if there are we get (2.24) with the additional terms concerning the collisions being encompassed in C. How these look like we will see below.

Now we want to use this equation also for relativistic particles and for this the Liouville operator can be expressed in a covariant and relativistic form as [10]

$$\hat{L} = p^\rho \frac{\partial}{dx^\rho} - \Gamma^\rho_{\mu\nu} p^\mu p^\nu \frac{\partial}{\partial p^\rho} \tag{2.30}$$

As we are interested in the expansion history of the universe we use the Friedman-Lemaître-Robert-Walker metric (for the case of a flat universe):

$$ds^2 = dt^2 - a(t)^2 d\vec{x}^2 \tag{2.31}$$

$$\Gamma^\rho_{\mu\nu} = \frac{1}{2} g^{\rho\sigma} \left(\frac{\partial g_{\sigma\nu}}{\partial x^\mu} + \frac{\partial g_{\mu\sigma}}{\partial x^\nu} - \frac{\partial g_{\mu\nu}}{\partial x^\sigma}\right) \tag{2.32}$$

The only non vanishing Christoffel symbols then evaluate as

$$\Gamma^k_{i0} = \frac{\dot{a}(t)}{a(t)}\delta^k_i\,, \qquad \Gamma^0_{ij} = a(t)\dot{a}(t)\delta_{ij} \tag{2.33}$$

Plugging it into (2.30) and assuming a spatially homogeneous phase space distribution $f(p^\mu, x^\mu) = f(E,t)$ leads to

$$L[f] = p^0\frac{\partial f}{\partial x^0} + p^i\underbrace{\frac{\partial f}{\partial x^i}}_{=0} - \Gamma^0_{\mu\nu}p^\mu p^\nu\frac{\partial f}{\partial p^0} - \Gamma^i_{\mu\nu}p^\mu p^\nu\underbrace{\frac{\partial f}{\partial p^i}}_{=0} \tag{2.34}$$

$$= E\frac{\partial f}{\partial t} - a(t)\dot{a}(t)\delta_{ij}p^i p^j\frac{\partial f}{\partial E} \tag{2.35}$$

As we operate in an expanding universe the metric gives us a slight deviation for the standard energy-momentum relation:

$$p^\mu p_\mu = g_{\mu\nu}p^\mu p^\nu = E^2 - a(t)^2\delta_{ij}p^i p^j = m^2 \tag{2.36}$$

Here we can now introduce a physical momentum $p^i_{\text{ph}} = a(t)p^i$ so that

$$E = \sqrt{m^2 + |\vec{p}_{\text{ph}}|^2} \tag{2.37}$$

i.e. we regain the standard relation through this. For ease of notation we can now just define

$$|\vec{p}|^2 \equiv |\vec{p}_{\text{ph}}|^2 = \delta_{ij}p^i_{\text{ph}}p^j_{\text{ph}} = a(t)^2\delta_{ij}p^i p^j \tag{2.38}$$

Inserting this into the expression for the Liouville operator then leads to the expression

$$\hat{L}[f(E,T)] = E\frac{\partial f}{\partial t} - \frac{\dot{a}}{a}|\vec{p}|^2\frac{\partial f}{\partial E} \tag{2.39}$$

With this we can now determine the evolution of a particle density described by $f(E,T)$, which is given as

$$n(t) = \frac{g}{(2\pi)^3}\int d^3p f(E,t) \tag{2.40}$$

Applying a time derivative on this:

$$\frac{dn}{dt} = \frac{g}{(2\pi)^3}\int d^3p\frac{\partial f(E,t)}{\partial t} \tag{2.41}$$

$$= \frac{g}{(2\pi)^3}\int d^3p\left[\frac{C[f]}{E} + \frac{\dot{a}}{a}\frac{|\vec{p}|^2}{E}\frac{\partial f}{\partial E}\right] \tag{2.42}$$

By making use of spherical coordinates in momentum space, for which I define $\rho = \sqrt{p_1^2 + p_2^2 + p_3^2} = |\vec{p}|$ and the relativistic energy momentum relation $E = \sqrt{\rho^2 + m^2}$ we can apply the chain rule on the energy derivative leading to:

$$\frac{\partial f}{\partial E} = \frac{\partial f}{\partial \rho}\frac{\partial \rho}{\partial E} = \frac{\partial f}{\partial \rho}\frac{E}{\rho} \tag{2.43}$$

and substituting in the integral $d^3p = d\rho\, 4\pi\rho^2$ we can then use partial integration like

$$\int d^3p\,\frac{|p|^2}{E}\frac{\partial f}{\partial E} = 4\pi\int d\rho\,\rho^2\frac{\rho^2}{E}\frac{E}{\rho}\frac{\partial f}{\partial \rho} \tag{2.44}$$

$$= 4\pi\int d\rho\,\rho^3\frac{\partial f}{\partial \rho} \tag{2.45}$$

$$= 4\pi\left[\cancelto{0}{\rho^3 f|_\partial} - \int d\rho\, 3\rho^2 f(\rho,t)\right] \tag{2.46}$$

$$= -3\int d^3p\, f(E,t) \tag{2.47}$$

Inserting this back into (2.42) then gives

$$\frac{dn}{dt} = -\frac{g}{(2\pi)^3}\int d^3p \underbrace{\frac{\dot{a}}{a}}_{=H} f(E,t) + \frac{g}{(2\pi)^3}\int d^3p \frac{C[f]}{E} \tag{2.48}$$

$$\Leftrightarrow \frac{dn}{dt} + 3Hn = \frac{g}{(2\pi)^3}\int d^3p \frac{C[f]}{E} \tag{2.49}$$

With each reaction that affects the number of a particle species X being summed over in the collision term like [30]

$$C = -\sum_{X\ldots\leftrightarrow Y\ldots}\left[\frac{n_X n_{\ldots}}{n_X^{eq} n_{\ldots}^{eq}}\gamma^{eq}(X\ldots\longrightarrow Y\ldots) - \frac{n_Y n_{\ldots}}{n_Y^{eq} n_{\ldots}^{eq}}\gamma^{eq}(Y\ldots\longrightarrow X\ldots)\right] \tag{2.50}$$

Chapter 3

Wash-in leptogenesis

Let's remind ourselves how we got from classical Baryogenesis to Leptogenesis: Instead of directly creating a baryon asymmetry we create a lepton asymmetry first which we can then convert into the desired baryon asymmetry. So what if we apply the same trick again for leptogenesis as well, by first having some other asymmetry generated which we can then maybe convert into the desired lepton asymmetry, to later facilitate a baryon asymmetry. The way to do this is to use interactions that usually wash out the lepton asymmetry to now"wash-in" a previously existing charge asymmetry into a lepton asymmetry.

3.1 Basic idea

What we use here is that in the presence of a non trivial primordial chemical background the standard linear relation between chemical potentials becomes an *affine* relation.

3.1.1 Construction of the Boltzmann equation

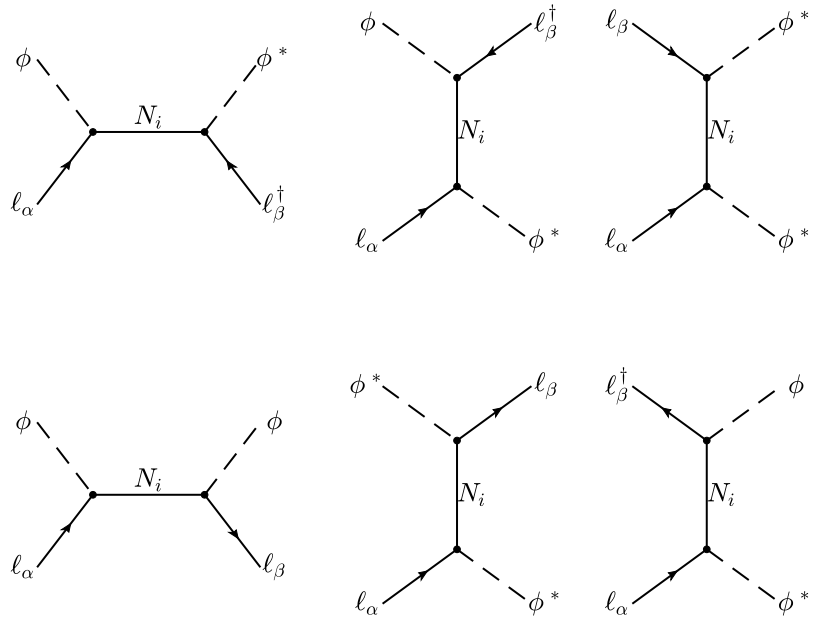

Figure 3.1: Tree level diagrams of relevant $2 \longrightarrow 2$ processes

To start we want to construct the Boltzmann equations that describe the evolution of the flavour asymmetries $\Delta_\alpha = \frac{B}{3} - L_\alpha$. For this we take into account the those $2 \longrightarrow 2$ interactions which violate

total lepton number by $\Delta L = 2$ and those conserving total lepton number $\Delta L = 0$ but still violating lepton flavour number $\Delta L_\alpha \neq 0$, i.e. those in which RHNs serve as the mediator. And of course the the decay of the neutrinos

Instead of modelling simply modelling the particle densities we study the behaviour of the difference between particles and antiparticles $q_x = n_x - n_{\bar{x}}$ [31]. As none of these interactions affect baryon number: $\Delta_\alpha \sim -L_\alpha$. The particle number density for such a charge would then be expressed as the sum of all the particles carrying this charge, with the average number of baryons so that

$$n_{\Delta_\alpha} = -n_{\ell_\alpha} - n_{e_\alpha} + \frac{1}{3}\left[\sum_i \frac{n_{Q_i}}{3} + \sum_q \frac{n_q}{3}\right] \tag{3.1}$$

$$\begin{aligned}
\frac{dq_{\Delta_\alpha}}{dt} + 3Hq_{\Delta_\alpha} = \sum_i^{N_R} \Bigg[& \frac{n_{\ell_\alpha} n_\phi}{n^{eq}_{\ell_\alpha} n^{eq}_\phi}\gamma^{eq}\left(\ell_\alpha\phi \to N_i\right) && - \frac{n_{N_i}}{n^{eq}_{N_i}}\gamma^{eq}\left(N_i \to \ell_\alpha\phi\right) \\
& - \frac{n_{\ell^\dagger_\alpha} n_{\phi^*}}{n^{eq}_{\ell^\dagger_\alpha} n^{eq}_{\phi^*}}\gamma^{eq}\left(\ell^\dagger_\alpha\phi^* \to N_i\right) && + \frac{n_{N_i}}{n^{eq}_{N_i}}\gamma^{eq}\left(N_i \to \ell^\dagger_\alpha\phi^*\right)\Bigg] \\
+ \sum_{\beta=e,\mu,\tau} \Bigg[& \frac{n_{\ell_\alpha} n_\phi}{n^{eq}_{\ell_\alpha} n^{eq}_\phi}\gamma^{eq}_{sub}\left(\ell_\alpha\phi \longrightarrow \ell^\dagger_\beta\phi^*\right) && - \frac{n_{\ell^\dagger_\beta} n_{\phi^*}}{n^{eq}_{\ell^\dagger_\beta} n^{eq}_{\phi^*}}\gamma^{eq}_{sub}\left(\ell^\dagger_\beta\phi^* \longrightarrow \ell_\alpha\phi\right) \\
& - \frac{n_{\ell^\dagger_\alpha} n_{\phi^*}}{n^{eq}_{\ell^\dagger_\alpha} n^{eq}_{\phi^*}}\gamma^{eq}_{sub}\left(\ell^\dagger_\alpha\phi^* \longrightarrow \ell_\beta\phi\right) && + \frac{n_{\ell_\beta} n_\phi}{n^{eq}_{\ell_\beta} n^{eq}_\phi}\gamma^{eq}_{sub}\left(\ell_\beta\phi \longrightarrow \ell^\dagger_\alpha\phi^*\right)\Bigg] \\
+ \sum_{\beta=e,\mu,\tau} \Bigg[& \frac{n_{\ell_\alpha} n_{\ell_\beta}}{n^{eq}_{\ell_\alpha} n^{eq}_{\ell_\beta}}\gamma^{eq}\left(\ell_\alpha\ell_\beta \to \phi^*\phi^*\right) && - \frac{2n_{\phi^*}}{2n^{eq}_{\phi^*}}\gamma^{eq}\left(\phi^*\phi^* \to \ell_\alpha\ell_\beta\right) \\
& - \frac{n_{\ell^\dagger_\alpha} n_{\ell^\dagger_\beta}}{n^{eq}_{\ell^\dagger_\alpha} n^{eq}_{\beta^\dagger}}\gamma^{eq}\left(\ell^\dagger_\alpha\ell^\dagger_\beta \to \phi\phi\right) && + \frac{2n_\phi}{2n^{eq}_\phi}\gamma^{eq}\left(\phi\phi \to \ell^\dagger_\alpha\ell^\dagger_\beta\right)\Bigg](1+\delta_{\alpha\beta}) \\
+ \sum_{\beta=e,\mu,\tau} \Bigg[& \frac{n_{\ell_\alpha} n_\phi}{n^{eq}_{\ell_\alpha} n^{eq}_\phi}\gamma^{eq}_{sub}\left(\ell_\alpha\phi \longrightarrow \ell_\beta\phi\right) && - \frac{n_{\ell_\beta} n_\phi}{n^{eq}_{\ell_\beta} n^{eq}_\phi}\gamma^{eq}_{sub}\left(\ell_\beta\phi \longrightarrow \ell_\alpha\phi\right) \\
& - \frac{n_{\ell^\dagger_\alpha} n_{\phi^*}}{n^{eq}_{\ell^\dagger_\alpha} n^{eq}_{\phi^*}}\gamma^{eq}_{sub}\left(\ell^\dagger_\alpha\phi^* \longrightarrow \ell^\dagger_\beta\phi^*\right) && + \frac{n_{\ell^\dagger_\beta} n_\phi}{n^{eq}_{\ell^\dagger_\beta} n^{eq}_\phi}\gamma^{eq}_{sub}\left(\ell^\dagger_\beta\phi^* \longrightarrow \ell^\dagger_\alpha\phi^*\right)\Bigg] \\
+ \sum_{\beta=e,\mu,\tau} \Bigg[& \frac{n_{\ell_\alpha} n_{\phi^*}}{n^{eq}_{\ell_\alpha} n^{eq}_{\phi^*}}\gamma^{eq}\left(\ell^\dagger_\alpha\phi^* \longrightarrow \ell^\dagger_\beta\phi^*\right) && - \frac{n_{\ell_\beta} n_{\phi^*}}{n^{eq}_{\ell_\beta} n^{eq}_{\phi^*}}\gamma^{eq}\left(\ell^\dagger_\beta\phi^* \longrightarrow \ell^\dagger_\alpha\phi^*\right) \\
& - \frac{n_{\ell^\dagger_\alpha} n_\phi}{n^{eq}_{\ell^\dagger_\alpha} n^{eq}_\phi}\gamma^{eq}\left(\ell^\dagger_\alpha\phi \longrightarrow \ell^\dagger_\beta\phi\right) && + \frac{n_{\ell^\dagger_\beta} n_\phi}{n^{eq}_{\ell^\dagger_\beta} n^{eq}_\phi}\gamma^{eq}\left(\ell^\dagger_\beta\phi \longrightarrow \ell^\dagger_\alpha\phi\right)\Bigg] \\
+ \sum_{\beta=e,\mu,\tau} \Bigg[& \frac{n_{\ell_\alpha} n_{\ell^\dagger_\beta}}{n^{eq}_{\ell_\alpha} n^{eq}_{\ell^\dagger_\beta}}\gamma^{eq}\left(\ell_\alpha\ell^\dagger_\beta \longrightarrow \phi\phi^*\right) && - \frac{n_\phi n_{\phi^*}}{n^{eq}_\phi n^{eq}_{\phi^*}}\gamma^{eq}\left(\phi\phi^* \longrightarrow \ell_\alpha\ell^\dagger_\beta\right) \\
& - \frac{n_{\ell^\dagger_\alpha} n_{\ell_\beta}}{n^{eq}_{\ell^\dagger_\alpha} n^{eq}_{\ell_\beta}}\gamma^{eq}\left(\ell^\dagger_\alpha\ell_\beta \longrightarrow \phi^*\phi\right) && + \frac{n_{\phi^*} n_\phi}{n^{eq}_{\phi^*} n^{eq}_\phi}\gamma^{eq}\left(\phi^*\phi \longrightarrow \ell^\dagger_\alpha\ell_\beta\right)\Bigg]
\end{aligned} \tag{3.2}$$

Assuming a Boltzmann distribution $f = \exp\left(\frac{E+\mu_X}{T}\right)$ the particle density can be calculated as

$$n_X(T) = g_X \int d^3p\, f(E;\mu_X)\,, \tag{3.3}$$

$$= \frac{g_X m_X^2 T \exp\left(\mu_X/T\right)}{2\pi^2} K_2\left(\frac{m_X}{T}\right) \tag{3.4}$$

From which the particle density in equilibrium n^{eq} can be derived from as the case with vanishing chemical potential $\mu = 0$, leading to

$$n_X^{eq}(T) = \frac{g_X m_X^2 T}{2\pi^2} K_2\left(\frac{m_X}{T}\right) \tag{3.5}$$

So we can express the fractions of the number densities as they appear in the Boltzmann equations, assuming $\frac{\mu_X}{T} \ll 1$:

$$\frac{n_X}{n_X^{eq}} = \exp\frac{\mu_X}{T} \simeq 1 + \frac{\mu_X}{T} \tag{3.6}$$

Furthermore we can assume that the chemical potentials for particles and antiparticles are of the same magnitude with opposite sign, so $\mu_X = -\mu_{\bar{X}}$

$$\begin{aligned}
\frac{dq_{\Delta_\alpha}}{dt} + 3Hq_{\Delta_\alpha} = \sum_i^{N_R} \Bigg[& \left(1 + \frac{\mu_{\ell_\alpha} + \mu_\phi}{T}\right)\gamma^{eq}\left(\ell_\alpha\phi \longrightarrow N_i\right) && - \left(1 + \frac{\mu_{N_i}}{T}\right)\gamma^{eq}\left(N_i \longrightarrow \ell_\alpha\phi\right) \\
& - \left(1 + \frac{-\mu_{\ell_\alpha} - \mu_\phi}{T}\right)\gamma^{eq}\left(\ell_\alpha^\dagger\phi^* \longrightarrow N_i\right) && + \left(1 + \frac{\mu_{N_i}}{T}\right)\gamma^{eq}\left(N_i \longrightarrow \ell_\alpha^\dagger\phi^*\right)\Bigg] \\
+ \sum_{\beta=e,\mu,\tau} \Bigg[& \left(1 + \frac{\mu_{\ell_\alpha} + \mu_\phi}{T}\right)\gamma_{sub}^{eq}\left(\ell_\alpha\phi \longrightarrow \ell_\beta^\dagger\phi^*\right) && - \left(1 + \frac{-\mu_{\ell_\beta} - \mu_\phi}{T}\right)\gamma_{sub}^{eq}\left(\ell_\beta^\dagger\phi^* \longrightarrow \ell_\alpha\phi\right) \\
& - \left(1 + \frac{-\mu_{\ell_\alpha} - \mu_\phi}{T}\right)\gamma_{sub}^{eq}\left(\ell_\alpha^\dagger\phi^* \longrightarrow \ell_\beta\phi\right) && + \left(1 + \frac{\mu_{\ell_\beta} + \mu_\phi}{T}\right)\gamma_{sub}^{eq}\left(\ell_\beta\phi \longrightarrow \ell_\alpha^\dagger\phi^*\right)\Bigg] \\
+ \sum_{\beta=e,\mu,\tau} (1+\delta_{\alpha\beta}) \Bigg[& \left(1 + \frac{\mu_{\ell_\alpha} + \mu_{\ell_\beta}}{T}\right)\gamma^{eq}\left(\ell_\alpha\ell_\beta \longrightarrow \phi^*\phi^*\right) && - \left(1 + \frac{-2\mu_\phi}{T}\right)\gamma^{eq}\left(\phi^*\phi^* \longrightarrow \ell_\alpha\ell_\beta\right) \\
& - \left(1 + \frac{-\mu_{\ell_\alpha} - \mu_{\ell_\beta}}{T}\right)\gamma^{eq}\left(\ell_\alpha^\dagger\ell_\beta^\dagger \longrightarrow \phi\phi\right) && + \left(1 + \frac{2\mu_\phi}{T}\right)\gamma^{eq}\left(\phi\phi \longrightarrow \ell_\alpha^\dagger\ell_\beta^\dagger\right)\Bigg] \\
+ \sum_{\beta=e,\mu,\tau} \Bigg[& \left(1 + \frac{\mu_{\ell_\alpha} + \mu_\phi}{T}\right)\gamma_{sub}^{eq}\left(\ell_\alpha\phi \longrightarrow \ell_\beta\phi\right) && - \left(1 + \frac{\mu_{\ell_\beta} + \mu_\phi}{T}\right)\gamma_{sub}^{eq}\left(\ell_\beta\phi \longrightarrow \ell_\alpha\phi\right) \\
& - \left(1 + \frac{-\mu_{\ell_\alpha} - \mu_\phi}{T}\right)\gamma_{sub}^{eq}\left(\ell_\alpha^\dagger\phi^* \longrightarrow \ell_\beta^\dagger\phi^*\right) && + \left(1 + \frac{-\mu_{\ell_\beta} - \mu_\phi}{T}\right)\gamma_{sub}^{eq}\left(\ell_\beta^\dagger\phi^* \longrightarrow \ell_\alpha^\dagger\phi^*\right) \\
+ \sum_{\beta=e,\mu,\tau} \Bigg[& \left(1 + \frac{\mu_{\ell_\alpha} - \mu_\phi}{T}\right)\gamma^{eq}\left(\ell_\alpha\phi^* \longrightarrow \ell_\beta\phi^*\right) && - \left(1 + \frac{\mu_{\ell_\beta} - \mu_\phi}{T}\right)\gamma^{eq}\left(\ell_\beta\phi^* \longrightarrow \ell_\alpha\phi^*\right) \\
& - \left(1 + \frac{-\mu_{\ell_\alpha} + \mu_\phi}{T}\right)\gamma^{eq}\left(\ell_\alpha^\dagger\phi \longrightarrow \ell_\beta^\dagger\phi\right) && + \left(1 + \frac{-\mu_{\ell_\alpha} + \mu_\phi}{T}\right)\gamma^{eq}\left(\ell_\beta^\dagger\phi \longrightarrow \ell_\alpha^\dagger\phi\right)\Bigg] \\
+ \sum_{\beta=e,\mu,\tau} \Bigg[& \left(1 + \frac{\mu_{\ell_\alpha} - \mu_{\ell_\beta}}{T}\right)\gamma^{eq}\left(\ell_\alpha\ell_\beta^\dagger \longrightarrow \phi\phi^*\right) && \left(1 + \frac{\mu_\phi - \mu_\phi}{T}\right)\gamma^{eq}\left(\phi\phi^* \longrightarrow \ell_\alpha\ell_\beta^\dagger\right) \\
& - \left(1 + \frac{-\mu_{\ell_\alpha} + \mu_{\ell_\beta}}{T}\right)\gamma^{eq}\left(\ell_\alpha^\dagger\ell_\beta \longrightarrow \phi^*\phi\right) && + \left(1 + \frac{-\mu_\phi + \mu_\phi}{T}\right)\gamma^{eq}\left(\phi^*\phi \longrightarrow \ell_\alpha^\dagger\ell_\beta\right)\Bigg]
\end{aligned}$$

Let's do some reordering now, grouping all the terms without the temperature/chemical potential dependence together. And also we want CPT invariance to *not* be violated from which follows that the CPT conjugated rates are identical: $\gamma^{eq}\left(XY \longrightarrow AB\right) = \gamma^{eq}\left(\bar{A}\bar{B} \longrightarrow \bar{X}\bar{Y}\right)$

$$
\begin{aligned}
\frac{dq_{\Delta_\alpha}}{dt} + 3Hq_{\Delta_\alpha} =& 2\sum_i^{N_R}\left[\gamma^{eq}\left(\ell_\alpha\phi \longrightarrow N_i\right) - \gamma^{eq}\left(\ell_\alpha^\dagger\phi^* \longrightarrow N_i\right)\right] \\
&+\sum_i^{N_R}\frac{\mu_{N_i}}{T}\left[\gamma^{eq}\left(\ell_\alpha\phi \longrightarrow N_i\right) - \gamma^{eq}\left(\ell_\alpha^\dagger\phi^* \longrightarrow N_i\right)\right] \\
&+\sum_i^{N_R}\frac{\mu_{\ell_\alpha}+\mu_\phi}{T}\left[\gamma^{eq}\left(\ell_\alpha\phi \longrightarrow N_i\right) + \gamma^{eq}\left(\ell_\alpha^\dagger\phi^* \longrightarrow N_i\right)\right] \\
&+2\sum_{\beta=e,\mu,\tau}\gamma^{eq}_{sub}\left(\ell_\alpha\phi \longrightarrow \ell_\beta^\dagger\phi^*\right) - \gamma^{eq}_{sub}\left(\ell_\alpha^\dagger\phi^* \longrightarrow \ell_\beta\phi\right) \\
&+2\sum_{\beta=e,\mu,\tau}\left\{\gamma^{eq}\left(\ell_\alpha\ell_\beta \longrightarrow \phi^*\phi^*\right) - \gamma^{eq}\left(\ell_\alpha^\dagger\ell_\beta^\dagger \longrightarrow \phi\phi\right)\right\}(1+\delta_{\alpha\beta}) \\
&+2\sum_{\beta=e,\mu,\tau}\gamma^{eq}_{sub}\left(\ell_\alpha\phi \longrightarrow \ell_\beta\phi\right) - \gamma^{eq}_{sub}\left(\ell_\alpha^\dagger\phi^* \longrightarrow \ell_\beta^\dagger\phi^*\right) \\
&+2\sum_{\beta=e,\mu,\tau}\gamma^{eq}\left(\ell_\alpha\phi^* \longrightarrow \ell_\beta\phi^*\right) - \gamma^{eq}\left(\ell_\alpha^\dagger\phi \longrightarrow \ell_\beta^\dagger\phi\right) \\
&+2\sum_{\beta=e,\mu,\tau}\gamma^{eq}\left(\ell_\alpha\ell_\beta^\dagger \longrightarrow \phi\phi\right) - \gamma^{eq}\left(\ell_\alpha^\dagger\ell_\beta \longrightarrow \phi^*\phi\right)\Big] \\
&+\sum_{\beta=e,\mu,\tau}\frac{\mu_{\ell_\alpha}+\mu_{\ell_\beta}+2\mu_\phi}{T}\left[\gamma^{eq}_{sub}\left(\ell_\alpha\phi \longrightarrow \ell_\beta^\dagger\phi^*\right) + \gamma^{eq}_{sub}\left(\ell_\alpha^\dagger\phi^* \longrightarrow \ell_\beta\phi\right)\right] \\
&+\sum_{\beta=e,\mu,\tau}\frac{\mu_{\ell_\alpha}+\mu_{\ell_\beta}+2\mu_\phi}{T}\left[\gamma^{eq}\left(\ell_\alpha\ell_\beta \longrightarrow \phi^*\phi^*\right) + \gamma^{eq}\left(\ell_\alpha^\dagger\ell_\beta^\dagger \longrightarrow \phi\phi\right)\right](1+\delta_{\alpha\beta}) \\
&+\sum_{\beta=e,\mu,\tau}\frac{\mu_{\ell_\alpha}-\mu_{\ell_\beta}}{T}\left[\gamma^{eq}_{sub}\left(\ell_\alpha\phi \longrightarrow \ell_\beta\phi\right) + \gamma^{eq}\left(\ell_\alpha^\dagger\phi^* \longrightarrow \ell_\beta^\dagger\phi^*\right)\right] \\
&+\sum_{\beta=e,\mu,\tau}\frac{\mu_{\ell_\alpha}-\mu_{\ell_\beta}}{T}\left[\gamma^{eq}\left(\ell_\alpha\phi^* \longrightarrow \ell_\beta\phi^*\right)\right] + \gamma^{eq}\left(\ell_\alpha^\dagger\phi \longrightarrow \ell_\beta^\dagger\phi\right) \\
&+\sum_{\beta=e,\mu,\tau}\frac{\mu_{\ell_\alpha}-\mu_{\ell_\beta}}{T}\left[\gamma^{eq}\left(\ell_\alpha\ell_\beta^\dagger \longrightarrow \phi\phi^*\right) + \gamma^{eq}\left(\ell_\alpha^\dagger\ell_\beta \longrightarrow \phi^*\phi\right)\right] \qquad (3.7)
\end{aligned}
$$

The only terms for which we allow CP violation ($\not{CP}$) is those with real RHN participating, therefore we can say for the $2 \longrightarrow 2$ rates which do no not require RIS subtraction, that the difference between them and their CP conjugate has to vanish:

$$
\begin{aligned}
&\gamma^{eq}\left(\ell_\alpha\ell_\beta \longrightarrow \phi^*\phi^*\right) - \gamma^{eq}\left(\ell_\alpha^\dagger\ell_\beta^\dagger \longrightarrow \phi\phi\right) = 0 \\
&\gamma^{eq}\left(\ell_\alpha\phi^* \longrightarrow \ell_\beta\phi^*\right) - \gamma^{eq}\left(\ell_\alpha^\dagger\phi \longrightarrow \ell_\beta^\dagger\phi\right) = 0 \\
&\gamma^{eq}\left(\ell_\alpha\ell_\beta^\dagger \longrightarrow \phi\phi^*\right) - \gamma^{eq}\left(\ell_\alpha^\dagger\ell_\beta \longrightarrow \phi^*\phi\right) = 0 \qquad (3.8)
\end{aligned}
$$

The reaction rates for the RHN decay and inverse decay can be expresses through the (a)symmetry parameters p, ε and a universal decay rate γ_i

$$
\gamma^{eq}\left(N_i \longrightarrow \ell_\alpha\phi\right) - \gamma^{eq}\left(N_i \longrightarrow \ell_\alpha^\dagger\phi^*\right) = \varepsilon_{i\alpha}\gamma_i \qquad (3.9)
$$

$$
\gamma^{eq}\left(N_i \longrightarrow \ell_\alpha\phi\right) + \gamma^{eq}\left(N_i \longrightarrow \ell_\alpha^\dagger\phi^*\right) = p_{i\alpha}\gamma_i \qquad (3.10)
$$

$$
(3.11)
$$

Where we can express:

$$\varepsilon_{i\alpha} = \frac{\Gamma\left(N_i \to \ell_\alpha \phi\right) - \Gamma\left(N_i \to \ell_\alpha^\dagger \phi^*\right)}{\sum_\sigma \Gamma\left(N_i \to \ell_\sigma \phi\right) + \Gamma\left(N_i \to \ell_\sigma^\dagger \phi^*\right)} = \mathcal{BR}\left(N_i \to \ell_\alpha \phi\right) - \mathcal{BR}\left(N_i \to \ell_\alpha^\dagger \phi^*\right) \tag{3.12}$$

$$p_{i\alpha} = \frac{\Gamma\left(N_i \to \ell_\alpha \phi\right) + \Gamma\left(N_i \to \ell_\alpha^\dagger \phi^*\right)}{\sum_\sigma \Gamma\left(N_i \to \ell_\sigma \phi\right) + \Gamma\left(N_i \to \ell_\sigma^\dagger \phi^*\right)} = \mathcal{BR}\left(N_i \to \ell_\alpha \phi\right) + \mathcal{BR}\left(N_i \to \ell_\alpha^\dagger \phi^*\right) \tag{3.13}$$

$$\gamma^{eq}\left(N_i \longrightarrow \ell_\alpha \phi\right) = \gamma^{eq}\left(\ell_\alpha^\dagger \phi^* \longrightarrow N_i\right) = \frac{1}{2}\left(p_{i\alpha} + \varepsilon_{i\alpha}\right)\gamma_i = \mathcal{BR}\left(N_i \to \ell_\alpha \phi\right)\gamma_i \tag{3.14}$$

$$\gamma^{eq}\left(N_i \longrightarrow \ell_\alpha^\dagger \phi^*\right) = \gamma^{eq}\left(\ell_\alpha \phi \longrightarrow N_i\right) = \frac{1}{2}\left(p_{i\alpha} - \varepsilon_{i\alpha}\right)\gamma_i = \mathcal{BR}\left(N_i \to \ell_\alpha^\dagger \phi^*\right)\gamma_i \tag{3.15}$$

The rates with the subtracted RIS we need to consider separately and we write them as

$$\gamma_{sub}^{eq}\left(\ell_\alpha \phi \longrightarrow \ell_\beta \phi\right) = \gamma^{eq}\left(\ell_\alpha \phi \longrightarrow \ell_\beta \phi\right) - \sum_i^{N_R} \gamma^{eq}\left(\ell_\alpha \phi \longrightarrow N_i\right)\mathcal{BR}\left(N_i \to \ell_\beta \phi\right) \quad etc. \tag{3.16}$$

$$\tag{3.17}$$

With the unsubtracted part not violating CP, so:

$$\begin{aligned}
&\gamma_{sub}^{eq}\left(\ell_\alpha \phi \longrightarrow \ell_\beta^\dagger \phi^*\right) - \gamma_{sub}^{eq}\left(\ell_\alpha^\dagger \phi^* \longrightarrow \ell_\beta \phi\right) \\
&\quad = -\sum_i^{N_R} \gamma^{eq}\left(\ell_\alpha \phi \longrightarrow N_i\right)\mathcal{BR}\left(N_i \to \ell_\beta^\dagger \phi^*\right) + \sum_i^{N_R} \gamma^{eq}\left(\ell_\alpha^\dagger \phi^* \longrightarrow N_i\right)\mathcal{BR}\left(N_i \to \ell_\beta \phi\right) \\
&\quad = -\sum_i^{N_R} \frac{1}{4}\left(p_{i\alpha} - \varepsilon_{i\alpha}\right)\left(p_{i\beta} - \varepsilon_{i\beta}\right) + \sum_i^{N_R} \frac{1}{4}\left(p_{i\alpha} + \varepsilon_{i\alpha}\right)\left(p_{i\beta} + \varepsilon_{i\beta}\right)\gamma_i \\
&\quad = \sum_i^{N_R} \frac{1}{4}\left(-p_{i\alpha}p_{i\beta} + p_{i\alpha}\varepsilon_{i\beta} + p_{i\beta}\varepsilon_{i\alpha} - \varepsilon_{i\alpha}\varepsilon_{i\beta} + p_{i\alpha}p_{i\beta} + p_{i\alpha}\varepsilon_{i\beta} + p_{i\beta}\varepsilon_{i\alpha} + \varepsilon_{i\alpha}\varepsilon_{i\beta}\right)\gamma_i \\
&\quad = \sum_i^{N_R} \frac{1}{2}\left(p_{i\alpha}\varepsilon_{i\beta} + p_{i\beta}\varepsilon_{i\alpha}\right)\gamma_i
\end{aligned} \tag{3.18}$$

$$\begin{aligned}
&\gamma_{sub}^{eq}\left(\ell_\alpha \phi \longrightarrow \ell_\beta \phi\right) - \gamma_{sub}^{eq}\left(\ell_\alpha^\dagger \phi^* \longrightarrow \ell_\beta^\dagger \phi^*\right) \\
&\quad = -\sum_i^{N_R} \gamma^{eq}\left(\ell_\alpha \phi \longrightarrow N_i\right)\mathcal{BR}\left(N_i \to \ell_\beta \phi\right) + \sum_i^{N_R} \gamma^{eq}\left(\ell_\alpha^\dagger \phi^* \longrightarrow N_i\right)\mathcal{BR}\left(N_i \to \ell_\beta^\dagger \phi^*\right) \\
&\quad = -\sum_i^{N_R} \frac{1}{4}\left(p_{i\alpha} - \varepsilon_{i\alpha}\right)\left(p_{i\beta} + \varepsilon_{i\beta}\right) + \sum_i^{N_R} \frac{1}{4}\left(p_{i\alpha} + \varepsilon_{i\alpha}\right)\left(p_{i\beta} - \varepsilon_{i\beta}\right)\gamma_i \\
&\quad = \sum_i^{N_R} \frac{1}{4}\left(-p_{i\alpha}p_{i\beta} - p_{i\alpha}\varepsilon_{i\beta} + p_{i\beta}\varepsilon_{i\alpha} + \varepsilon_{i\alpha}\varepsilon_{i\beta} + p_{i\alpha}p_{i\beta} - p_{i\alpha}\varepsilon_{i\beta} + p_{i\beta}\varepsilon_{i\alpha} - \varepsilon_{i\alpha}\varepsilon_{i\beta}\right)\gamma_i \\
&\quad = \sum_i^{N_R} \frac{1}{2}\left(-p_{i\alpha}\varepsilon_{i\beta} + p_{i\beta}\varepsilon_{i\alpha}\right)\gamma_i
\end{aligned} \tag{3.19}$$

So this now takes care of all the CP odd terms. For the CP symmetric reaction rates we can

introduce as a shorthand notation: $\gamma^{eq}\left(XY \longrightarrow AB\right) + \gamma^{eq}\left(\bar{X}\bar{Y} \longrightarrow \bar{A}\bar{B}\right) = \gamma^{XY}_{AB}$

$$\begin{aligned}
\frac{dq_{\Delta_\alpha}}{dt} + 3Hq_{\Delta_\alpha} =& -\sum_i^{N_R}\left(2+\frac{\mu_{N_i}}{T}\right)\varepsilon_{i\alpha}\gamma_i \\
&+\sum_i^{N_R}\frac{\mu_{\ell_\alpha}+\mu_\phi}{T}p_{i\alpha}\gamma_i \\
&+\sum_i^{N_R}\sum_{\beta=e,\mu,\tau}\left(p_{i\alpha}\varepsilon_{i\beta}+p_{i\beta}\varepsilon_{i\alpha}-p_{i\alpha}\varepsilon_{i\beta}+p_{i\beta}\varepsilon_{i\alpha}\right)\gamma_i \\
&+\sum_{\beta=e,\mu,\tau}\frac{\mu_{\ell_\alpha}+\mu_{\ell_\beta}+2\mu_\phi}{T}\left[\gamma^{\ell_\alpha\phi}_{\ell^\dagger_\beta\phi^*,\ sub}+\gamma^{\ell_\alpha\ell_\beta}_{\phi^*\phi^*}\left(1+\delta_{\alpha\beta}\right)\right] \\
&+\sum_{\beta=e,\mu,\tau}\frac{\mu_{\ell_\alpha}-\mu_{\ell_\beta}}{T}\left[\gamma^{\ell_\alpha\phi}_{\ell_\beta\phi,\ sub}+\gamma^{\ell_\alpha\phi^*}_{\ell_\beta\phi^*}+\gamma^{\ell_\alpha\ell^\dagger_\beta}_{\phi\phi^*}\right] \qquad (3.20)\\
=&\sum_i^{N_R}\left[-\left(2+\frac{\mu_{N_i}}{T}\right)\varepsilon_{i\alpha}+\frac{\mu_{\ell_\alpha}+\mu_\phi}{T}p_{i\alpha}+2\sum_{\beta=e,\mu,\tau}p_{i\beta}\varepsilon_{i\alpha}\right]\gamma_i \\
&+\sum_{\beta=e,\mu,\tau}\frac{\mu_{\ell_\alpha}+\mu_{\ell_\beta}+2\mu_\phi}{T}\gamma^{\Delta L=2}_{\alpha\beta}+\frac{\mu_{\ell_\alpha}-\mu_{\ell_\beta}}{T}\gamma^{\Delta L=0}_{\alpha\beta} \qquad (3.21)
\end{aligned}$$

Then we can simplify by using $\sum_{\beta=e,\mu,\tau}p_{i\beta}=1$ and resubstituting: $\frac{\mu_{N_i}}{T}=\left(\frac{n_{N_i}}{n^{eq}_{N_i}}-1\right)$ and $\Gamma_i=\frac{\gamma_i}{n^{eq}_{N_i}}$

$$\begin{aligned}
\frac{dq_{\Delta_\alpha}}{dt} + 3Hq_{\Delta_\alpha} =& -\sum_i^{N_R}\left(n_{N_i}-n^{eq}_{N_i}\right)\varepsilon_{i\alpha}\Gamma_i+\sum_i^{N_R}\frac{\mu_{\ell_\alpha}+\mu_\phi}{T}\overbrace{p_{i\alpha}\gamma_i}^{=\gamma_{i\alpha}} \\
&+\sum_{\beta=e,\mu,\tau}\frac{\mu_{\ell_\alpha}+\mu_\phi}{T}\left(\gamma^{\Delta L=2}_{\alpha\beta}+\gamma^{\Delta L=0}_{\alpha\beta}\right)+\frac{\mu_{\ell_\beta}+\mu_\phi}{T}\left(\gamma^{\Delta L=2}_{\alpha\beta}-\gamma^{\Delta L=0}_{\alpha\beta}\right)
\end{aligned}$$

$$\begin{aligned}
\sum_{\beta=e,\mu,\tau}\frac{\mu_{\ell_\alpha}+\mu_\phi}{T}\left(\gamma^{\Delta L=2}_{\alpha\beta}+\gamma^{\Delta L=0}_{\alpha\beta}\right) &= \sum_{\sigma=e,\mu,\tau}\frac{\mu_{\ell_\alpha}+\mu_\phi}{T}\left(\gamma^{\Delta L=2}_{\alpha\sigma}+\gamma^{\Delta L=0}_{\alpha\sigma}\right) \\
&= \sum_{\sigma=e,\mu,\tau}\sum_{\beta=e,\mu,\tau}\delta_{\alpha\beta}\frac{\mu_{\ell_\beta}+\mu_\phi}{T}\left(\gamma^{\Delta L=2}_{\alpha\sigma}+\gamma^{\Delta L=0}_{\alpha\sigma}\right) \qquad (3.22)
\end{aligned}$$

$$\begin{aligned}
\sum_{\beta=e,\mu,\tau}\frac{\mu_{\ell_\beta}+\mu_\phi}{T}\left(\gamma^{\Delta L=2}_{\alpha\beta}-\gamma^{\Delta L=0}_{\alpha\beta}\right) &= \sum_{\sigma=e,\mu,\tau}\frac{\mu_{\ell_\sigma}+\mu_\phi}{T}\left(\gamma^{\Delta L=2}_{\alpha\sigma}-\gamma^{\Delta L=0}_{\alpha\sigma}\right) \\
&= \sum_{\beta=e,\mu,\tau}\sum_{\sigma=e,\mu,\tau}\delta_{\sigma\beta}\frac{\mu_{\ell_\beta}+\mu_\phi}{T}\left(\gamma^{\Delta L=2}_{\alpha\sigma}-\gamma^{\Delta L=0}_{\alpha\sigma}\right) \qquad (3.23)
\end{aligned}$$

Also defining the rate for the washout through inverse decays:

$$\gamma^{ID}_{\alpha\beta}=\sum_i^{N_R}\gamma_{i\alpha}\delta_{\alpha\beta} \qquad (3.24)$$

we can now write the total washout rate

$$\gamma^{W}_{\alpha\beta}=\gamma^{ID}_{\alpha\beta}+\sum_{\sigma=e,\mu,\tau}\left(\gamma^{\Delta L=2}_{\alpha\sigma}+\gamma^{\Delta L=0}_{\alpha\sigma}\right)\delta_{\alpha\beta}+\left(\gamma^{\Delta L=2}_{\alpha\sigma}-\gamma^{\Delta L=0}_{\alpha\sigma}\right)\delta_{\sigma\beta} \qquad (3.25)$$

Leading to a compact form of writing the Boltzmann equations

$$\frac{dq_{\Delta_\alpha}}{dt} + 3Hq_{\Delta_\alpha} = -\sum_i^{N_R}\left(n_{N_i}-n^{eq}_{N_i}\right)\varepsilon_{i\alpha}\Gamma_i+\sum_{\beta=e,\mu,\tau}\frac{\mu_{\ell_\beta}+\mu_\phi}{T}\gamma^{W}_{\alpha\beta} \qquad (3.26)$$

3.1.2 Interrelation of chemical potentials in the Standard model at low temperatures

We want to look at the chemical potentials of all the SM particles:

$$\mathcal{P} = \{e, \mu, \tau, \ell_e, \ell_\mu, \ell_\tau, u, c, t, d, s, b, Q_1, Q_2, Q_3, \phi\} \tag{3.27}$$

And we cleverly choose a set of interactions which are linearly independent in particle space [32].

$$Y_t, \mathrm{SS}, \mathrm{WS}, Y_b, Y_\tau, Y_c, Y_\mu, Y_{sb}, Y_s, Y_d, Y_{ds}, Y_e \tag{3.28}$$

Y here refers to the different types of Yukawa interactions with the index indicating the effected fermion, while SS, WS refer to strong and weak sphalerons respectively.

Take as an example the strange quark Yukawa interaction $Y_s = s\phi \longleftrightarrow Q_2$ while it is in thermal equilibrium the chemical potentials follow the relation:

$$\mu_s + \mu_\phi = \mu_{Q_2} \Leftrightarrow \mu_{Q_2} - \mu_s - \mu_\phi = 0 \tag{3.29}$$

We can now write the particles involved in this interaction in vector form, with all the SM particle as particles like:

$$\vec{n}^{Y_s} = (\overset{e}{0}, \overset{\mu}{0}, \overset{\tau}{0}, \overset{\ell_e}{0}, \overset{\ell_\mu}{0}, \overset{\ell_\tau}{0}, \overset{u}{0}, \overset{c}{0}, \overset{t}{0}, \overset{d}{0}, \overset{s}{-1}, \overset{b}{0}, \overset{Q_1}{0}, \overset{Q_2}{1}, \overset{Q_3}{0}, \overset{\phi}{-1}) \tag{3.30}$$

So writing the chemical potentials into a 16-dim vector as well we can write (3.29) as:

$$\sum_i n_i^{Y_s} \mu_i = \vec{n}^{Y_s} \cdot \vec{\mu} = 0 \tag{3.31}$$

This we can do for all the previously listed interactions and we get a set of 12 constraint equations for the SM chemical potentials. To fully solvable set of equations we need 16 equations though, so we also consider four in the SM globally conserved charges, those being the electroweak Hypercharge Y and the lepton flavour asymmetries $\Delta_\alpha = \frac{B}{3} - L_\alpha$.

We can define a similar charge vector for these, encompassing all the particles making up the respective charge:

$$\vec{n}^{Y} = \left(-1, -1, -1, -\frac{1}{2}, -\frac{1}{2}, -\frac{1}{2}, \frac{2}{3}, \frac{2}{3}, \frac{2}{3}, -\frac{1}{3}, -\frac{1}{3}, -\frac{1}{3}, \frac{1}{6}, \frac{1}{6}, \frac{1}{6}, \frac{1}{6}, \frac{1}{2}\right) \tag{3.32}$$

$$\vec{n}^{\Delta_e} = \left(-1, 0, 0, -1, 0, 0, \frac{1}{9}, \frac{1}{9}, \frac{1}{9}, \frac{1}{9}, \frac{1}{9}, \frac{1}{9}, \frac{1}{9}, \frac{1}{9}, \frac{1}{9}, 0\right) \tag{3.33}$$

$$\vec{n}^{\Delta_\mu} = \left(0, -1, 0, 0, -1, 0, \frac{1}{9}, \frac{1}{9}, \frac{1}{9}, \frac{1}{9}, \frac{1}{9}, \frac{1}{9}, \frac{1}{9}, \frac{1}{9}, \frac{1}{9}, 0\right) \tag{3.34}$$

$$\vec{n}^{\Delta_\tau} = \left(0, 0, -1, 0, 0, -1, \frac{1}{9}, \frac{1}{9}, \frac{1}{9}, \frac{1}{9}, \frac{1}{9}, \frac{1}{9}, \frac{1}{9}, \frac{1}{9}, \frac{1}{9}, 0\right) \tag{3.35}$$

And we can define an effective potential μ_C to these charges as

$$\sum_i n_i^C g_i \mu_i^{ini} = \left(\vec{n}^C \circ \vec{g}\right) \cdot \vec{\mu}^{ini} \tag{3.36}$$

With $\vec{g}$ containing the colour and weak isospin multiplicities of the SM fields:

$$\vec{g} = (1, 1, 1, 2, 2, 2, 3, 3, 3, 3, 3, 3, 6, 6, 6, 4) \tag{3.37}$$

By collecting all the charges associated with the interactions and the conserved charges into a Matrix we can write all the 16 constraint equations in the very compact form

$$\underline{M}\vec{\mu} = m \Leftrightarrow \vec{\mu} = \underline{M}^{-1} m \tag{3.38}$$

$$\text{With } \underline{M} = \begin{pmatrix} (\vec{n}^I)^T \\ \left(\vec{n}^C \circ \vec{g}\right) \end{pmatrix}, \qquad m = \begin{pmatrix} 0 \\ \mu_C \end{pmatrix} \tag{3.39}$$

So when all the aforementioned are indeed in equilibrium we get as a full matrix equation

$$\begin{pmatrix}
0 & 0 & 0 & 0 & 0 & 0 & 0 & 0 & -1 & 0 & 0 & 0 & 0 & 0 & 1 & 1 \\
0 & 0 & 0 & 0 & 0 & 0 & -1 & -1 & -1 & -1 & -1 & -1 & 2 & 2 & 2 & 0 \\
0 & 0 & 0 & 1 & 1 & 1 & 0 & 0 & 0 & 0 & 0 & 0 & 3 & 3 & 3 & 0 \\
0 & 0 & 0 & 0 & 0 & 0 & 0 & 0 & 0 & 0 & 0 & -1 & 0 & 0 & 1 & -1 \\
0 & 0 & -1 & 0 & 0 & 1 & 0 & 0 & 0 & 0 & 0 & 0 & 0 & 0 & 0 & -1 \\
0 & 0 & 0 & 0 & 0 & 0 & 0 & -1 & 0 & 0 & 0 & 0 & 0 & 1 & 0 & 1 \\
0 & -1 & 0 & 0 & 1 & 0 & 0 & 0 & 0 & 0 & 0 & 0 & 0 & 0 & 0 & -1 \\
0 & 0 & 0 & 0 & 0 & 0 & 0 & 0 & 0 & 0 & -1 & 0 & 0 & 0 & 1 & -1 \\
0 & 0 & 0 & 0 & 0 & 0 & 0 & 0 & 0 & 0 & -1 & 0 & 0 & 1 & 0 & -1 \\
0 & 0 & 0 & 0 & 0 & 0 & 0 & 0 & 0 & -1 & 0 & 0 & 1 & 0 & 0 & -1 \\
0 & 0 & 0 & 0 & 0 & 0 & 0 & 0 & 0 & -1 & 0 & 0 & 0 & 1 & 0 & -1 \\
-1 & 0 & 0 & 1 & 0 & 0 & 0 & 0 & 0 & 0 & 0 & 0 & 0 & 0 & 0 & -1 \\
-1 & -1 & -1 & -1 & -1 & -1 & 2 & 2 & 2 & -1 & -1 & -1 & 1 & 1 & 1 & 2 \\
-1 & 0 & 0 & -2 & 0 & 0 & \frac{1}{3} & \frac{1}{3} & \frac{1}{3} & \frac{1}{3} & \frac{1}{3} & \frac{1}{3} & \frac{2}{3} & \frac{2}{3} & \frac{2}{3} & 0 \\
0 & -1 & 0 & 0 & -2 & 0 & \frac{1}{3} & \frac{1}{3} & \frac{1}{3} & \frac{1}{3} & \frac{1}{3} & \frac{1}{3} & \frac{2}{3} & \frac{2}{3} & \frac{2}{3} & 0 \\
0 & 0 & -1 & 0 & 0 & -2 & \frac{1}{3} & \frac{1}{3} & \frac{1}{3} & \frac{1}{3} & \frac{1}{3} & \frac{1}{3} & \frac{2}{3} & \frac{2}{3} & \frac{2}{3} & 0
\end{pmatrix}^{-1}
\begin{pmatrix} 0 \\ 0 \\ 0 \\ 0 \\ 0 \\ 0 \\ 0 \\ 0 \\ 0 \\ 0 \\ 0 \\ 0 \\ 0 \\ \mu_{\Delta_e} \\ \mu_{\Delta_\mu} \\ \mu_{\Delta_\tau} \end{pmatrix}
=
\begin{pmatrix} \mu_e \\ \mu_\mu \\ \mu_\tau \\ \mu_{\ell_1} \\ \mu_{\ell_2} \\ \mu_{\ell_3} \\ \mu_u \\ \mu_c \\ \mu_t \\ \mu_d \\ \mu_s \\ \mu_b \\ \mu_{Q_1} \\ \mu_{Q_2} \\ \mu_{Q_3} \\ \mu_\phi \end{pmatrix}$$

Here I made use of the gauged nature of $U(1)_Y$ to determine that $\mu_Y = 0$ always holds. This now allows us to express any SM potential as a linear combination of the effective potentials associated with the leptons flavour asymmetries Δ_α, especially the potential combinations we're interested in for our Boltzmann equation, which we can express as

$$\mu_{\ell_\alpha} + \mu_\phi = -\sum_\beta C_{\alpha\beta}\mu_{\Delta_\beta} \tag{3.40}$$

where C is the according flavour coupling matrix and the minus sign is convention. Or explicitly:

$$\begin{pmatrix} \mu_{\ell_e} + \mu_\phi \\ \mu_{\ell_\mu} + \mu_\phi \\ \mu_{\ell_\tau} + \mu_\phi \end{pmatrix} = \begin{pmatrix} -\frac{257}{711} & -\frac{20}{711} & -\frac{20}{711} \\ -\frac{20}{711} & -\frac{257}{711} & -\frac{20}{711} \\ -\frac{20}{711} & -\frac{20}{711} & -\frac{257}{711} \end{pmatrix} \begin{pmatrix} \mu_{\Delta_e} \\ \mu_{\Delta_\mu} \\ \mu_{\Delta_\tau} \end{pmatrix} \tag{3.41}$$

3.1.3 Out of equilibrium electron Yukawa

The problem with this approach so far is that we assumed all the interaction to be in equilibrium, which only holds for temperatures $T \lesssim 10^5\,\mathrm{GeV}$. Going to higher temperatures, i.e. at earlier times in the evolution of the universe, the electron Yukawa interaction Y_e becomes less efficient and goes out of equilibrium and we can no longer assume $\vec{n}^{Y_e} \cdot \vec{\mu} = 0$.

What we do instead is to observe that between those active interactions the electron Yukawa is the only one affecting right handed electrons e, so when this interactions has become inefficient the number density n_e, and hence the chemical potential μ_e, remains untouched and can therefore be a conserved quantity, and we treat it like the other (globally) conserved charges from before.

Doing so changes the matrix equation from before to:

$$\begin{pmatrix}
0 & 0 & 0 & 0 & 0 & 0 & 0 & 0 & -1 & 0 & 0 & 0 & 0 & 0 & 1 & 1 \\
0 & 0 & 0 & 0 & 0 & 0 & -1 & -1 & -1 & -1 & -1 & -1 & 2 & 2 & 2 & 0 \\
0 & 0 & 0 & 1 & 1 & 1 & 0 & 0 & 0 & 0 & 0 & 0 & 3 & 3 & 3 & 0 \\
0 & 0 & 0 & 0 & 0 & 0 & 0 & 0 & 0 & 0 & 0 & -1 & 0 & 0 & 1 & -1 \\
0 & 0 & -1 & 0 & 0 & 1 & 0 & 0 & 0 & 0 & 0 & 0 & 0 & 0 & 0 & -1 \\
0 & 0 & 0 & 0 & 0 & 0 & 0 & -1 & 0 & 0 & 0 & 0 & 0 & 1 & 0 & 1 \\
0 & -1 & 0 & 0 & 1 & 0 & 0 & 0 & 0 & 0 & 0 & 0 & 0 & 0 & 0 & -1 \\
0 & 0 & 0 & 0 & 0 & 0 & 0 & 0 & 0 & 0 & -1 & 0 & 0 & 0 & 1 & -1 \\
0 & 0 & 0 & 0 & 0 & 0 & 0 & 0 & 0 & 0 & -1 & 0 & 0 & 1 & 0 & -1 \\
0 & 0 & 0 & 0 & 0 & 0 & 0 & 0 & 0 & -1 & 0 & 0 & 1 & 0 & 0 & -1 \\
0 & 0 & 0 & 0 & 0 & 0 & 0 & 0 & 0 & -1 & 0 & 0 & 0 & 1 & 0 & -1 \\
1 & 0 & 0 & 0 & 0 & 0 & 0 & 0 & 0 & 0 & 0 & 0 & 0 & 0 & 0 & 0 \\
-1 & -1 & -1 & -1 & -1 & -1 & 2 & 2 & 2 & -1 & -1 & -1 & 1 & 1 & 1 & 2 \\
-1 & 0 & 0 & -2 & 0 & 0 & \frac{1}{3} & \frac{1}{3} & \frac{1}{3} & \frac{1}{3} & \frac{1}{3} & \frac{1}{3} & \frac{2}{3} & \frac{2}{3} & \frac{2}{3} & 0 \\
0 & -1 & 0 & 0 & -2 & 0 & \frac{1}{3} & \frac{1}{3} & \frac{1}{3} & \frac{1}{3} & \frac{1}{3} & \frac{1}{3} & \frac{2}{3} & \frac{2}{3} & \frac{2}{3} & 0 \\
0 & 0 & -1 & 0 & 0 & -2 & \frac{1}{3} & \frac{1}{3} & \frac{1}{3} & \frac{1}{3} & \frac{1}{3} & \frac{1}{3} & \frac{2}{3} & \frac{2}{3} & \frac{2}{3} & 0
\end{pmatrix}^{-1}
\begin{pmatrix} 0 \\ 0 \\ 0 \\ 0 \\ 0 \\ 0 \\ 0 \\ 0 \\ 0 \\ 0 \\ \mu_e \\ 0 \\ \mu_{\Delta_e} \\ \mu_{\Delta_\mu} \\ \mu_{\Delta_\tau} \end{pmatrix}
=
\begin{pmatrix} \mu_e \\ \mu_\mu \\ \mu_\tau \\ \mu_{\ell_1} \\ \mu_{\ell_2} \\ \mu_{\ell_3} \\ \mu_u \\ \mu_c \\ \mu_t \\ \mu_d \\ \mu_s \\ \mu_b \\ \mu_{Q_1} \\ \mu_{Q_2} \\ \mu_{Q_3} \\ \mu_\phi \end{pmatrix}$$

from which we can already see that the relation between the potentials changes from the simple linear relation in (3.40) into an affine relation:

$$\mu_{\ell_\alpha} + \mu_\phi = \mu_\alpha^0 - \sum_\beta C_{\alpha\beta}\mu_{\Delta_\beta} \tag{3.42}$$

with the pre existing (primordial) potentials written as $\vec{\mu}^0$, which here only encompass μ_e. Explicitly this now looks like

$$\begin{pmatrix} \mu_{\ell_e} + \mu_\phi \\ \mu_{\ell_\mu} + \mu_\phi \\ \mu_{\ell_\tau} + \mu_\phi \end{pmatrix} = \begin{pmatrix} -\frac{5}{13} \\ \frac{4}{37} \\ \frac{4}{37} \end{pmatrix} \mu_e - \begin{pmatrix} \frac{6}{13} & 0 & 0 \\ 0 & \frac{41}{111} & \frac{4}{111} \\ 0 & \frac{4}{111} & \frac{41}{111} \end{pmatrix} \begin{pmatrix} \mu_{\Delta_e} \\ \mu_{\Delta_\mu} \\ \mu_{\Delta_\tau} \end{pmatrix} \tag{3.43}$$

It is important to mention here that we assume $\mu_e \neq 0$, which is the core aspect of wash-in leptogenesis, and introduces through the differing sign in the shift vector $\vec{\mu}^0$ that what under previously considered circumstances would simply result in an asymmetry wash out, now leads to a new equilibrium, which is offset from the original $B - L = 0$ line. Thereby we can use this mechanism to create a situation where $B - L \neq 0$ even if originally $B - L = 0$ without even needing the explicit violation of CP through the RHN

3.1.4 At even higher temperatures

As we go to even higher temperatures we see more and more interactions going out of equilibrium. One can now divide the temperature range the universe goes through after reheating until all the Interactions are in thermal equilibrium ($10^{15}\,\text{GeV} \rightarrow 10^5\,\text{GeV}$) into five sections, in which each a subset of interactions goes into/out of equilibrium. An overview of these temperature regimes as the interactions starting to go off equilibrium can be see in Table 3.1.

Another effect one needs to account for is that at temperatures of $T \gtrsim 10^{13}\,\text{GeV}$, when all the charged lepton Yukawa interactions are out of thermal equilibrium, no SM interaction can probe the flavour composition of charged lepton states any more. Which means we have to treat charged leptons as one fully coherent field. Similarly this has to be taken into account in the temperature regime down to $T \gtrsim 10^9\,\text{GeV}$ when the muon Yukawa interaction has not yet reached thermal equilibrium, leaving

T [GeV]	Interaction leaving equilibrium	New conserved charge
$(10^5, 10^6)$	Y_e	e
$(10^6, 10^9)$	Y_{ds}	$2B_1 - B_2 - B_3$
	Y_d	$u - d$
$(10^9, 10^{11\sim12})$	Y_s	$d - s$
	Y_{sb}	$B_1 - B_2$
	Y_μ	μ
$(10^{11\sim12}, 10^{13})$	Y_c	$u - c$
	Y_τ	τ
	Y_b	$d - b$
	WS	B
$(10^{13}, 10^{15})$	SS	u

Table 3.1: Temperature regions and the interactions that leave thermal equilibrium in each region along with the new conserved charges arising from this

us with the τ state and a coherent $e - \mu$ lepton state. In this work I will not further go into these effects as I will primarily focus on the low end of this temperature scale.

It is clear that this rough subdivision into temperature regimes, in which we simply assume that an interaction is either fully *in* or fully *out of* equilibrium, does not capture the full picture. For each interaction there is a transition regime in which the efficiency of the interactions transitions smoothly from 0 to 1. I will later have a detailed look at this transition regime for the electron Yukawa interaction ($T \lesssim 10^5$ GeV) in Chapter 4.

3.2 Calculation of the reaction rates

To determine the rate at which the processes contributing to the wash-out / wash-in occur I follow [24, 25] calculations of the relevant rates, while ignoring the extra attention they paid to the resummation of the Yukawa couplings, as they focus on the scenario of resonant leptogenesis, which requires highly degenerate RHN masses (see Section 2.2.3.1), while the wash-in scenario requires a strong mass hierarchy between the RHS. For the sake of comparison this means $\bar{h}^\nu_+ = h^\nu$ and $\bar{h}^\nu_- = h^{\nu *}$.

In general any reaction rate of a process $X \longrightarrow Y$ can be expressed as

$$\gamma^{eq}\left(X \longrightarrow Y\right) = \int d\pi_X d\pi_Y \, (2\pi)^4 \delta^{(4)}(p_X - p_Y) e^{-p^0_X/T} |\mathcal{M}(X \longrightarrow Y)|^2 \tag{3.44}$$

with the phase space factors being shortened as

$$d\pi_X = \frac{1}{S_X} \prod_{i=1}^{n_X} \delta(p_i^2 - m_i^2)\theta(p_i^0) \tag{3.45}$$

$S_X = n_{id}!$ here being a symmetry factor if X contains any identical particles, and n_X referring to the total number of individual particles in X.

For a $1 \to 2$ process (i.e. a decay) of the form $X \longrightarrow AB$ this simplifies into

$$\gamma^{eq}\left(A \longrightarrow BC\right) = n_X^{eq} \frac{K_1(y)}{K_2(y)} \Gamma(A \longrightarrow BC) \tag{3.46}$$

here $y = \frac{m_A}{T}$ and the decay width of the particle Γ_A and K_n being modified Bessel functions of the second kind, of order n.

As the particle density of A is calculated via

$$n_A(T) = g_A \int \frac{d^3\mathbf{p}}{(2\pi)^3} e^{-(E_A - \mu_A)/T}, \qquad E_A = \sqrt{p^2 + m_A^2} \tag{3.47}$$

$$= \frac{g_A m_A^2 T e^{\mu_A/T}}{2\pi^2} K_2\left(\frac{m_A}{T}\right) \tag{3.48}$$

from which we can get the equilibrium distribution from the case where $\mu_A = 0$, i.e.

$$n_A^{eq} = \frac{g_A m_A^2 T}{2\pi^2} K_2(y) \tag{3.49}$$

hence conveniently cancelling the $K_2(y)$ in (3.46) leading to

$$\gamma^{eq}(A \longrightarrow BC) = \frac{g_A m_A^3}{2\pi^2 y} K_1(y) \Gamma(A \longrightarrow BC) \tag{3.50}$$

$$\gamma^{eq}\left(\bar{A} \longrightarrow \bar{B}\bar{C}\right) = \frac{g_A m_A^3}{2\pi^2 y} K_1(y) \Gamma(\bar{A} \longrightarrow \bar{B}\bar{C}) \tag{3.51}$$

For $2 \longrightarrow 2$ processes, one can use the reduced cross section $\hat{\sigma}(s)$ in (3.44) like, to arrive at

$$\gamma^{eq}(X \longrightarrow Y) + \gamma^{eq}\left(\bar{X} \longrightarrow \bar{Y}\right) \equiv \gamma_Y^X = \frac{m_A^4}{64\pi^4 y} \int_{x_0}^{\infty} dx \sqrt{x} K_1(z\sqrt{x}) \hat{\sigma}_Y^X(x) \tag{3.52}$$

Here $x = \frac{s}{m_A^2}$ with the standard mandelstam variable s, and x_{thr} being the the kinematic threshold for the given scattering process.

In the following we will of course use as the reference energy scale the mass of the lightest heavy neutrino M_1.

3.2.1 Decays and inverse decays

For the simple decay processes (and their inverse) the rate at which these occur in a comoving volume is given through the relatively simple expression.

$$\gamma_{i\alpha} = p_{i\alpha}\gamma_i = \gamma^{eq}(N_i \to \ell_\alpha \phi) + \gamma^{eq}\left(N_i \to \ell_\alpha^\dagger \phi^*\right) \tag{3.53}$$

$$= \frac{g_{N_i} M_i^2 T}{\pi^2} K_1\left(\frac{M_i}{T}\right) \Gamma_{N_i} \tag{3.54}$$

Here we introduce a and c as parameters to express the relative size of the RHN masses and the RHN decay width Γ to the lightest RHN mass M_1 as a dimensionless parameter:

$$z = \frac{M_1}{T}, \qquad a_i = \left(\frac{M_i}{M_1}\right)^2, \qquad c_i^\alpha = \left(\frac{\Gamma_i^\alpha}{M_1}\right)^2 \tag{3.55}$$

With the decay width of a RHN of generation i decaying into a lepton (or antilepton) of flavour α being given as

$$\Gamma_i^\alpha = \Gamma_{N_i}^\alpha = \Gamma(N_i \longrightarrow \ell_\alpha \phi) + \Gamma(N_i \longrightarrow \ell_\alpha^\dagger \phi^*) \tag{3.56}$$

$$= \frac{M_i}{8\pi} h_{\alpha i}^{\nu *} h_{\alpha i} \tag{3.57}$$

These dimensionless parameters and inserting the internal degrees of freedom for the RHN $g_{N_i} = 2$ then give rise to the following form of the decay rate

$$\gamma_{i\alpha} = \frac{M_1^4 a_i \sqrt{c_i^\alpha}}{\pi^2 z} K_1(z\sqrt{a_i}) \tag{3.58}$$

In order to give some numerical examples I to choose 12 essentially free parameters (or 15 real degrees of freedom) as I already showed in section 2.2.1. My choice for those parameters is shown in Table 3.2. While most of these values are essentially random, I placed the lightest RHN mass in the range I later want to look at, so a bit below 100 TeV, while the two heavier neutrinos I choose to be several orders of magnitude higher.

M_1	$50\,\text{TeV}$	x	$0.7 + 0.5i$	s_1	-0.07	σ_1	$1/12\,\pi$
M_2	$M_1 \times 10^3$	y	$-0.2 + 0.4i$	s_2	0.9	σ_2	$2/3\,\pi$
M_3	$M_1 \times 10^4$	z	$-0.4 - 0.2i$	s_3	-0.8	m_1	$1\,\text{meV}$

Table 3.2: Benchmark parameters I choose to calculate a neutrino Yukawa matrix

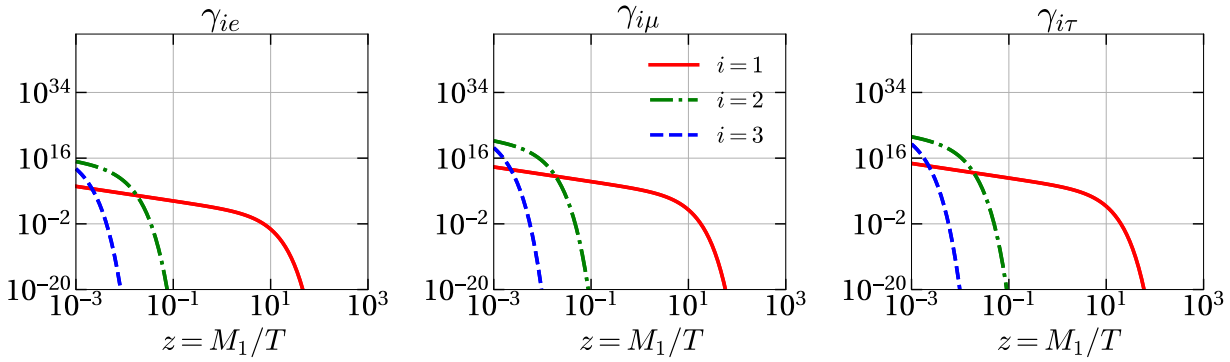

Figure 3.2: Shown here are the CP symmetric reaction rate of the decay (and inverse decay) of the RHN $\gamma_{i\alpha}$. It's the rate N_i decays into a lepton-Higgs pair or anti-lepton conjugate Higgs pair, with the lepton of flavour α. It is clearly visible that until the temperature exceeds the mass of the respective RHN N_i the rate drops of with z^{-1}, after which it experiences exponential suppression coming from the modified Bessel function.
It becomes also clear that around $z = 1$ therefore only the lightest RNH contributes in any significant way to wash-out, assuming a strong enough hierarchy.

The form these rates appear in the Boltzmann equations are summed over the RHN generations, and projected into the lepton flavour basis like. A numerical example for these rates is shown in Figure 3.3

$$\gamma^{\text{ID}}_{\alpha\beta} = \sum_i^{N_R} \gamma_{i\alpha}\delta_{\alpha\beta} \tag{3.59}$$

$$= \sum_i^{N_R} \gamma_i \begin{pmatrix} p_{ie} & 0 & 0 \\ 0 & p_{i\mu} & 0 \\ 0 & 0 & p_{i\tau} \end{pmatrix}_{\alpha\beta} \tag{3.60}$$

Indeed seeing that for a large mass hierarchy for the RHNs only the lightest RHN contributes to the total rate, in the temperature regime we're looking at, it is sufficient to only consider its contribution and therefore ignore the sum and just take the $i = 1$ parts:

$$\gamma^{\text{ID}}_{\alpha\beta} = \gamma \begin{pmatrix} p_e & 0 & 0 \\ 0 & p_\mu & 0 \\ 0 & 0 & p_\tau \end{pmatrix}, \qquad p_\alpha \equiv p_{1\alpha}\,, \quad \gamma = \gamma_1 \tag{3.61}$$

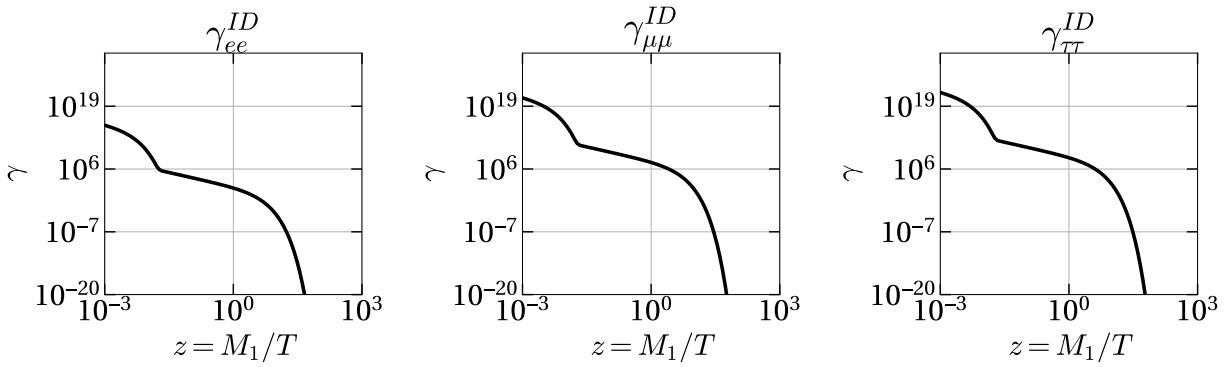

Figure 3.3: The rate $\gamma^{\rm ID}_{\alpha\beta}$ is the sum of the (inverse) decay rates of all the heavy neutrino species. As we can see aside from very small values for z it's the lightest RHN indeed dominates

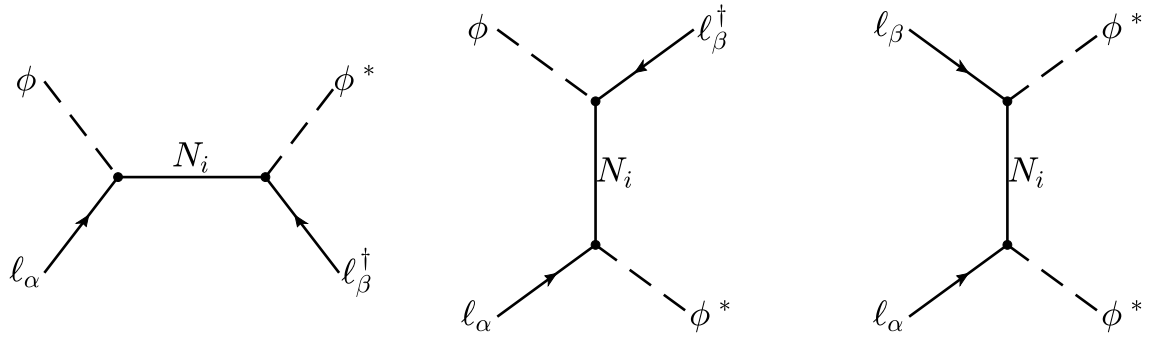

Figure 3.4: Feynman diagrams for the $\Delta L = 2$ violating processes

3.2.2 $\Delta L = 2$ cross sections

To determine the reaction rates for the $\Delta L = 2$ violating processes I use (3.52). The reduced cross section for the process $\ell_\alpha \phi \longleftrightarrow \ell^\dagger_\beta \phi^*$ is given by [25]

$$\begin{aligned}\sigma^{\ell_\alpha \phi}_{\ell^\dagger_\beta \phi^*} = \sum_{i,j} \Re \Big\{ & \left[h^{\nu *}_{\alpha i} h^{\nu}_{\alpha j} h^{\nu *}_{\beta i} h^{\nu}_{\beta j} + h^{\nu}_{\alpha i} h^{\nu *}_{\alpha j} h^{\nu}_{\beta i} h^{\nu *}_{\beta j} \right] \mathcal{A}^{(ss)}_{ij} \\ & + 2 \left[h^{\nu *}_{\beta i} h^{\nu}_{\beta j} h^{\nu *}_{\alpha i} h^{\nu}_{\alpha j} + h^{\nu}_{\beta i} h^{\nu *}_{\beta j} h^{\nu}_{\alpha i} h^{\nu *}_{\alpha j} \right] \mathcal{A}^{(st)*}_{ij} \\ & + 2 \left[h^{\nu *}_{\alpha i} h^{\nu}_{\alpha j} h^{\nu *}_{\beta i} h^{\nu}_{\beta j} \right] \mathcal{A}^{(tt)}_{ij} \Big\} \end{aligned} \tag{3.62}$$

The functions $\mathcal{A}^{(ss)}, \mathcal{A}^{(tt)}$ describe the s-channel and t-channel contributions respectively, while $\mathcal{A}^{(st)}$ describes the accounts for their interference. These functions are defined as [24]

$$\mathcal{A}_{ij}^{(ss)} = \begin{cases} \dfrac{x a_i}{4\pi |D_i^2|}, & \text{if } i = j \\ \dfrac{x\sqrt{a_i a_j}}{4\pi P_i^* P_j}, & \text{if } i \neq j \end{cases} \tag{3.63}$$

$$\mathcal{A}_{ij}^{(st)} = \frac{\sqrt{a_i a_j}}{2\pi P_i^*}\left[1 - \frac{x + a_j}{x}\ln\frac{x + a_j}{a_j}\right] \tag{3.64}$$

$$\mathcal{A}_{ij}^{(tt)} = \begin{cases} \dfrac{\sqrt{a_i a_j}}{2\pi x(a_i - a_j)}\left[(x + a_j)\ln\dfrac{x + a_j}{a_j} - (x + a_i)\ln\dfrac{x + a_i}{a_i}\right], & \text{if } i \neq j \\ \dfrac{a_i}{2\pi x}\left[\dfrac{x}{a_i} - \ln\dfrac{x + a_i}{a_i}\right], & \text{if } i = j \end{cases} \tag{3.65}$$

P_i here is the s-Channel Propagator of the heavy Neutrinos, which appears due to the s-channel process creating propagating RHNs. As we assume temperatures around the lightest heavy neutrino mass also the production of real intermediate neutrinos has to be considered, as is included in the substitution of the squared propagator $|P_i|^2$ with $|D_i|^2$ in the $i = j$ case. For that case the production of on-shell neutrinos has to be subtracted in order to avoid double counting, as they are already accounted for in the Boltzmann equations. The (inverse) propagator is given by

$$P_i^{-1} = \frac{1}{x - a_i + i\sqrt{a_i c_i}} \tag{3.66}$$

$$|D_i^{-1}|^2 = |P_i^{-1}|^2 - \frac{\pi}{\sqrt{a_i c_i}}\delta(x - a_i) \tag{3.67}$$

Furthermore c_i here refers to the decay width summed over the left handed lepton flavours relative to the lightest RHN mass:

$$c_i = \left(\frac{\sum_{\alpha=e,\mu,\tau}\Gamma_i^\alpha}{M_1}\right)^2 \quad \left(\neq \sum_{\alpha=e,\mu,\tau} c_i^\alpha\right) \tag{3.68}$$

I also want to look at the asymptotic behaviour of these functions (a more detailed calculation can be found in Appendix A) which turn out to be

	$x \ll a_i$	$x \gg a_i$
$\Re\mathcal{A}^{(ss)}$		$\mathcal{O}(1/x)$
$\Im\mathcal{A}^{(ss)}$		$\mathcal{O}\left(1/x^2\right)$
$\Re\mathcal{A}^{(st)}$	$\mathcal{O}(x)$	$\mathcal{O}(\ln x/x)$
$\Im\mathcal{A}^{(st)}$		$\mathcal{O}\left(\ln x/x^2\right)$
$\mathcal{A}^{(tt)}$		const

Table 3.3: Asymptotics of $\mathcal{A}$

Figure 3.5 now show numerical examples, confirming the analytical observations. Especially for $\mathcal{A}^{(tt)}$ the behaviour clearly follows a linear growth in the beginning and then assumes a constant value at large energies. For the off diagonal components ($i \neq j$) there is also some transitory regime between the respective mass scales occurring (a_i, a_j). $\mathcal{A}^{(ss)}$ and $\mathcal{A}^{(st)}$ also show the expected linear growth behaviour at low energies and the $\frac{1}{x}$ $\left(\frac{1}{x^2}\right)$ suppression at higher energies for the real (imaginary) parts. For the energies in between though the nature of the propagators become obvious leading to the sharp peaks around energies of the mass scales of the respective heavy neutrino (a_i).

For the process $\ell_\alpha\ell_\beta \longleftrightarrow \phi^*\phi^*$ the expression is a lot simpler as it does not involve any s-channel contributions and is given by [24, 25]

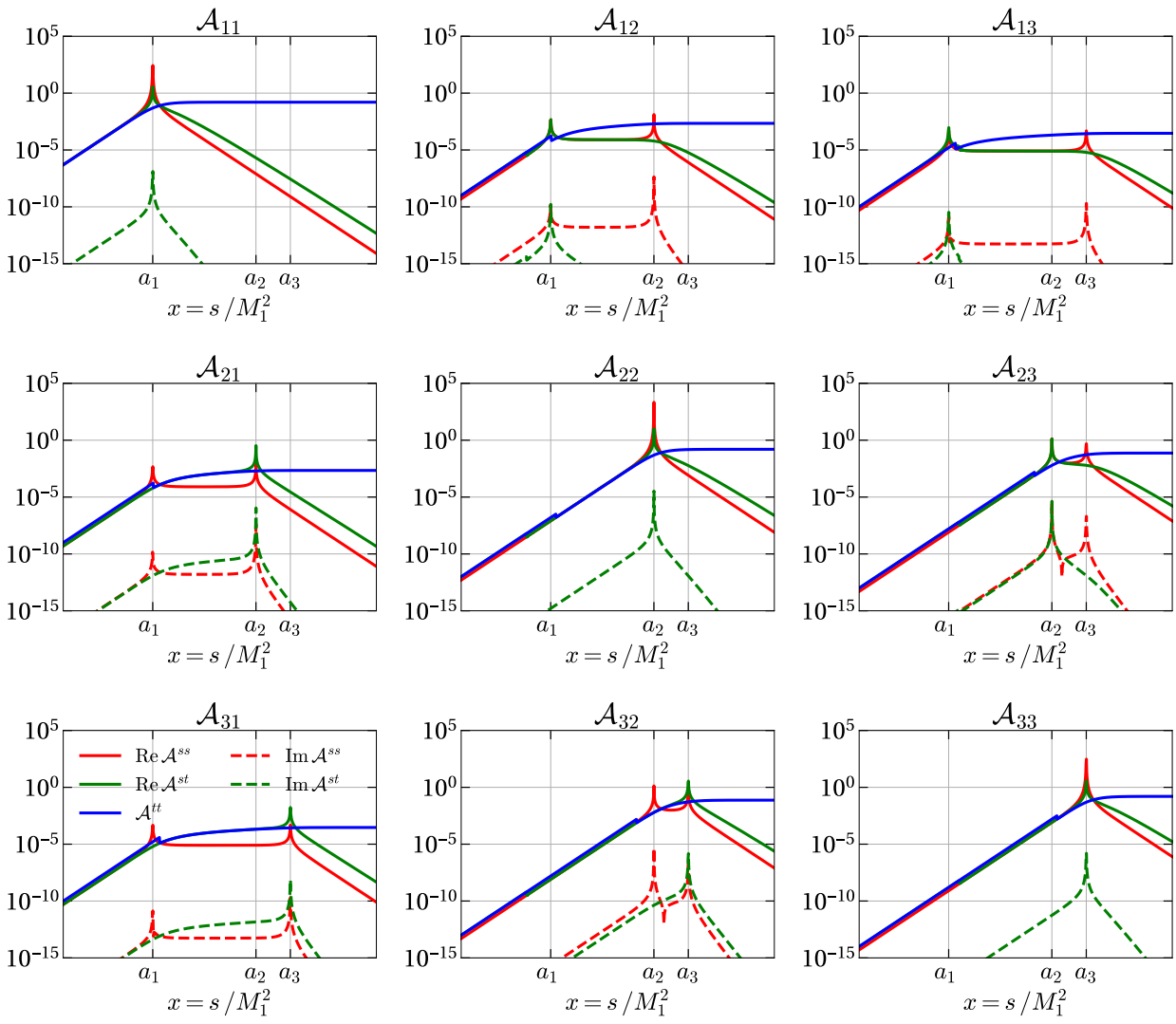

Figure 3.5: Shown here are numerical results for the different components for the 3 $\mathcal{A}$ functions. I display the absolute value to also have the negative parts visible while retaining the logarithmic scaling on the y-axis. For $\mathcal{A}^{(ss)}$ and $\mathcal{A}^{(st)}$ both real and imaginary part are shown.
Note the small discontinuities in some components of $\mathcal{A}^{(st)}$ and $\mathcal{A}^{(tt)}$. These are the results of numerical instabilities from terms containing numbers of vastly different orders of magnitude. To fix those I implemented an approximate expression for values below a cutoff at which this instability occurs. As these plots mainly serve to show the qualitative behaviour of these functions, this is not a problem.
Furthermore I do not include the subtraction term intended to deal with the on-shell production of RHN, as numerically implementing a δ function can be very tricky

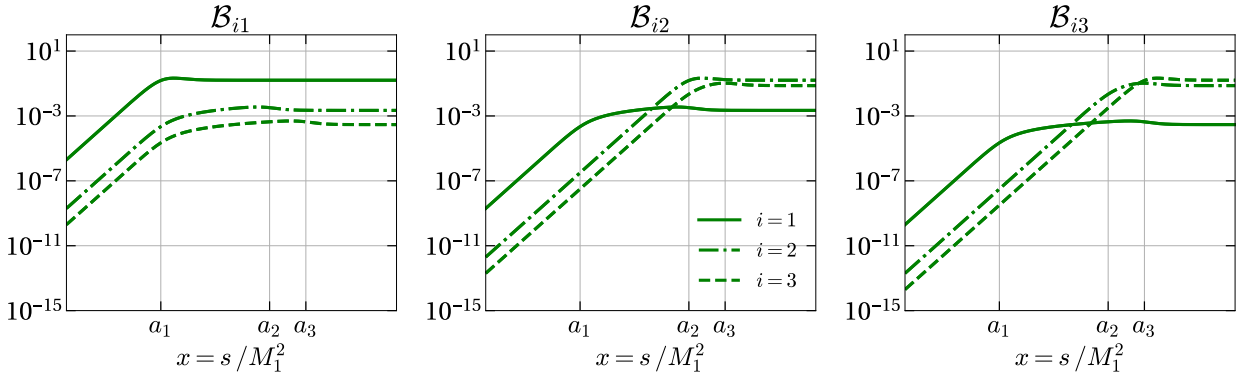

Figure 3.6: Plots for $\mathcal{B}_{ij}$ shown in a more reduced way

$$\hat{\sigma}^{\ell_\alpha \ell_\beta}_{\phi^* \phi^*} = \sum_{i,j} \Re\left[h^{\nu *}_{\alpha i} h^{\nu}_{\alpha j} h^{\nu *}_{\beta i} h^{\nu}_{\beta j}\right] \mathcal{B}_{ij} \tag{3.69}$$

$$\text{with} \quad \mathcal{B}_{ij} = \begin{cases} \dfrac{\sqrt{a_i a_j}}{2\pi} \left[\dfrac{1}{a_i - a_j} \ln \dfrac{a_i (x + a_j)}{a_j (x + a_i)} + \dfrac{1}{x + a_i + a_j} \ln \dfrac{(x + a_i)(x + a_j)}{a_i a_j} \right], & \text{if } i \neq j \\ \dfrac{1}{2\pi} \left[\dfrac{x}{x + a_i} + \dfrac{2 a_i}{x + 2 a_i} \ln \dfrac{x + a_i}{a_i} \right], & \text{if } i = j \end{cases} \tag{3.70}$$

Figure 3.6 shows $\mathcal{B}$, which exhibits a very similar behaviour as $\mathcal{A}^{(tt)}$, in that it is linearly growing for small x and assumes a constant value at larges energies. Indeed the asymptotics turn our to be the same:

$$\mathcal{B} \overset{x \ll a_i}{\sim} \mathcal{O}(x) \qquad\qquad \mathcal{B} \overset{x \gg a_i}{\approx} \text{const} \tag{3.71}$$

We can also see that the $i = j$ components, corresponding to processes in which the RHN flavour does not change give the largest contribution.

Lastly I also show the effective cross sections resulting from these form functions in Figure 3.7. What we can mainly see is as the cross sections are effectively a weighted sum of all the components of the form functions, weighted with different index combinations of the neutrino Yukawa matrix, that the dominant asymptotic behaviour remains conserved in that for low energies the cross section grows linearly, until the energy matches the mass of the first heavy neutrino at $x = a_1$. After this we see some sort of a plateau region, until it starts growing again around when the energy is at the threshold for the next heavy neutrino and remaining constant at the end. We also see the enhancement for the cross section $\ell_\alpha \phi \longleftrightarrow \ell^\dagger_\beta \phi^*$ at the energies of the heavy neutrinos, as due to the s-channel contributions real intermediate RHN can be produced, which for this numerical example I have not subtracted.

As all of these functions are being summed up both cross sections end up with the same dominant asymptotic behaviour

$$\hat{\sigma} \overset{x \ll a_1}{\sim} \mathcal{O}(x) \qquad\qquad \hat{\sigma} \overset{x \gg a_3}{\approx} \text{const} \tag{3.72}$$

as well as depending on the combination of Yukawa couplings to the fourth power

3.2.3 $\Delta L = 0$ cross sections

The treatment of the $\Delta L = 0$ processes remains very similar as for the $\Delta L = 2$ processes, though now one needs to keep in mind that scatterings for which $\alpha = \beta$ do *not* contribute to our Boltzmann equation as in these cases both $\Delta L = 0$ *and* $\Delta L_\alpha = 0\,, \forall \alpha$. To see if this actually has computational consequences let us look at the full term for the wash-out rate, as it appears in the Boltzmann equations.

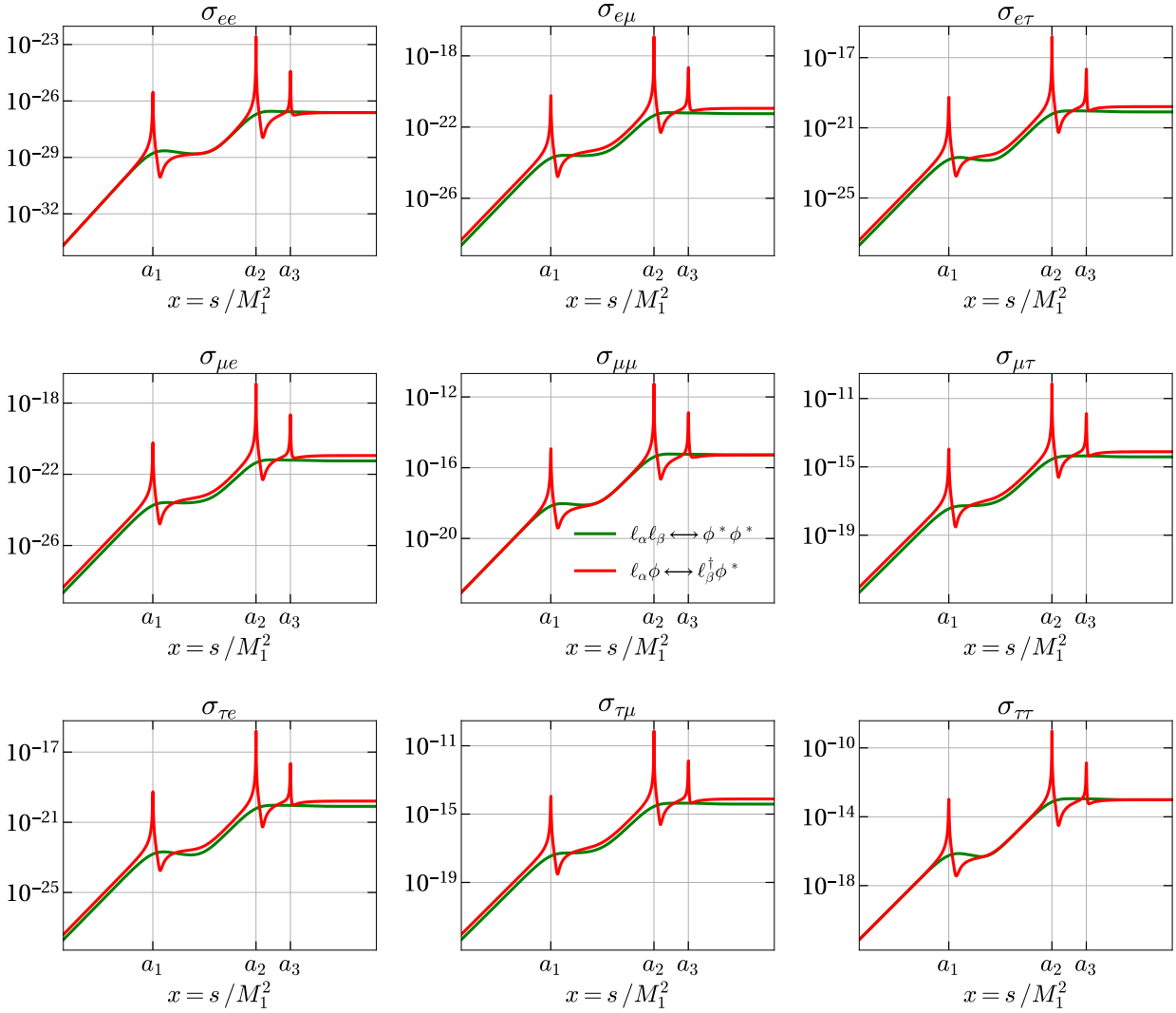

Figure 3.7: Plots for the reduced cross sections for the $\Delta L = 2$ processes. Again the subtraction of real intermediate RHNs is not included leading to very pronounced peaks in the red curves.
Even though it is barely visible the green curves do indeed rise around $x = a_3$.

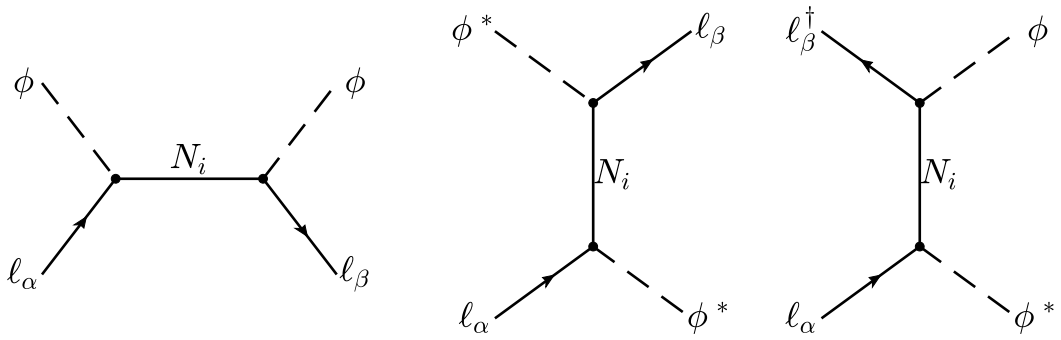

Figure 3.8: Tree level Feynman diagrams for the $\Delta L = 0$ processes

Straight forwardly we can just subtract the diagonal components from $\gamma^{\Delta L=0}$

$$\gamma^W_{\alpha\beta} = \gamma^{ID}_{\alpha\beta} + \sum_\sigma \left(\gamma^{\Delta L=2}_{\alpha\sigma} + \gamma^{\Delta L=0}_{\alpha\sigma}(1-\delta_{\alpha\sigma})\right)\delta_{\alpha\beta} - \left(\gamma^{\Delta L=0}_{\alpha\sigma} - \gamma^{\Delta L=0}_{\alpha\sigma}(1-\delta_{\alpha\sigma})\right)\delta_{\sigma\beta} \tag{3.73}$$

If we then only focus on the $\Delta L = 0$ terms:

$$\begin{aligned}\sum_\sigma \left\{\gamma^{\Delta L=0}_{\alpha\sigma}(1-\delta_{\alpha\sigma})\delta_{\alpha\beta} - \gamma^{\Delta L=0}_{\alpha\sigma}(1-\delta_{\alpha\sigma})\delta_{\sigma\beta}\right\} &= \sum_\sigma \gamma^{\Delta L=0}_{\alpha\sigma}(1-\delta_{\alpha\sigma})(\delta_{\alpha\beta}-\delta_{\sigma\beta}) \\ &= \sum_\sigma \left\{\gamma^{\Delta L=0}_{\alpha\sigma}(\delta_{\alpha\beta}-\delta_{\sigma\beta}) - \gamma^{\Delta L=0}_{\alpha\sigma}\delta_{\alpha\sigma}(\delta_{\alpha\beta}-\delta_{\sigma\beta})\right\} \\ &= \sum_\sigma \left\{\gamma^{\Delta L=0}_{\alpha\sigma}(\delta_{\alpha\beta}-\delta_{\sigma\beta}) - \gamma^{\Delta L=0}_{\alpha\beta}(\delta_{\alpha\beta}-\delta_{\alpha\beta})\right\}\end{aligned}$$

So we can pretty much neglect how to actually remove the $\alpha = \beta$ terms as they will cancel out in the final rate.

Now the cross section for the process $\ell_\alpha\phi \longleftrightarrow \ell_\beta\phi$ is given by [25]

$$\hat{\sigma}^{\ell_\alpha\phi}_{\ell_\beta\phi} = \sum_{i,j}\left[h^{\nu*}_{\beta i}h^\nu_{\alpha i}h^\nu_{\beta j}h^{\nu*}_{\alpha j} + h^\nu_{\beta i}h^{\nu*}_{\alpha i}h^{\nu*}_{\beta j}h^\nu_{\alpha j}\right]\mathcal{C}_{ij} \tag{3.74}$$

$$\text{with} \qquad \mathcal{C}_{ij} = \begin{cases} \dfrac{x a_i}{4\pi|D_i^2|}, & \text{if } i = j \\ \dfrac{x\sqrt{a_i a_j}}{4\pi P_i^* P_j}, & \text{if } i \neq j \end{cases} \tag{3.75}$$

The propagator is defined as before in (3.66) and (3.67). On closer look we can see that this form factor function is indeed identical to the one we saw before for (pure) s-channel contribution of $\ell_\alpha\phi \longleftrightarrow \ell^\dagger_\beta\phi^*$. I.e.

$$\mathcal{C}_{ij} = \mathcal{A}^{(ss)}_{ij}$$

This is of course only natural as these processes are almost identical, except of the conjugate particles in the end state. And as any potential CP violation will be encompassed in the Yukawa coupling, and this function only describes the scattering dynamics, we end up with the same expression. Consequently this leads to the same asymptotics as $\mathcal{A}^{(ss)}$

Next we have a look at the process $\ell_\alpha\phi^* \longleftrightarrow \ell_\beta\phi^*$, which exhibits a very similar structure as the t-channel interaction for $\ell_\alpha\phi \longleftrightarrow \ell^\dagger_\beta\phi^*$, leading to a very similar expression

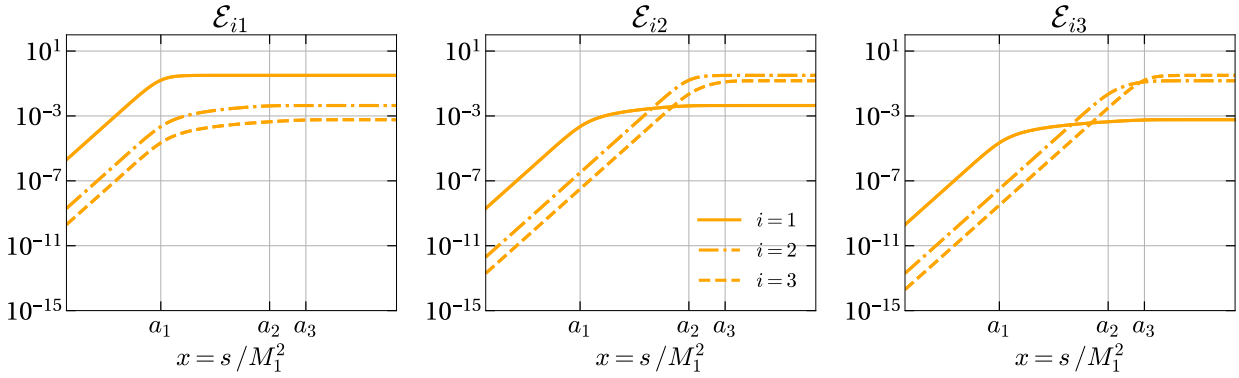

Figure 3.9: The form factors for the $\mathcal{E}$ functions. As $\mathcal{C}$ and $\mathcal{D}$ are already covered in the previous cases I omitted them to allow for a less busy plot

$$\hat{\sigma}^{\ell_\alpha \phi^*}_{\ell_\beta \phi^*} = \sum_{i,j} \Re\left(h^{\nu *}_{\beta i} h^{\nu}_{\alpha i} h^{\nu}_{\beta j} h^{\nu *}_{\alpha j}\right) \mathcal{D}_{ij} \tag{3.76}$$

$$\text{With} \qquad \mathcal{D}_{ij} = \begin{cases} \dfrac{\sqrt{a_i a_j}}{\pi x (a_i - a_j)} \left[(x + a_j) \ln \dfrac{x + a_j}{a_j} - (x + a_i) \ln \dfrac{x + a_i}{a_i} \right], & \text{if } i \neq j \\ \dfrac{a_i}{\pi x} \left[\dfrac{x}{a_i} - \ln \dfrac{x + a_i}{a_i} \right], & \text{if } i = j \end{cases} \tag{3.77}$$

In fact

$$\mathcal{D}_{ij} = 2\mathcal{A}^{(tt)}_{ij} \tag{3.78}$$

So the asymptotics simply follow from $\mathcal{A}^{(tt)}$.

The last process $\ell_\alpha \ell^\dagger_\beta \longleftrightarrow \phi \phi^*$ we cannot simply copy from before, but it turns out rather simple.

$$\hat{\sigma}^{\ell_\alpha \ell^\dagger_\beta}_{\phi \phi^*} = \sum_{i,j} \Re\left(h^{\nu *}_{\beta i} h^{\nu}_{\alpha i} h^{\nu}_{\beta j} h^{\nu *}_{\alpha j}\right) \mathcal{E}_{ij} \tag{3.79}$$

$$\text{With} \qquad \mathcal{E}_{ij} = \begin{cases} \dfrac{\sqrt{a_i a_j}}{\pi (a_i - a_j)} \ln \dfrac{a_i (x + a_j)}{a_j (x + a_i)}, & \text{if } i \neq j \\ \dfrac{x}{\pi (x + a_i)}, & \text{if } i = j \end{cases} \tag{3.80}$$

Which also exhibits a the same asymptotic behaviour as the functions before

$$\mathcal{E} \overset{x \ll a_i}{\sim} \mathcal{O}(x) \,, \qquad \mathcal{E} \overset{x \gg a_i}{\approx} \text{const} \tag{3.81}$$

So now Figure 3.9 shows a numerical example for the components of $\mathcal{E}_{ij}$, which again confirms the prior analytical observations, in that they start out growing linearly and assume a constant value for high energies.

In Figure 3.10 I now show the resulting reduced cross sections from the $\Delta L = 0$ processes. The t-channel processes exhibit the same behaviour we saw previously for the $\ell_\alpha \ell_\beta \longleftrightarrow \phi^* \phi^*$ process, in that it start growing linearly at low energies until around the mass of the first heavy neutrino and continues in this step like pattern until it assumes a constant value at high energies.

The s-channel process is very similar to the previously seen s-channel process in that it also starts growing linearly at low energies, has some very stark peaks around the heavy neutrino masses due to the propagator and ending in a $\frac{1}{x}$ suppression for very high energies.

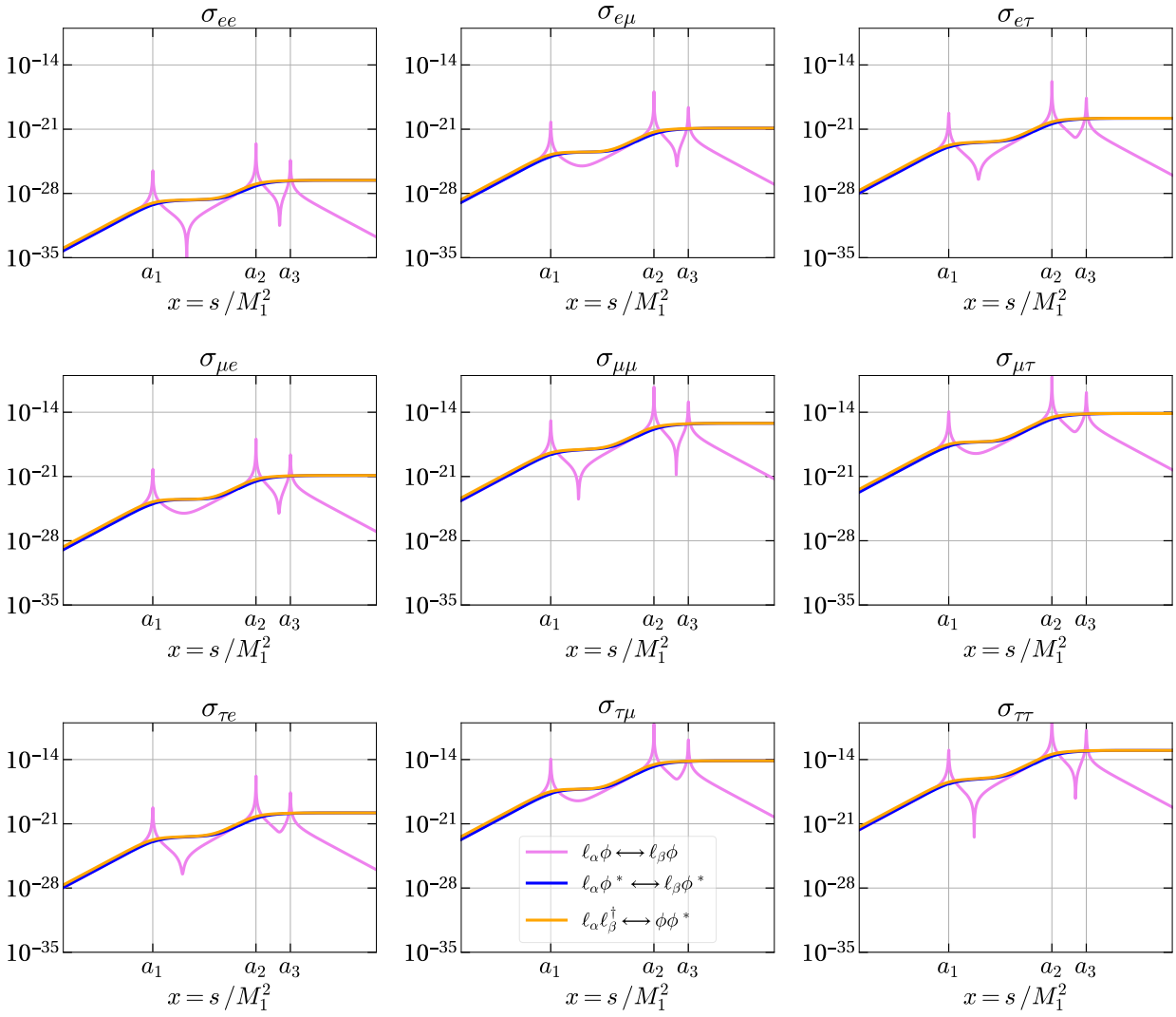

Figure 3.10: Reduced cross sections for $\Delta L = 0$ processes, even though they don't appear in the final rates for the Boltzmann equations I included the cross sections for the $\alpha = \beta$ cases

3.2.4 Real intermediate state subtraction

So far all the numerical calculations ignored the subtraction of real intermediate states, as the subtraction in (3.67) consists of a delta function, which is numerically difficult to implement. On the other hand a delta function makes the analytical evaluation of integrals a lot easier and as the reaction rates are calculated through the integration of the reduced cross section we can make use of that.

Starting out with the full contributions to the wash-out rate, as in (3.25)

$$\gamma^W_{\alpha\beta} = \gamma^{ID}_{\alpha\beta} + \sum_\sigma (\gamma^{\Delta L=2}_{\alpha\sigma} + \gamma^{\Delta L=0}_{\alpha\sigma})\delta_{\alpha\beta} + (\gamma^{\Delta L=2}_{\alpha\sigma} - \gamma^{\Delta L=0}_{\alpha\sigma})\delta_{\sigma\beta}$$

I now want to consider the on-shell contributions which are being subtracted in the $2 \to 2$ rates, which I write as

$$\begin{aligned}
\Delta L = 2: \ \gamma'^{\ell_\alpha\phi}_{\ell^\dagger_\sigma\phi^*} &= \gamma^{eq}_{sub}(\ell_\alpha\phi \to \ell^\dagger_\sigma\phi^*) + \gamma^{eq}_{sub}(\ell^\dagger_\sigma\phi^* \to \ell_\alpha\phi) \\
&= \gamma^{eq}(\ell_\alpha\phi \to \ell^\dagger_\sigma\phi^*) - \gamma^{eq}_{on-shell}(\ell_\alpha\phi \to \ell^\dagger_\sigma\phi^*) + \gamma^{eq}(\ell^\dagger_\sigma\phi^* \to \ell_\alpha\phi) - \gamma^{eq}_{on-shell}(\ell^\dagger_\sigma\phi^* \to \ell_\alpha\phi) \\
&= \gamma^{\ell_\alpha\phi}_{\ell^\dagger_\sigma\phi^*} - \gamma^{\ell_\alpha\phi}_{\ell^\dagger_\sigma\phi^*, on-shell} \\
\Delta L = 0: \ \gamma'^{\ell_\alpha\phi}_{\ell_\sigma\phi} &= \gamma^{eq}_{sub}(\ell_\alpha\phi \to \ell_\sigma\phi) + \gamma^{eq}_{sub}(\ell_\sigma\phi \to \ell_\alpha\phi) \\
&= \gamma^{eq}(\ell_\alpha\phi \to \ell_\sigma\phi) - \gamma^{eq}_{on-shell}(\ell_\alpha\phi \to \ell_\sigma\phi) + \gamma^{eq}(\ell_\sigma\phi \to \ell_\alpha\phi) - \gamma^{eq}_{on-shell}(\ell_\sigma\phi \to \ell_\alpha\phi) \\
&= \gamma^{\ell_\alpha\phi}_{\ell_\sigma\phi} - \gamma^{\ell_\alpha\phi}_{\ell_\sigma\phi, on-shell}
\end{aligned}$$

The on-shell contributions are each then given through

$$\gamma^{\ell_\alpha\phi}_{\ell^\dagger_\sigma\phi^*, on-shell} = \frac{M_1^4}{64\pi^4 z}\int_{x_{thr}}^\infty dx\sqrt{x}K_1(z\sqrt{x})\hat{\sigma}^{\ell_\alpha\phi}_{\ell^\dagger_\sigma\phi^*, on-shell} \tag{3.82}$$

$$\gamma^{\ell_\alpha\phi}_{\ell_\sigma\phi, on-shell} = \frac{M_1^4}{64\pi^4 z}\int_{x_{thr}}^\infty dx\sqrt{x}K_1(z\sqrt{x})\hat{\sigma}^{\ell_\alpha\phi}_{\ell_\sigma\phi, on-shell} \tag{3.83}$$

The reduced cross section for $\ell_\alpha\phi \longleftrightarrow \ell^\dagger_\sigma\phi^*$ is then by as seen before:

$$\begin{aligned}
\hat{\sigma}^{\ell_\alpha\phi}_{\ell^\dagger_\sigma\phi^*, on-shell} &= \sum_{i,j} \Re\left\{\left[h^{\nu*}_{\alpha i}h^\nu_{\alpha j}h^{\nu*}_{\sigma i}h^\nu_{\sigma j} + h^\nu_{\alpha i}h^{\nu*}_{\alpha j}h^\nu_{\sigma i}h^{\nu*}_{\sigma j}\right]\mathcal{A}^{(ss),on-shell}_{ij}\right\} \\
\text{With } \mathcal{A}^{(ss)}_{ij} &= \mathcal{A}^{(ss),total}_{ij} - \mathcal{A}^{(ss),on-shell}_{ij} \\
&= \frac{x\sqrt{a_i a_j}}{4\pi P_i^* P_j} - \underbrace{\frac{xa_i}{4\sqrt{a_i c_i}}\delta(x-a_i)\delta_{ij}}_{=\text{on-shell part}} \\
\Rightarrow \hat{\sigma}^{\ell_\alpha\phi}_{\ell^\dagger_\sigma\phi^*, on-shell} &= \sum_{i,j} \Re\left\{\left[h^{\nu*}_{\alpha i}h^\nu_{\alpha j}h^{\nu*}_{\sigma i}h^\nu_{\sigma j} + h^\nu_{\alpha i}h^{\nu*}_{\alpha j}h^\nu_{\sigma i}h^{\nu*}_{\sigma j}\right]\frac{xa_i}{4\sqrt{a_i c_i}}\delta(x-a_i)\delta_{ij}\right\} \\
&= \sum_i \Re\left\{\left[h^{\nu*}_{\alpha i}h^\nu_{\alpha i}h^{\nu*}_{\sigma i}h^\nu_{\sigma i} + h^\nu_{\alpha i}h^{\nu*}_{\alpha i}h^\nu_{\sigma i}h^{\nu*}_{\sigma i}\right]\frac{xa_i}{4\sqrt{a_i c_i}}\delta(x-a_i)\right\} \\
&= 2\sum_i \Re\left\{h^{\nu*}_{\alpha i}h^\nu_{\alpha i}h^{\nu*}_{\sigma i}h^\nu_{\sigma i}\frac{xa_i}{4\sqrt{a_i c_i}}\delta(x-a_i)\right\} \\
&= \frac{1}{2}\sum_i \Re\left\{h^{\nu*}_{\alpha i}h^\nu_{\alpha i}h^{\nu*}_{\sigma i}h^\nu_{\sigma i}\frac{xa_i}{\sqrt{a_i c_i}}\delta(x-a_i)\right\}
\end{aligned} \tag{3.84}$$

Reinserting this expression for the reduced cross section into the integral for γ^{eq} then allows us to

eliminate the integral:

$$\begin{aligned}\gamma^{\ell_\alpha\phi}_{\ell^\dagger_\sigma\phi^*,\,on-shell} &= \frac{M_1^4}{128\pi^4 z}\sum_i \int_{x_{thr}}^{\infty} dx\sqrt{x}K_1(z\sqrt{x})\Re\left\{h^{\nu*}_{\alpha i}h^{\nu}_{\alpha i}h^{\nu*}_{\sigma i}h^{\nu}_{\sigma i}\frac{xa_i}{\sqrt{a_i c_i}}\delta(x-a_i)\right\}\\ &= \frac{M_1^4}{128\pi^4 z}\sum_i \sqrt{a_i}K_1(z\sqrt{a_i})\Re\left\{h^{\nu*}_{\alpha i}h^{\nu}_{\alpha i}h^{\nu*}_{\sigma i}h^{\nu}_{\sigma i}\frac{a_i a_i}{\sqrt{a_i c_i}}\right\}\\ &= \sum_i \frac{M_i^4}{128\pi^4 z}K_1(z\sqrt{a_i})\Re\left\{h^{\nu*}_{\alpha i}h^{\nu}_{\alpha i}h^{\nu*}_{\sigma i}h^{\nu}_{\sigma i}\frac{M_1}{\Gamma_{N_i}}\right\}\end{aligned} \tag{3.85}$$

Similarly in the $\ell_\alpha\phi \longleftrightarrow \ell_\sigma\phi$ case:

$$\begin{aligned}\hat{\sigma}^{\ell_\alpha\phi}_{\ell_\sigma\phi,\,on-shell} &= \sum_{i,j}\Re\left\{\left[h^{\nu*}_{\sigma i}h^{\nu}_{\alpha i}h^{\nu}_{\sigma j}h^{\nu*}_{\alpha j}+h^{\nu}_{\sigma i}h^{\nu*}_{\alpha i}h^{\nu*}_{\sigma j}h^{\nu}_{\alpha j}\right]\frac{xa_i}{4\sqrt{a_i c_i}}\delta(x-a_i)\delta_{ij}\right\}\\ &= \frac{1}{2}\sum_i \Re\left\{h^{\nu*}_{\alpha i}h^{\nu}_{\alpha i}h^{\nu*}_{\sigma i}h^{\nu}_{\sigma i}\frac{xa_i}{\sqrt{a_i c_i}}\delta(x-a_i)\right\} = \hat{\sigma}^{\ell_\alpha\phi}_{\ell^\dagger_\sigma\phi^*,\,on-shell}\end{aligned} \tag{3.86}$$

Thereby:

$$\gamma^{\ell_\alpha\phi}_{\ell_\sigma\phi,\,on-shell} = \sum_i \frac{M_i^4}{128\pi^4 z}K_1(z\sqrt{a_i})\Re\left\{h^{\nu*}_{\alpha i}h^{\nu}_{\alpha i}h^{\nu*}_{\sigma i}h^{\nu}_{\sigma i}\frac{M_1}{\Gamma_{N_i}}\right\} = \gamma^{\ell_\alpha\phi}_{\ell^\dagger_\sigma\phi^*,\,on-shell} \tag{3.87}$$

The decay width and Yukawa couplings are of course linked by:

$$\begin{aligned}\Gamma^{\alpha}_{N_i} &= \frac{M_i}{8\pi}h^{\nu*}_{\alpha i}h^{\nu}_{\alpha i}\\ \Leftrightarrow h^{\nu*}_{\alpha i}h^{\nu}_{\alpha i} &= \frac{8\pi}{M_i}\Gamma^{\alpha}_{N_i}\end{aligned}$$

Using that in (3.85) and (3.87) we get:

$$\begin{aligned}\gamma^{\ell_\alpha\phi}_{\ell_\sigma\phi,\,on-shell} &= \sum_i \frac{M_i^4}{128\pi^4 z}K_1(z\sqrt{a_i})\Re\left\{\frac{64\pi^2}{M_i^2}\Gamma^{\alpha}_{N_i}\Gamma^{\sigma}_{N_i}\frac{M_1}{\Gamma_{N_i}}\right\} = \gamma^{\ell_\alpha\phi}_{\ell^\dagger_\sigma\phi^*,\,on-shell}\\ &= \sum_i \frac{M_i^2 M_1^2\sqrt{c_i^\alpha}}{2\pi^2 z}K_1(z\sqrt{a_i})\frac{\Gamma^{\sigma}_{N_i}}{\Gamma_{N_i}}\\ &= \frac{1}{2}\sum_i \frac{M_1^4 a_i\sqrt{c_i^\alpha}}{\pi^2 z}K_1(z\sqrt{a_i})\frac{\Gamma^{\sigma}_{N_i}}{\Gamma_{N_i}}\\ &= \frac{1}{2}\sum_i \frac{\Gamma^{\sigma}_{N_i}}{\Gamma_{N_i}}\gamma_{i\alpha}\\ &= \frac{1}{2}\sum_i \frac{\Gamma^{\sigma}_{N_i}}{\Gamma_{N_i}}\left(\gamma^{eq}(N_i\to\ell_\alpha\phi)+\gamma^{eq}(N_i\to\ell^\dagger_\alpha\phi^*)\right)\end{aligned}$$

As it appears in the wash-in/wash-out terms:

$$\gamma^{\ell_\alpha\phi}_{\ell^\dagger_\sigma\phi^*,on-shell}+\gamma^{\ell_\alpha\phi}_{\ell_\sigma\phi,on-shell} = \sum_i \frac{\Gamma^{\sigma}_{N_i}}{\Gamma_{N_i}}\gamma_{i\alpha} \tag{3.88}$$

$$\gamma^{\ell_\alpha\phi}_{\ell^\dagger_\sigma\phi^*,on-shell}-\gamma^{\ell_\alpha\phi}_{\ell_\sigma\phi,on-shell} = 0 \tag{3.89}$$

Summed up:

$$\begin{aligned}\sum_\sigma\left(\gamma^{\ell_\alpha\phi}_{\ell^\dagger_\sigma\phi^*,on-shell}+\gamma^{\ell_\alpha\phi}_{\ell_\sigma\phi,on-shell}\right)\delta_{\alpha\beta} &= \sum_{i,\sigma}\frac{\Gamma^{\sigma}_{N_i}}{\Gamma_{N_i}}\gamma_{i\alpha}\delta_{\alpha\beta}\\ &= \sum_i \gamma_{i\alpha}\delta_{\alpha\beta} = \gamma^{ID}_{\alpha\beta}\end{aligned} \tag{3.90}$$

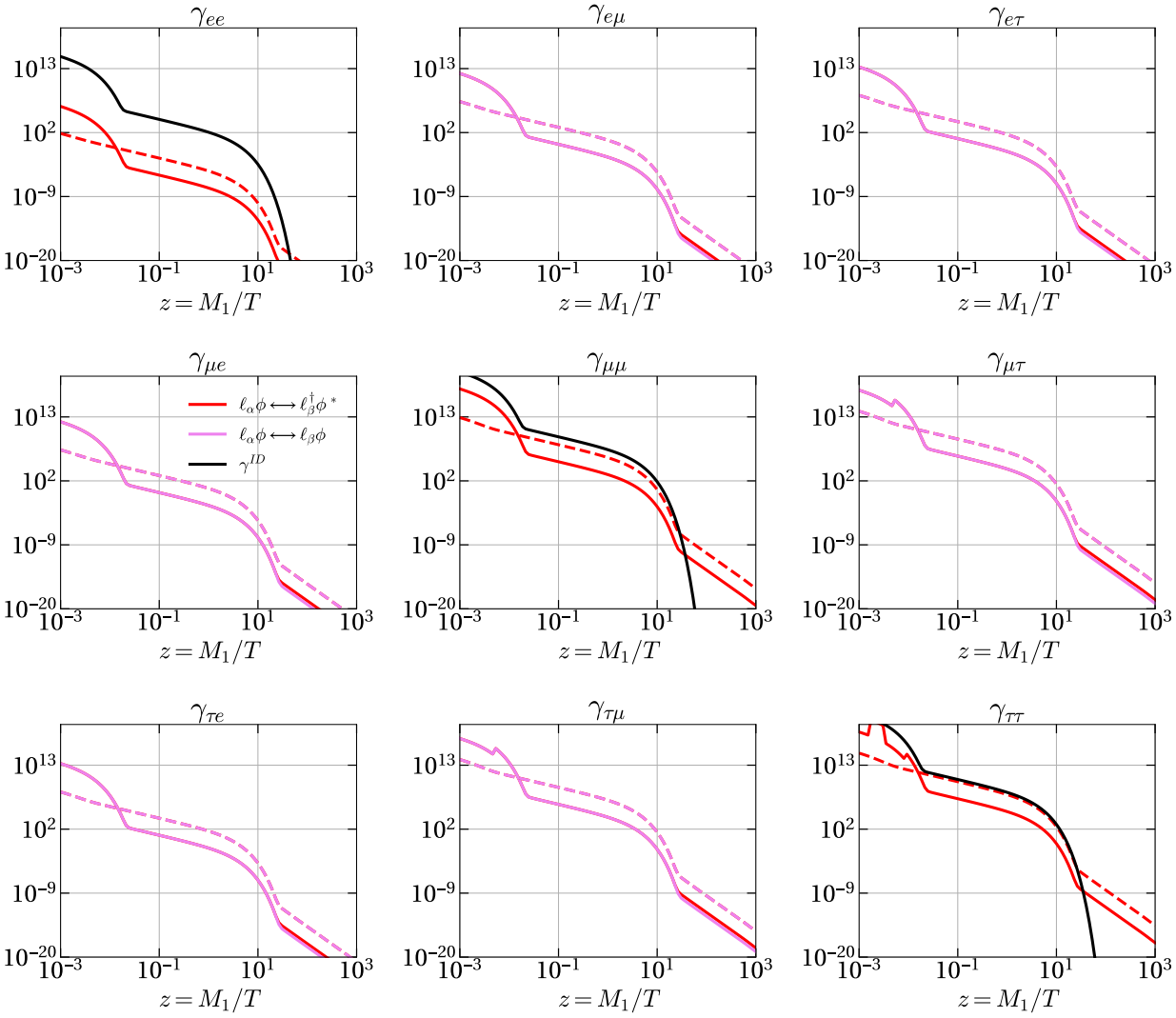

Figure 3.11: Comparison between the RIS containing rates, without the subtraction applied. In dashed lines also the numerically determined on-shell contribution as per (3.82) and (3.83) is included.
The reason the on-shell contribution seems to be greater than the base rate including this on-shell contribution is due to numerical difficulties arising from trying to integrate over the poles of the propagator, which occur at different orders of magnitude, and the same for implementing a δ function numerically.
For comparison I also show γ^{ID}, and we can see that qualitatively the on-shell contributions lead to a very similar shape, as we would expect from the analytical results

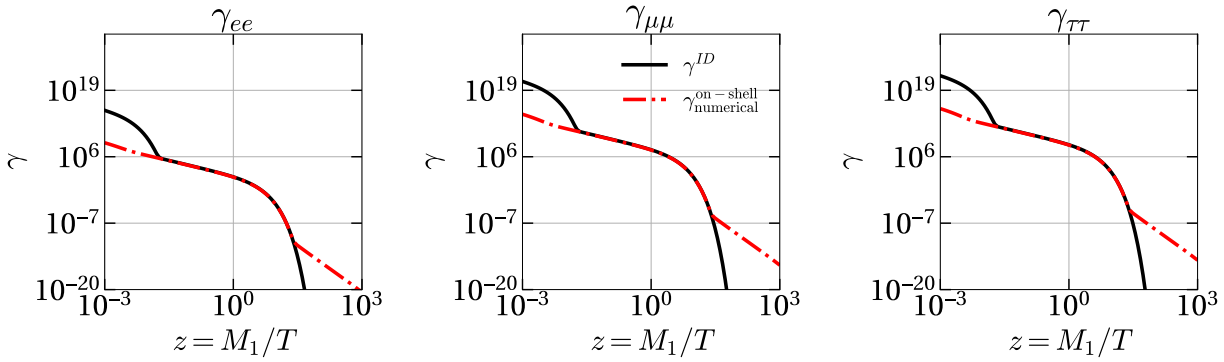

Figure 3.12: Comparison between the on shell contribution as they appear in the final expression to γ^{ID}. We can see it well coinciding with the expected analytical result in the intermediate part of the z-range, but shows strong deviation at high and low z, as again z stretches over a wide range of magnitudes and it leads to the numerical approximation used for the δ function to become unreliable

3.2.5 Comparison of the rates

As one can see especially from the subtraction of intermediate states the numerical calculation of the rates becomes a bit difficult, mainly as a result of the numerical integration. For this reason I have been looking at the asymptotic behaviour of the functions before, to identify if any rates are subdominant and can be neglected in the determination of the total wash-out rate.

We saw before that the reduced cross section for all the $2 \longrightarrow 2$ rates behaves for all interactions like

$$\hat{\sigma}(x) \sim |h^\nu|^4 \mathcal{F}(x) \tag{3.91}$$

Where $\mathcal{F}(x)$ represents the form factors appearing in the different interactions. As we sum over the different rates it is sufficient to look only at the leading order contribution among all the rates.

We arrive this behaviour by analysing the general Form of the reaction rates being

$$\gamma^{eq} = \frac{M_1^4}{64\pi^4 z} \int_{x_0}^{\infty} dx\, \sqrt{x} K_1(z\sqrt{x}) \hat{\sigma}(x) \tag{3.92}$$

$$\sim \frac{M_1^4}{z} \int_{x_0}^{\infty} dx\, \sqrt{x} K_1(z\sqrt{x}) |h^\nu|^4 \mathcal{F}(x) \tag{3.93}$$

For small $z \to 0$ we can approximate the modified Bessel function in the integrand as

$$\sqrt{x} K_1(z\sqrt{x}) \sim \frac{1}{z} \theta(z^{-2} - x) \tag{3.94}$$

Leading to

$$\gamma^{eq} \overset{z \ll 1}{\sim} \frac{M_1^4}{64\pi^4 z} \int_{x_0}^{\infty} dx\, \frac{1}{z} \theta(z^{-2} - x) |h^\nu|^4 \mathcal{F}(x) \tag{3.95}$$

$$\sim \frac{M_1^4 |h^\nu|^4}{z^2} \int_{x_0}^{z^{-2}} \mathcal{F}(x)\, dx \tag{3.96}$$

When z is small enough the dominant contribution in the integral will be the constant part of $\mathcal{F}$ at high energies, so we can approximate it as such in the integral:

$$\gamma^{eq} \overset{z \ll 1}{\sim} \frac{M_1^4 |h^\nu|^4}{z^2} \int_{x_0}^{z^{-2}} dx \tag{3.97}$$

$$= \frac{M_1^4 |h^\nu|^4}{z^2} \left(z^{-2} - x_0\right) \sim \frac{M_1^4 |h^\nu|^4}{z^4} \tag{3.98}$$

For large z the form factor is dominated by the linear growth part of $\mathcal{F}$ at low energies. So as long as $z^{-2} \gg x_0$:

$$\gamma^{eq} \overset{z\gg 1}{\sim} \frac{M_1^4 |h^\nu|^4}{z^2} \int_{x_0}^{z^{-2}} x\, dx \tag{3.99}$$

$$= \frac{M_1^4 |h^\nu|^4}{z^2} \left(\frac{1}{2} z^{-4} - \frac{1}{2} x_0^2 \right) \sim \frac{M_1^4 |h^\nu|^4}{z^6} \tag{3.100}$$

To get a better picture how the scaling behaves for even larger values for z, we have to treat the asymptotic behaviour of the modified Bessel function more carefully, which is given by:

$$K_1(z) \overset{z\gg 1}{\sim} \sqrt{\frac{2\pi}{z}} e^{-z} \tag{3.101}$$

So for the integral

$$\gamma^{eq} \overset{z\gg 1}{\sim} \frac{M_1^4}{64\pi^4 z} \int_{x_0}^{\infty} dx\, \sqrt{x} \sqrt{\frac{2\pi}{z\sqrt{x}}} e^{-z\sqrt{x}} |h^\nu|^4 \mathcal{F}(x)\,, \quad u = z\sqrt{x}\,, dx = \frac{2u}{z^2} du \tag{3.102}$$

$$\sim \frac{M_1^4 |h^\nu|^4}{z} \int_{z\sqrt{x_0}}^{\infty} du\, \frac{u}{z^2} \frac{u}{z} \sqrt{\frac{1}{u}} e^{-u} \underbrace{\mathcal{F}\left(\frac{u^2}{z^2} \right)}_{\sim \frac{u^2}{z^2}} \tag{3.103}$$

$$\sim \frac{M_1^4 |h^\nu|^4}{z^6} \int_{z\sqrt{x_0}}^{\infty} u^{\frac{7}{2}} e^{-u} \tag{3.104}$$

$$= \frac{M_1^4 |h^\nu|^4}{z^6} \Gamma\left(\frac{9}{2}; z\sqrt{x_0} \right) \tag{3.105}$$

Which then shows us for sufficiently large z there will be an exponential suppression of the reaction rate, as the incomplete Γ function appearing here behaves like $\Gamma(x; y) \xrightarrow{y\to\infty} e^{-y}$

Now we of course have to compare this to the inverse decay rate, which is considerably easier to analyse, as it does not involve any further integrals. Simply by using (3.101) again we see that

$$\gamma_{i\alpha} \overset{z\gg 1}{\simeq} \frac{M_1^4 M_i^2 \Gamma_i^\alpha}{M_1^2 M_1 \pi^2 z} \sqrt{\frac{2\pi\, M_i}{z\, M_1}} e^{-z\frac{M_i}{M_1}} \tag{3.106}$$

$$\sim \frac{M_1^{\frac{1}{2}} M_i^{\frac{7}{2}} |h^\nu|^2}{z^{\frac{3}{2}}} e^{-z\frac{M_i}{M_1}} \tag{3.107}$$

From which we can see that an exponential suppression will kick in a lot earlier than compared to the $2 \longrightarrow 2$ rates, and also that the heavier RHN will already play no role any more at larger values for z. So we can just focus on the case for the lightest RHN:

$$\gamma_{1\alpha} \sim \frac{M_1^4 |h^\nu|^2}{z^{\frac{3}{2}}} e^{-z} \tag{3.108}$$

It can also be interesting to look at the case for small z here. Then the modified Bessel function takes the asymptotic form:

$$K_1(y) \sim \frac{1}{y} \tag{3.109}$$

This asymptotic behaviour will only apply to the lightest RHN at the values for z we are interested in, so they will remain in the regime of exponential suppression, as long as $z \gg \frac{1}{\sqrt{a_i}}$, which will be fulfilled down to very small z as we assume a significant hierarchy of masses among the RNH.

$$\gamma_{i\alpha} \simeq \frac{M_1^4 M_i^2 \Gamma_i^\alpha}{M_1^2 M_1 \pi^2 z} \frac{M_1}{z\, M_i} \tag{3.110}$$

$$\sim \frac{M_1^4 |h^\nu|^2}{z^2} \tag{3.111}$$

What we see from this is that at earlier times the inverse decays indeed contribute the most to the total washout rate, due to only being suppressed by two powers of the Yukawa matrix, and will drop off more slowly, before the exponential cut off kicks in.

Furthermore we can numerically check how well all of this holds in Figure 3.13, and we see that indeed up to values $z \sim 20$ the inverse decays indeed dominate over the $2 \longrightarrow 2$ rates and also outpace the expansion of the universe in form of the Hubble rate H. The reaction rates has to be compared to the expansion of the universe given by the Hubble rate, which at early times in a radiation dominated universe is given by

$$H = \sqrt{\frac{g_*\pi^2}{90}}\frac{T^2}{M_{Pl}} = \sqrt{\frac{g_*\pi^2}{90}}\frac{M_1^2}{z^2 M_{Pl}} \tag{3.112}$$

as well as to the lepton number density n_ℓ

$$n_\ell = \frac{3}{4}\frac{\zeta(3) g_\ell T^3}{\pi^2} = \frac{3}{4}\frac{\zeta(3) M_1^3}{z^3\pi^2} \tag{3.113}$$

If then $\dfrac{\gamma^{eq}}{H n_\ell} > 1$ the contribution of the given rate is significant, while for $\dfrac{\gamma^{eq}}{H n_\ell} < 1$ it cannot compete with the expansion of the universe.

With this we can see in Figure 3.13 that indeed the inverse decays dominate over the $2 \longrightarrow 2$ scatterings in the relevant regions around $z = 1$. Though this is of course highly dependent on the choice of Yukawa couplings. From the analytical treatment one can say as long as sufficiently many components of h^ν are of small enough magnitude the suppression of $|h^\nu|^4$ will be strong enough to leave the inverse decays to be the dominant contribution.

This is of course also the case for the $s-$channel scatterings which exhibit the same asymptotic behaviour (or are more strongly suppressed in the case of $\mathcal{C}(x)$), aside from the large contributions from around the poles of the propagator. As they are supposed to be subtracted this leaves a total scattering rate, very much comparable to the others.

In total this now means that one can ignore the contributions of the $2 \longrightarrow 2$ scatterings to the total wash-in rate, at least in temperature regimes up to potentially $10^6\,\mathrm{GeV}$.

3.3 Analytical solution

As we can see that at low temperatures $T \sim 100\,\mathrm{TeV}$ the inverse decays are dominating the wash out term, allowing us to ignore further contributions. With that we can actually achieve an analytical solution for the Boltzmann equations

As the Boltzmann equations are linear in q_{Δ_α} we can split them up into a thermal leptogenesis contribution and a wash-in contribution $q^{\mathrm{win}}_{\Delta_\alpha}$ so that

$$\begin{aligned}\left(\frac{\partial}{\partial t} + 3H\right) q^{win}_{\Delta_\alpha} &= \sum_\beta \frac{6}{T^3}\gamma^W_{\alpha\beta}\left(q^0_\beta - \sum_\sigma C_{\beta\sigma} q^{win}_{\Delta_\sigma}\right) \\ &= \sum_\beta \Gamma^W_{\alpha\beta}\left(q^0_\beta - \sum_\sigma C_{\beta\sigma} q^{win}_{\Delta_\sigma}\right)\end{aligned} \tag{3.114}$$

From having one interaction dominating we get that we can factorise the wash-in rate as $\Gamma^W_{\alpha\beta} = \Gamma^W P_{\alpha\beta}$, where Γ^W now encompasses the flavour neutral interaction rate, while all the flavour structure is absorbed into $P_{\alpha\beta}$. In the temperature regime we want to look at it's the inverse decays dominating, so P is a diagonal matrix with the branching ratios into the different flavours on the diagonal.

$$\left(\frac{\partial}{\partial t} + 3H\right) q^{win}_{\Delta_\alpha} = \sum_\beta \Gamma^W P_{\alpha\beta}\left(q^0_\beta - \sum_\sigma C_{\beta\sigma} q^{win}_{\Delta_\sigma}\right) \tag{3.115}$$

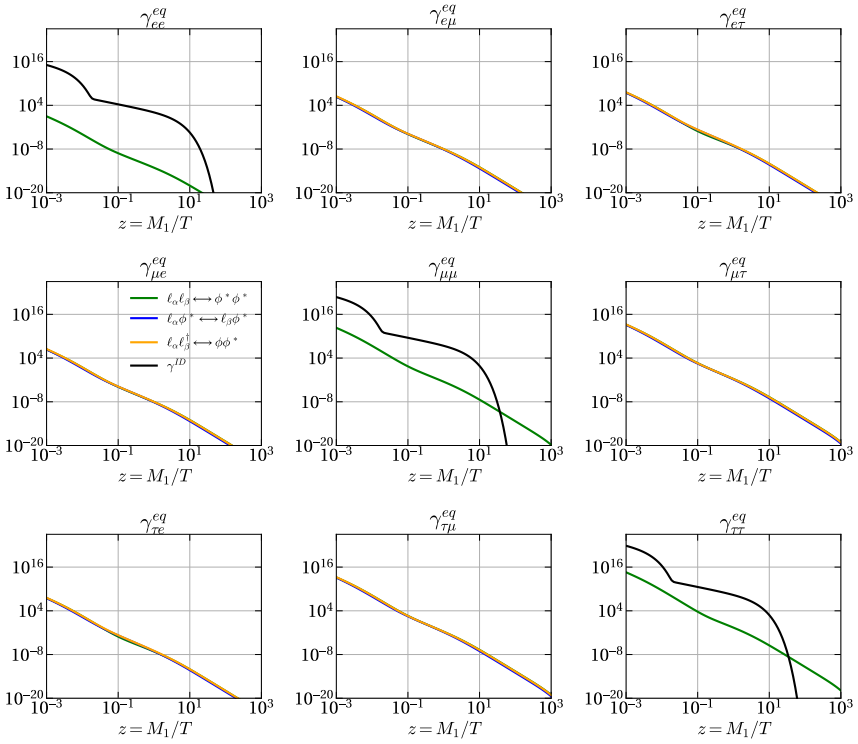

(a) The reaction rates that do not require the subtraction of RIS, compared to the rate of inverse decays

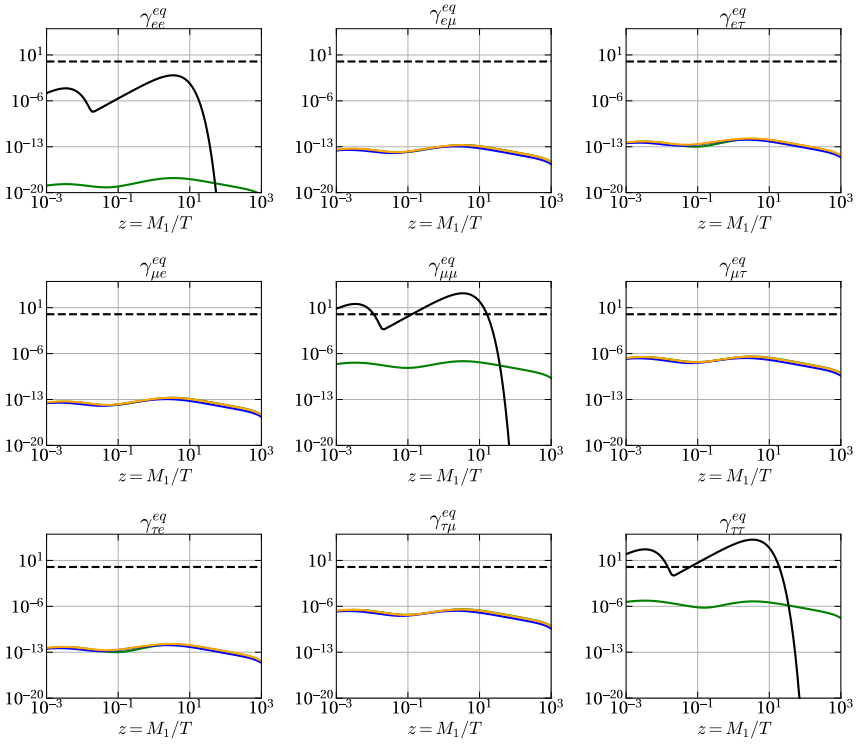

(b) The same rates as above now normalised to the expansion rate of the universe H and the lepton density n_ℓ. We can see that the shown $2 \longrightarrow 2$ rates are too weak to compete with the expansion of the universe (dashed line)

Figure 3.13: The behaviour of the $2 \longrightarrow 2$ reaction rates compared to the inverse decay rates and Hubble expansion

At this point it is helpful to formulate these Boltzmann equations in a comoving frame

$$\begin{aligned} Q_\alpha = a^3 q^{in}_{\Delta_\alpha} \longrightarrow \frac{dQ_\alpha}{dt} &= a^3 \frac{dq^{\text{win}}_{\Delta_\alpha}}{dt} + q^{\text{win}}_{\Delta_\alpha} \frac{d\, a^3}{dt} \\ &= a^3 \frac{dq^{\text{win}}_{\Delta_\alpha}}{dt} + a^3 q^{\text{win}}_{\Delta_\alpha} 3 \underbrace{\frac{\dot{a}}{a}}_{=H} \\ &= a^3 \left(\frac{dq^{\text{win}}_{\Delta_\alpha}}{dt} + 3H q^{\text{win}}_{\Delta_\alpha} \right) \\ &= \sum_\beta \Gamma^W P_{\alpha\beta} \left(\underbrace{a^3 q^0_\beta}_{\equiv Q^0_\beta} - \sum_\sigma C_{\beta\sigma} Q_\sigma \right) \end{aligned} \tag{3.116}$$

Or in a more compact matrix notation, and in dependence of $z = \frac{M_1}{T}$ so that with $H \sim \frac{1}{2t}$ $\frac{d}{dt} = Hz\frac{d}{dz}$

$$\begin{aligned} \frac{d}{dz}\vec{Q} &= \frac{\Gamma^W}{zH} \mathbf{P} \left(\vec{Q}^0 - \mathbf{C}\vec{Q} \right) \\ &= W(z) \mathbf{PC} \left(\mathbf{C}^{-1}\vec{Q}^0 - \vec{Q} \right) \end{aligned} \tag{3.117}$$

We can assume that there exists a matrix $\mathbf{B}$ that diagonalises $\mathbf{PC}$ again, so that $\mathbf{D} = \mathbf{B}\,\mathbf{PC}\,\mathbf{B}^{-1}$. Then defining

$$\mathcal{Q} = \mathbf{B}\vec{Q} \qquad\qquad \mathcal{Q}^{eq} = \mathbf{B}\vec{Q}^{eq} = \mathbf{BC}^{-1}\vec{Q}^0 \tag{3.118}$$

So then

$$\begin{aligned} \frac{d}{dz}\vec{Q} &= W(z)\mathbf{B}^{-1}\mathbf{D}\,\mathbf{B} \left(\vec{Q}^{eq} - \vec{Q} \right) \\ \Leftrightarrow \frac{d}{dz}\mathcal{Q} &= W(z)\mathbf{D} \left(\mathcal{Q}^{eq} - \mathcal{Q} \right) \end{aligned} \tag{3.119}$$

To analytically solve this equation now we can introduce a shift $\mathcal{Y} = \mathcal{Q} - \mathcal{Q}^{eq}$ so that

$$\frac{d\mathcal{Q}}{dz} = \frac{d\mathcal{Y}}{dz} + \frac{d\mathcal{Q}^{eq}}{dz} = -W(z)\mathbf{D}\mathcal{Y}(z) \tag{3.120}$$

By introducing an integrating factor

$$\mathbf{E}(z_0, z) = \exp \int_{z_0}^{z} dz' W(z')\mathbf{D} \tag{3.121}$$

and multiplying the Boltzmann equation with it we arrive at

$$\mathbf{E}(z_0, z)\frac{d\mathcal{Y}}{dz} + E(z_0, z)\frac{d\mathcal{Q}^{eq}}{dz} = -\mathbf{E}(z_0, z)\frac{d\mathcal{Q}^{eq}}{dz} \tag{3.122}$$

$$\frac{d}{dz}\left(\mathcal{Y}(z)\mathbf{E}(z_0, z) \right) = -\mathbf{E}(z_0, z)\frac{d\mathcal{Q}^{eq}}{dz} \tag{3.123}$$

Now integrating both sides

$$\int_{z_0}^{z} dz' \frac{d}{dz'} \left(\mathcal{Y}(z')\mathbf{E}(z_0, z') \right) = -\int_{z_0}^{z} dz'\, \mathbf{E}(z_0, z')\frac{d\mathcal{Q}^{eq}}{dz'} \tag{3.124}$$

$$\mathbf{E}(z_0, z)\mathcal{Y}(z) = -\int_{z_0}^{z} dz' \mathbf{E}(z_0, z')\frac{d\mathcal{Q}^{eq}}{dz} + \mathbf{E}(z_0, z_0)\mathcal{Y}(z_0) \tag{3.125}$$

Resubstituting $\mathcal{Y}$ then leads to

$$\begin{aligned}\mathbf{E}(z_0,z)\mathcal{Q}(z) &= \mathbf{E}(z_0,z)\mathcal{Q}^{eq}(z) + \mathcal{Q}(z_0) - \mathcal{Q}^{eq}(z_0) - \int_{z_0}^{z} dz' \mathbf{E}(z_0,z')\frac{d\mathcal{Q}^{eq}}{dz} \\ \mathcal{Q}(z) &= \mathcal{Q}^{eq}(z) + \mathbf{E}(z,z_0)\left[\mathcal{Q}(z_0) - \mathcal{Q}^{eq}(z_0)\right] - \int_{z_0}^{z} dz' \mathbf{E}(z,z')\frac{d\mathcal{Q}^{eq}}{dz'}\end{aligned} \tag{3.126}$$

Here we made use of

$$\mathbf{E}(z,z_0)^{-1} = \exp - \int_{z_0}^{z} dz'\, W(z)\mathbf{D} = \exp \int_{z}^{z_0} dz'\, W(z)\mathbf{D} = \mathbf{E}(z_0,z) \tag{3.127}$$

Considering that we started out looking at the specific temperature range $10^5\,\mathrm{GeV} \leq T \leq 10^6\,\mathrm{GeV}$ in which we focus on a specific conserved charge - here of course $\vec{q}^0 \sim q_e$ - which as the name suggests is in fact conserved, meaning in a comoving frame it's value remains constant, i.e.

$$\mathcal{Q}^{eq} = \mathbf{B}\mathbf{C}^{-1}\, a^3 \vec{q}^0 = \text{const} \tag{3.128}$$

Therefore its derivative vanishes and the integral term drops out, leaving

$$\mathcal{Q}(z) = \mathcal{Q}^{eq} + \mathbf{E}(z,z_0)\left[\mathcal{Q}(z_0) - \mathcal{Q}^{eq}\right] \tag{3.129}$$

Now we need to rotate it back into its original basis, but as $\mathbf{D}$ is a diagonal Matrix and its exponential is diagonalised by the same matrix - in this case $\mathbf{B}$ - we simply have

$$\mathbf{B}^{-1}\mathbf{E}(z,z_0)\mathbf{B} = \exp\left\{-\int_{z_0}^{z} dz'\, W(z)\mathbf{P}\mathbf{C}\right\} \equiv \hat{\mathbf{E}} \tag{3.130}$$

So that we simply arrive at

$$\vec{Q}(z) = \vec{Q}^{eq} + \hat{\mathbf{E}}\left[\vec{Q}^{\mathrm{ini}} - \vec{Q}^{eq}\right] \tag{3.131}$$

In order to reach a form closer to the original Boltzmann equation we can leave the comoving frame again and write it out in its components again, in order to compare with [31]

$$q^{\mathrm{win}}_{\Delta_\alpha}(z) = q^{eq}_{\Delta_\alpha} + \hat{E}_{\alpha\beta}\left(\left(\frac{a_{\mathrm{ini}}}{a}\right)^3 q^{\mathrm{ini}}_{\Delta_\beta} - q^{eq}_{\Delta_\beta}\right) \tag{3.132}$$

$$= \sum_\beta \left(\delta_{\alpha\beta} - \hat{E}_{\alpha\beta}\right) q^{eq}_{\Delta_\beta} + \sum_\beta \hat{E}_{\alpha\beta} q^{\mathrm{ini}}_{\Delta_\beta}\left(\frac{a_{\mathrm{ini}}}{a}\right)^3 \tag{3.133}$$

When we assume no initial asymmetry we get as an expression for the final asymmetry after wash-in leptogenesis has happened

Assuming no initial asymmetry this has an exact solution:

$$q^{\mathrm{win}}_{\Delta_\alpha} = \sum_\beta (\delta_{\alpha\beta} - E_{\alpha\beta}) q^{\mathrm{eq}}_{\Delta_\beta} \tag{3.134}$$

Here we now have to be careful to take into account the entire evolution history into $\mathbf{E}$, i.e. we take the limit $z \to \infty$ and $z_0 \to 0$. As we also saw before it's only the lightest RHN that contribute as any asymmetry created previously N_2 and N_3 will already be washed out again, so that $\mathbf{P}$ is not only diagonal but contains only the branching ratios for N_1, i.e. $P_{\alpha\beta} = p_{1\alpha}\delta_{\alpha\beta}$ so that

$$E = \exp\left\{-p_{1\alpha} C_{\alpha\beta} \int_0^\infty dz\, W(z)\right\} \tag{3.135}$$

How to calculate $W(z) = \frac{\Gamma^W}{zH}$ and $\Gamma^W = \frac{6\gamma}{T^3}$ as seen in (3.61).

In the case of strong wash-in, translating to a high decay rate of the RHN, the exponential is of course suppressed, as long as we one also assumes a generic flavour structure, in which the branching ratios are roughly of the same size and $p_{1\alpha} \ll 1$. So then (3.134) reads as

$$q^{\text{win}}_{\Delta_\alpha} \simeq q^{\text{eq}}_{\Delta_\alpha} \tag{3.136}$$

Meaning for the total washed in $B-L$ asymmetry:

$$q^{\text{win}}_{B-L} \simeq q^{\text{eq}}_{B-L} = \sum_\alpha q^{\text{eq}}_{\Delta_\alpha} = -\frac{3}{10} q_e \tag{3.137}$$

3.4 Potential mechanisms to create the primordial charge(s)

The great advantage of this mechanism for leptogenesis is that it allows for a wide variety of different mechanisms to produce the required primordial charge asymmetries. Therefore one has a great amount of flexibility in model building.

3.4.1 Axion inflation

The previously described scenario of Baryogenesis through axion inflation (see section **??**) can also be the source of other primordial charges, thereby leading to a more flexible scenario for the model.

Through the coupling of the fermion currents to the gauge fields, we can then get (chiral) fermionic charges which can then be used as the desired non trivial chemical background to employ wash-in leptogenesis. In [33] the authors demonstrate how they can produce the following set of fermionic charges:

$$q_e\,, \qquad q_{u-d}\,, \qquad q_\mu\,, \qquad q_\tau\,, \qquad q_B\,, \qquad q_u \tag{3.138}$$

Whose amplitude can be quantified through one single effective parameter χ

3.4.2 Primordial Black hole evaporation

Another way to produce primordial asymmetry, is - similar to the classic Baryogenesis scenario - just to have a very heavy particle decaying asymmetrically into whatever asymmetry is desired. In order to produce these heavy particle, which might have masses above the reheating temperature, is to have them be produced via evaporating primordial black holes (PBHs).

In [34] the authors consider simple scenarios with a heavy Majorana fermion X which through it's decay creates an asymmetry in right handed electrons, i.e. produces q_e. For this to work they also introduce an additional scalar field S which couples to X in a Yukawa-like term:

$$\mathcal{L} \supset y X e_R S \tag{3.139}$$

They then investigate for different PBH masses m_{PBH} and asymmetron masses m_X how much a q_e charge can be produced assuming a specific Yukawa (-like) coupling y

This mechanism could of course also work to produce other asymmetries given the right type of "asymmetron", which could then also be used for wash-in leptogenesis.

3.4.3 Gravitational Chargegenesis

One more way to to produce a set of primordial charges is through introducing a gravitational coupling of the form [35]

$$\mathcal{L} \supset \frac{1}{M_*^2} \int d^4x \sqrt{-g} J^\mu_A \partial_\mu \mathcal{R} \tag{3.140}$$

In a FLRW universe this leads to an effective Potential

$$\mu^{\text{eff}}_A = \frac{\dot{\mathcal{R}}}{M_*^2} = \frac{3\rho\dot{\omega}}{M_*^2 M_P^2} + \frac{\sqrt{3}\,(1+\omega)\,(1-3\omega)}{M_*^2 M_P^3} \rho^{\frac{3}{2}} \tag{3.141}$$

A in this case can be just about any conserved charge that we might want to wash in.

3.4.4 Heavy Higgs decay

As a last pathway to create primordial asymmetries there is also the introduction of more Higgs doublets which through CP violation in their decay create the desired asymmetries.

In [36] the authors use a three-Higgs doublet model (3HDM), which in addition to the SM Higgs field also contains two heavier Higgs fields H_1, H_2 with a lot higher masses: $m_\phi \ll m_{H_1} < m_{H_2}$, but which have a vanishing vacuum expectation value. The introduction of these new fields then gives rise to a new set of Yukawa interactions, which for the leptons look like:

$$\mathcal{L}^Y_{HH} = -\ell^\dagger_\alpha H_a Y^a_{\alpha\beta} e_\beta + \ell^\dagger_\alpha \bar{H}_a h^{\nu,a}_{\alpha i} N_i + h.c. \tag{3.142}$$

Assuming heavy Higgs masses are larger than the lightest Majorana mass: $M_1 < m_{H_1} \lesssim m_{H_2} \ll M_2, M_3$, so that H_1 is below the reheating temperature and we can assume H_1 to be populated thermally, and $M_1 \in (10^5, 10^6)\,\text{GeV}$, so in a regime where only right handed electrons are out of equilibrium, we can consider the heavy Higgses only coupling to one lepton flavour, i.e. the electron.

Similar to other Baryogenesis and Leptogenesis scenarios the decay of the heavy Higgses now gives the CP violation needed to produce an asymmetry in right handed electrons.

Having now generated an asymmetry in right handed electrons at $T \gg 10^6\,\text{GeV}$ so when the universe cools off further and the wash-in mechanisms kicks in at $T \sim M_1$ we can get the observed baryon asymmetry.

Chapter 4

Wash-in leptogenesis below 100 Tev

As stated before, the description of a fully out of equilibrium electron Yukawa interaction is only valid down to about 100 GeV, when the strength of the Yukawa interaction becomes competitive with the expansion of the universe. Yet it cannot simply be taken to be fully equilibrated at this point, but mere partially equilibrated. This can also be modelled by also taking into account an additional Boltzmann equation for the conserved charge associated with the electron Yukwawa interaction, which as we saw before is the difference of right handed electrons and left handed positrons q_e.

4.1 A Boltzmann equation for right handed electrons

To construct the Boltzmann equation for right handed electrons we follow a very similar process as for the construction of the Boltzmann equation for lepton asymmetries Δ_α. The processes we take into account here are firstly the directly through the Yukawa interaction mediated $1 \longrightarrow 2$ processes in Figure 4.1, and additionally to those also $1n \longrightarrow 2n$ processes in which the in- and outcoming particles also emit soft gauge bosons. They do not however affect the charge in q_e and is mainly relevant in the computation of the reaction rates.

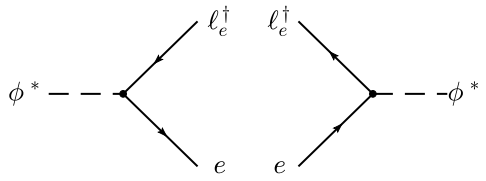

Figure 4.1: Feymans diagram for Higgs decay and inverse decay, without the inclusion of $1n \longrightarrow 2n$ processes that can occur due to the emission of gauge radiation

The $2 \longrightarrow 2$ processes which contribute to leading order consist of interactions with quarks (those lighter than top quarks are sufficiently strongly suppressed to be neglected) and are shown in Figure 4.2, as well as interactions with the electroweak gauge Bosons $V = W_i, B$, shown in Figure 4.3

To construct the BE we can also just split up the contributions into a $1 \longrightarrow 2$ part, one for the quark contributions to the $2 \longrightarrow 2$ scatterings and one for those including gauge Bosons in the scatterings, so that

$$\left(\frac{\partial}{\partial t} + 3H\right) q_e = \left(\frac{\partial}{\partial t} + 3H\right) \left(q_e^{1\to 2} + q_e^{\text{quarks}} + q_e^{\text{gauge}}\right) \tag{4.1}$$

So we get for the $1 \longrightarrow 2$ contribution, neglecting the gauge radiation as it does not affect the chemical potential structure of the BE

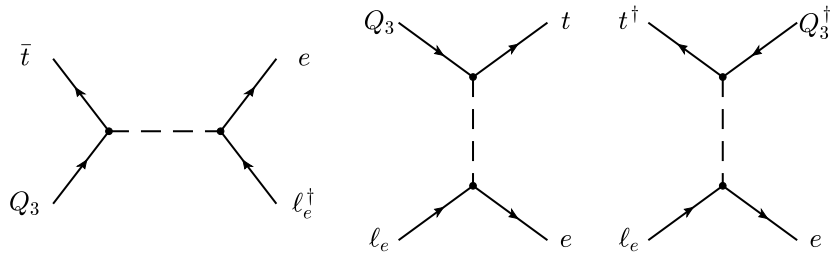

Figure 4.2: Feynman diagrams for the quark contributions to the BE for q_e

$$\left(\frac{\partial}{\partial t}+3H\right)q_e^{1\to 2}=\frac{n_{\phi^*}}{n_{\phi^*}^{eq}}\gamma^{eq}\left(\phi^*\longrightarrow \ell_e^\dagger e\right) - \frac{n_{\ell_e^\dagger}n_e}{n_{\ell_e^\dagger}^{eq}n_e^{eq}}\gamma^{eq}\left(\ell_e^\dagger e\longrightarrow \phi^*\right) - \frac{n_{\phi}}{n_{\phi}^{eq}}\gamma^{eq}\left(\phi\longrightarrow \ell_e e^\dagger\right) + \frac{n_{\ell_e}n_{e^\dagger}}{n_{\ell_e}^{eq}n_{e^\dagger}^{eq}}\gamma^{eq}\left(\ell_e e^\dagger\longrightarrow \phi\right) \tag{4.2}$$

Which as we saw before leads to some exponential factors we can expand around a small chemical potential, along with remembering that $\mu_X=-\mu_{\bar{X}}$ as well as making use of CPT symmetry

$$\begin{aligned}\left(\frac{\partial}{\partial t}+3H\right)q_e^{1\to 2}&=\left(2-\frac{\mu_e+\mu_{\ell_e}-\mu_\phi}{T}\right)\gamma^{eq}\left(\phi^*\longrightarrow \ell_e^\dagger e\right)-\left(2+\frac{\mu_e-\mu_{\ell_e}+\mu_\phi}{T}\right)\gamma^{eq}\left(\ell_e^\dagger e\longrightarrow \phi^*\right)\\ &=2\left[\underbrace{\gamma^{eq}\left(\phi^*\longrightarrow \ell_e^\dagger e\right)-\gamma^{eq}\left(\ell_e^\dagger e\longrightarrow \phi^*\right)}_{=0\,\text{due to no }\cancel{CP}}\right]+\left(\frac{-\mu_e+\mu_{\ell_e}-\mu_\phi}{T}\right)\gamma_{\ell_e^\dagger e}^{\phi^*}\end{aligned} \tag{4.3}$$

Where as before $\gamma_Y^X=\gamma^{eq}\left(X\longrightarrow Y\right)+\gamma^{eq}\left(Y\longrightarrow X\right)$

Very similarly we get for the for the quark contributions

$$\begin{aligned}\left(\frac{\partial}{\partial t}+3H\right)q_e^{\text{quarks}}=&\frac{n_{t^\dagger}n_{Q_3}}{n_{t^\dagger}^{eq}n_{Q_3}^{eq}}\gamma^{eq}\left(t^\dagger Q_3\longrightarrow e\ell_e^\dagger\right) - \frac{n_e n_{\ell_e^\dagger}}{n_e^{eq}n_{\ell_e^\dagger}^{eq}}\gamma^{eq}\left(\ell_e^\dagger e\longrightarrow Q_3 t^\dagger\right)\\ &-\frac{n_t n_{Q_3^\dagger}}{n_t^{eq}n_{Q_3^\dagger}^{eq}}\gamma^{eq}\left(tQ_3^\dagger\longrightarrow e^\dagger\ell_e\right) + \frac{n_{e^\dagger}n_{\ell_e}}{n_{e^\dagger}^{eq}n_{\ell_e}^{eq}}\gamma^{eq}\left(e^\dagger\ell_e\longrightarrow Q_3^\dagger t\right)\\ &+\frac{n_{Q_3}n_{\ell_e}}{n_{Q_3}^{eq}n_{\ell_e}^{eq}}\gamma^{eq}\left(Q_3\ell_e\longrightarrow te\right) - \frac{n_t n_e}{n_t^{eq}n_e^{eq}}\gamma^{eq}\left(te\longrightarrow Q_3\ell_e\right)\\ &-\frac{n_{Q_3^\dagger}n_{\ell_e^\dagger}}{n_{Q_3^\dagger}^{eq}n_{\ell_e^\dagger}^{eq}}\gamma^{eq}\left(Q_3^\dagger\ell_e^\dagger\longrightarrow t^\dagger e^\dagger\right) + \frac{n_{t^\dagger}n_{e^\dagger}}{n_{t^\dagger}^{eq}n_{e^\dagger}^{eq}}\gamma^{eq}\left(t^\dagger e^\dagger\longrightarrow Q_3^\dagger\ell_e^\dagger\right)\\ &+\frac{n_{t^\dagger}n_{\ell_e}}{n_{t^\dagger}^{eq}n_{\ell_e}^{eq}}\gamma^{eq}\left(t^\dagger\ell_e\longrightarrow Q_3^\dagger e\right) - \frac{n_{Q_3^\dagger}n_e}{n_{Q_3^\dagger}^{eq}n_e^{eq}}\gamma^{eq}\left(Q_3^\dagger e\longrightarrow t^\dagger\ell_e\right)\\ &-\frac{n_t n_{\ell_e^\dagger}}{n_t^{eq}n_{\ell_e^\dagger}^{eq}}\gamma^{eq}\left(t\ell_e^\dagger\longrightarrow Q_3 e^\dagger\right) + \frac{n_{Q_3}n_{e^\dagger}}{n_{Q_3}^{eq}n_{e^\dagger}^{eq}}\gamma^{eq}\left(Q_3 e^\dagger\longrightarrow t\ell_e^\dagger\right)\end{aligned} \tag{4.4}$$

Expanding in the chemical potentials and again cancelling CP asymmetric terms yields

$$\left(\frac{\partial}{\partial t}+3H\right)q_e^{\text{quarks}}=\left(\frac{\mu_{Q_3}-\mu_t-\mu_e+\mu_{\ell_e}}{T}\right)\left[\gamma_{e\ell_e^\dagger}^{t^\dagger Q_3}+\gamma_{te}^{Q_3\ell_e}+\gamma_{Q_3^\dagger e}^{t^\dagger\ell_e}\right] \tag{4.5}$$

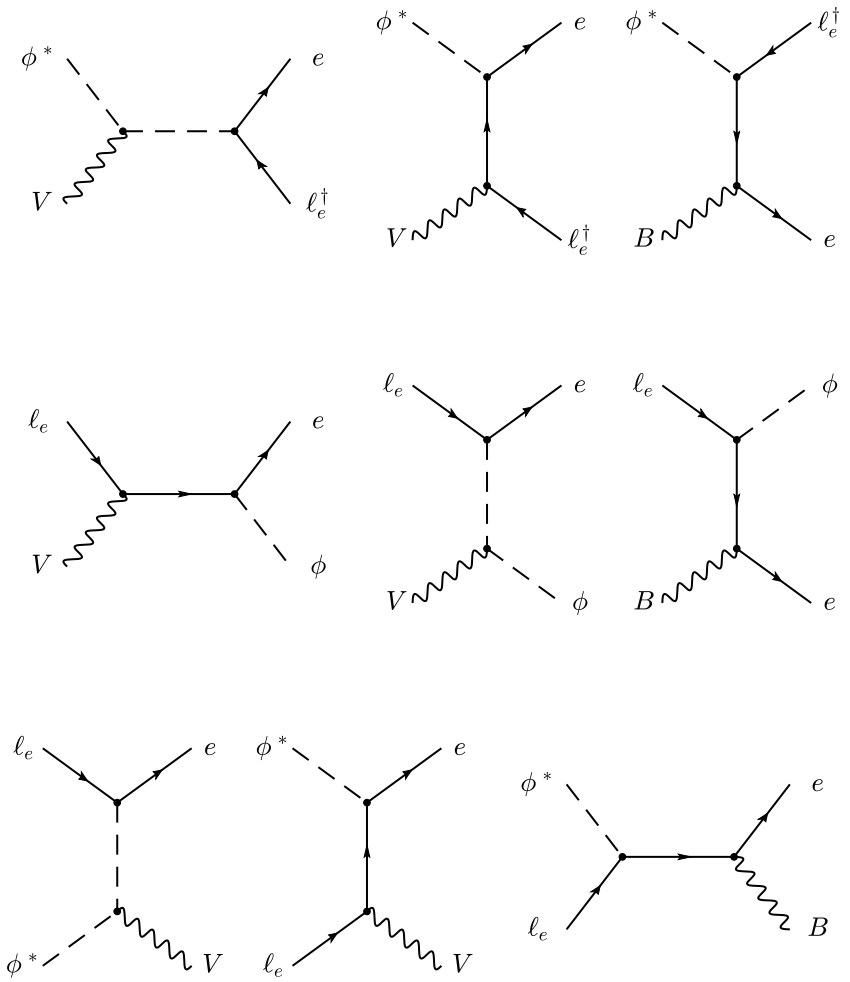

Figure 4.3: Feynman diagrams for the $2 \longrightarrow 2$ scatterings involving gauge bosons, consisting of $V\phi^* \longrightarrow \ell_e^\dagger e$ (first line), $V\ell_e \longrightarrow \phi e$ (second line) and $\ell_e\phi^* \longrightarrow Ve$ (third line)

For any temperature $T \lesssim 10^{13}\,\mathrm{GeV}$ the top Quark Yukawa interaction is of course in thermal equilibrium, which is obviously the case at $T \lesssim 100\,\mathrm{GeV}$, so

$$\mu_t = \mu_{Q_3} + \mu_\phi \quad \Leftrightarrow \quad \mu_{Q_3} - \mu_t = -\mu_\phi \tag{4.6}$$

and inserting that into (4.5) gives then

$$\left(\frac{\partial}{\partial t} + 3H\right) q_e^{\text{quarks}} = \left(\frac{-\mu_e + \mu_{\ell_e} - \mu_\phi}{T}\right) \gamma_e^{\text{quarks}} \tag{4.7}$$

At last we do the same for the $2 \longrightarrow 2$ scatterings involving gauge bosons:

$$\begin{aligned}\left(\frac{\partial}{\partial t}+3H\right) q_e^{\text{gauge}} = \sum_V \Bigg[& \frac{n_V n_{\phi^*}}{n_V^{eq} n_{\phi^*}^{eq}} \gamma^{eq}\left(V\phi^* \longrightarrow \ell_e^\dagger e\right) && - \frac{n_{\ell_e^\dagger} n_e}{n_{\ell_e^\dagger}^{eq} n_e^{eq}} \gamma^{eq}\left(\ell_e^\dagger e \longrightarrow V\phi^*\right) \\ & - \frac{n_V n_\phi}{n_V^{eq} n_\phi^{eq}} \gamma^{eq}\left(V\phi^* \longrightarrow \ell_e e^\dagger\right) && + \frac{n_{\ell_e} n_{e^\dagger}}{n_{\ell_e}^{eq} n_{e^\dagger}^{eq}} \gamma^{eq}\left(\ell_e e^\dagger \longrightarrow V\phi\right) \\ & + \frac{n_V n_{\ell_e}}{n_V^{eq} n_{\ell_e}^{eq}} \gamma^{eq}\left(V\ell_e \longrightarrow \phi\, e\right) && - \frac{n_\phi n_e}{n_\phi^{eq} n_e^{eq}} \gamma^{eq}\left(\phi\, e \longrightarrow V\ell_e\right) \\ & - \frac{n_V n_{\ell_e^\dagger}}{n_V^{eq} n_{\ell_e^\dagger}^{eq}} \gamma^{eq}\left(V\ell_e^\dagger \longrightarrow \phi^* e^\dagger\right) && + \frac{n_{\phi^*} n_{e^\dagger}}{n_{\phi^*}^{eq} n_{e^\dagger}^{eq}} \gamma^{eq}\left(\phi^* e^\dagger \longrightarrow V\ell_e^\dagger\right) \\ & + \frac{n_{\ell_e} n_{\phi^*}}{n_{\ell_e}^{eq} n_{\phi^*}^{eq}} \gamma^{eq}\left(\ell_e\phi^* \longrightarrow V\, e\right) && - \frac{n_V n_e}{n_V^{eq} n_e^{eq}} \gamma^{eq}\left(V\, e \longrightarrow \ell_e\phi^*\right) \\ & - \frac{n_{\ell_e^\dagger} n_\phi}{n_{\ell_e^\dagger}^{eq} n_\phi^{eq}} \gamma^{eq}\left(\ell_e^\dagger\phi \longrightarrow V\, e^\dagger\right) && + \frac{n_V n_{e^\dagger}}{n_V^{eq} n_{e^\dagger}^{eq}} \gamma^{eq}\left(V\, e^\dagger \longrightarrow \ell_e^\dagger\phi\right) \Bigg] \end{aligned} \tag{4.8}$$

$$\tag{4.9}$$

After making use of CPT symmetry and again expanding around small chemical potential this simplifies to

$$\left(\frac{\partial}{\partial t}+3H\right) q_e^{\text{gauge}} = \sum_V \left(\frac{\mu_V - \mu_e + \mu_{\ell_e} - \mu_\phi}{T}\right)\left[\gamma_{\ell_e^\dagger e}^{V\phi^*} + \gamma_{\phi e}^{V\ell_e} + \gamma_{V\, e}^{\ell_e\phi^*}\right] \tag{4.10}$$

As V denotes the electroweak gauge bosons we have $\mu_V = 0$ due to the nature of the gauge symmetry and thereby we end up with the same combination of chemical potentials again

$$\left(\frac{\partial}{\partial t}+3H\right) q_e^{\text{gauge}} = \left(\frac{-\mu_e + \mu_{\ell_e} - \mu_\phi}{T}\right)\gamma_e^{\text{gauge}} \tag{4.11}$$

When we now combine all the contributions into for the BE into one equation again, with $\gamma_e = \gamma_e^{1\to 2} + \gamma_e^{\text{quarks}} + \gamma_e^{\text{gauge}}$ and using the constraint equations from Section 3.1.2 to relate the chemical potentials appearing here to the charges we're solving for, we get:

$$\begin{aligned}\frac{\partial q_e}{\partial t} + 3Hq_e &= \gamma_e\left(\frac{\mu_{\ell_e} - \mu_e - \mu_\phi}{T}\right) \\ &= \frac{\gamma_e}{T}\left(-\frac{711}{481}\mu_e - \frac{5}{13}\mu_{\Delta_e} + \frac{4}{37}\left(\mu_{\Delta_\mu} + \mu_{\Delta_\tau}\right)\right)\end{aligned} \tag{4.12}$$

To determine reaction rate γ_e we can use the expressions derived in [37]. The contributions from the $1 \longrightarrow 2$ interactions, without taking into account the gauge radiation turn out to be negligible, so I drop those, while the contribution from multiple soft scattering in the Higgs (inverse) decays is computed using the so called Landau-Pomeranchuk-Migdal resummation, LPM for short. I denote the resulting (approximate) rate as γ_e^{LPM}. The $2 \longrightarrow 2$ reactions are combined into one $\gamma_e^{2\to 2}$ rate

$$\gamma_e^{2\to 2} = \frac{h_e^2 T^4}{2048\pi}\left[h_t^2 c_t + \left(3g^2 + g'^2\right)\left(c_\ell + \log\frac{1}{3g^2+g'^2}\right) + 4g'^2\left(c_e + \log\frac{1}{4g'^2}\right)\right] \tag{4.13}$$

$$\gamma_e^{LPM} \approx \frac{h_e^2 T^4}{2048\pi}\left[h_t^2 d_t + \left(3g^2 + g'^2\right) d_\ell + 4g'^2 d_e\right] \tag{4.14}$$

where c_i, d_i are factors determined through numerical integration. As these rates are purposefully constructed to have the same form, one can just combine them into one single rate as

$$\begin{aligned}\gamma_e &\simeq \frac{h_e^2 T^4}{2048\pi}\left[h_t^2 b_t + \left(3g^2 + g'^2\right)\left(b_\ell + \log\frac{1}{3g^2+g'^2}\right) + 4g'^2\left(b_{e_R} + \log\frac{1}{4g'^2}\right)\right] \\ &= T^4 C\end{aligned} \tag{4.15}$$

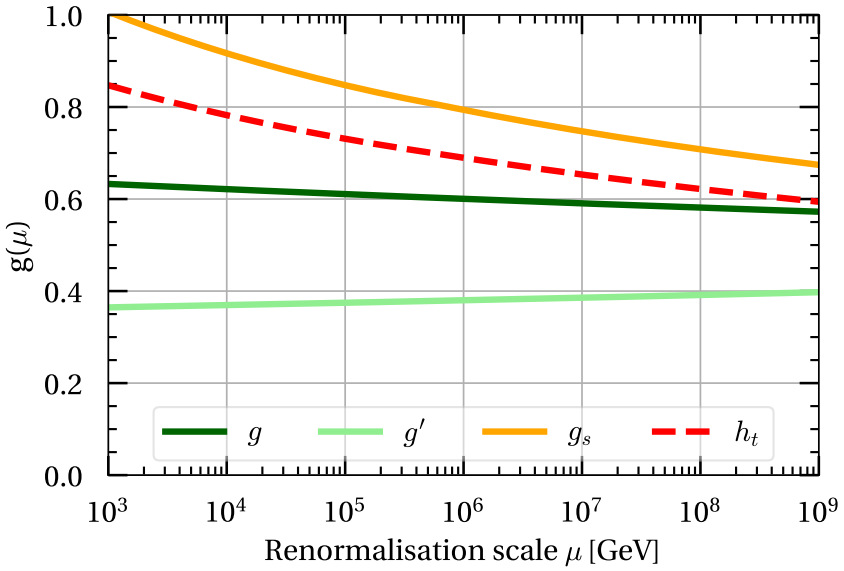

Figure 4.4: Running of the SM couplings and the top-quark Yukawa coupling

For which the combined numerical factors come out to be

$$b_t = c_t + d_t \simeq 4.3\,, \qquad b_\ell = c_\ell + d_\ell \simeq 4.296\,, \qquad b_e = c_e + d_e \simeq 4.72 \tag{4.16}$$

g, g' here are of course the gauge couplings for $SU(2)_L$ and $U(1)_Y$ respectively. As they also depend on the energy scale we calculate the running of these couplings through the following β functions

$$\frac{dg}{d\log\mu} = -\frac{1}{16\pi^2}\frac{19}{6}g^3 \tag{4.17}$$

$$\frac{dg'}{d\log\mu} = \frac{1}{16\pi^2}\frac{41}{6}g'^3 \tag{4.18}$$

Then there are also the electron and top quark Yukawa couplings h_e, h_t that appear, for which we only need to consider the running of h_t as h_e varies little due to it's small size, so we consider it as constant: $h_e = \sqrt{2\sqrt{G_F}}m_e$, where $m_e = 0.511\,\text{MeV}$ is the regular electron mass and $G_F = 1.1664 \times 10^{-5}\,\text{GeV}^{-2}$ Fermi's constant. To describe the running of h_t we also need to include the evolution of the $SU(3)_C$ coupling g_s, which therefore adds the following two β-functions

$$\frac{dg_s}{d\log\mu} = -\frac{1}{16\pi^2}7g_s^3 \tag{4.19}$$

$$\frac{dh_t}{d\log\mu} = \frac{1}{16\pi^2}\left[\left(-\frac{17}{12}g'^2 - \frac{9}{4}g^2 - 8g_s^2\right)h_t + \frac{9}{2}h_t^3\right] \tag{4.20}$$

As a reference energy scale we use the mass of the Z-boson $m_Z \simeq 91\,\text{GeV}$ and as the renormalisation scale πT. The values for the couplings at energies of m_Z we have

$$g(m_Z) = \sqrt{4\pi\alpha_w}\,, \qquad \alpha_w = 0.0338 \tag{4.21}$$

$$g'(m_Z) = \sqrt{4\pi\frac{3}{5}\alpha'}\,, \qquad \alpha' = 0.0169 \tag{4.22}$$

$$g_s(m_Z) = \sqrt{4\pi\cdot\alpha_s}\,, \qquad \alpha_s = 0.1184 \tag{4.23}$$

$$h_t(m_Z) = \sqrt{2\sqrt{2}G_F}\cdot m_t \tag{4.24}$$

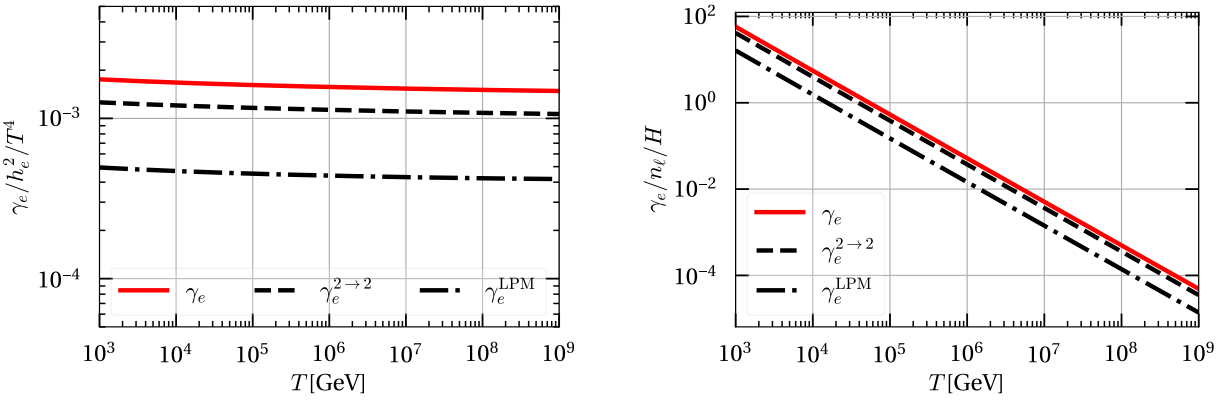

Figure 4.5: The left plot shows right handed electron interaction rate and it's components, scaled in units of $h_e^2 T^4$ for comparison with [37] and the left plot shows this rate in comparison to the expansion of the universe

where the top quark mass is taken as $m_t = 173\,\text{GeV}$

In Figure 4.5 we see the strength of the interaction rate, and see it's pretty much stable, i.e. it doesn't change much over a large temperature range. Comparing it to the expansion rate of the universe as done before we see that indeed at temperatures above $T \sim 80\,\text{TeV}$ these interaction cannot compete any more, as expected when we assumed the electron Yukawa interaction to be fully out of equilibrium at temperatures above 100 TeV

4.2 Implementation

In order to solve the Boltzmann equations numerically it is helpful to reformulate them in a comoving frame, so the $+3H$ term gets absorbed in the charges. Additionally it is common to formulate the BEs in terms of a leptogenesis variable $z = \frac{M_1}{T}$, so that the main action going on around $T \sim M_1$ occurs at around $z = 1$. It allows for better comparison of the behaviour for different heavy neutrino masses. Furthermore one can also normalise the charge to the initial right-handed electron charge q_e^{ini}, which makes it easier to see how efficient the conversion from primordial asymmetry to final $B - L$ asymmetry is.

To do that we first have the charge densities (normalised) in a comoving frame as

$$Q_x = \left(\frac{a}{a_{ini}}\right)^3 \frac{q_x}{q_e^{ini}}\,, \qquad x \in \{\Delta_\alpha, e\} \tag{4.25}$$

Which then let's us write the Boltzmann equations in a rescaled way analogously to as we saw before in (3.116), and inserting back the RHS then leads to

$$\frac{dQ_{\Delta_\alpha}}{dt} = \left(\frac{a}{a_{ini}}\right)^3 \frac{1}{q_e^{ini}} \left[\sum_\beta \left(\frac{\mu_{\ell_\beta} + \mu_\phi}{T}\right) \gamma^W_{\alpha\beta}\right] \tag{4.26}$$

$$= \left(\frac{a}{a_{ini}}\right)^3 \frac{1}{q_e^{ini}} \sum_\beta \left[\begin{pmatrix} -\frac{5}{13} \\ \frac{4}{37} \\ \frac{4}{37} \end{pmatrix} \mu_e - \begin{pmatrix} \frac{6}{13} & 0 & 0 \\ 0 & \frac{41}{111} & \frac{4}{111} \\ 0 & \frac{4}{111} & \frac{41}{111} \end{pmatrix} \begin{pmatrix} \mu_{\Delta_e} \\ \mu_{\Delta_\mu} \\ \mu_{\Delta_\tau} \end{pmatrix}\right]_\beta \frac{\gamma^W_{\alpha\beta}}{T} \tag{4.27}$$

$$= 6 \sum_\beta \left[\begin{pmatrix} -\frac{5}{13} \\ \frac{4}{37} \\ \frac{4}{37} \end{pmatrix} Q_e - \begin{pmatrix} \frac{6}{13} & 0 & 0 \\ 0 & \frac{41}{111} & \frac{4}{111} \\ 0 & \frac{4}{111} & \frac{41}{111} \end{pmatrix} \begin{pmatrix} Q_{\Delta_e} \\ Q_{\Delta_\mu} \\ Q_{\Delta_\tau} \end{pmatrix}\right]_\beta \frac{\gamma^W_{\alpha\beta}}{T^3} \tag{4.28}$$

$$\frac{dQ_e}{dt} = \frac{6\gamma_e}{T^3}\left[-\frac{711}{481} Q_e - \frac{5}{13} Q_{\Delta_e} + \frac{4}{37}\left(Q_{\Delta_\mu} + Q_{\Delta_\tau}\right)\right] \tag{4.29}$$

Here in the last step we used $\mu_x = \frac{6q_x}{T^2}$ As we know during radiation domination $H \sim \frac{1}{2t}$ which helps us convert the derivative with respect to time, into a derivative with respect to z

$$H = \sqrt{\frac{g_*\pi^2}{90}}\frac{M_1^2}{z^2 M_{Pl}} = \frac{M_1^2}{z^2 M_*} \qquad M_* = M_{Pl}\sqrt{\frac{90}{g_*\pi^2}} \tag{4.30}$$

$$H \sim \frac{1}{2t} \Rightarrow t \sim \frac{M_* z^2}{2M_1^2} \qquad dt = \frac{M_* z}{M_1^2}dz = \frac{1}{Hz}dz \tag{4.31}$$

Inserting this into the Boltzmann equations again, and writing $\Gamma^W_{\alpha\beta} = \frac{6\gamma^W_{\alpha\beta}}{T^3}\,, \quad \Gamma_e = \frac{6\gamma_e}{T^3}$

$$\frac{dQ_x}{dt} = Hz\frac{dQ_x}{dz} \tag{4.32}$$

$$\Leftrightarrow \frac{dQ_{\Delta_\alpha}}{dz} = \sum_\beta \left[\begin{pmatrix} -\frac{5}{13} \\ \frac{4}{37} \\ \frac{4}{37} \end{pmatrix} Q_e - \begin{pmatrix} \frac{6}{13} & 0 & 0 \\ 0 & \frac{41}{111} & \frac{4}{111} \\ 0 & \frac{4}{111} & \frac{41}{111} \end{pmatrix} \begin{pmatrix} Q_{\Delta_e} \\ Q_{\Delta_\mu} \\ Q_{\Delta_\tau} \end{pmatrix} \right]_\beta \frac{\Gamma^W_{\alpha\beta}}{Hz} \tag{4.33}$$

$$\frac{dQ_e}{dz} = \frac{\Gamma_e}{Hz}\left[-\frac{711}{481}Q_e - \frac{5}{13}Q_{\Delta_e} + \frac{4}{37}\left(Q_{\Delta_\mu} + Q_{\Delta_\tau}\right)\right] \tag{4.34}$$

As of now we'd need to fix about 15 free parameters in order to use the Casas-Ibarra parametrisation to arrive at values for the neutrino Yukawa matrix, which is far to many to meaningfully scan over. So what we'll do now is to reduce the number of parameter by reformulating the Boltzmann equations in the term of just four *effective parameters*.

To do so we first come back that the washout term $\gamma^W_{\alpha\beta}$ is dominated by the inverse decays, with the $2 \longrightarrow 2$ interactions being negligible. Thus allowing us to write:

$$\gamma^W_{\alpha\beta} \simeq \gamma^{ID}_{\alpha\beta} = \sum_i \gamma_{i\alpha}\delta_{\alpha\beta} = \sum_i p_{i\alpha}\gamma_i\delta_{\alpha\beta} \tag{4.35}$$

$$= \underbrace{\sum_i \gamma_i}_{=\gamma^W} \underbrace{\begin{pmatrix} p_e & 0 & 0 \\ 0 & p_\mu & 0 \\ 0 & 0 & p_\tau \end{pmatrix}}_{=P_{\alpha\beta}} \tag{4.36}$$

As we also saw only the lightest RHN plays a role, i.e.

$$\sum_i \gamma_i \approx \gamma_1 = \frac{M_1^3\Gamma_1}{\pi^2 z}K_1(z) \tag{4.37}$$

And also we absorb all further temperature dependence into the rate:

$$\Gamma^W = \frac{6\gamma^W}{T^3} = \frac{6z^2\Gamma_1}{\pi^2}K_1(z) \tag{4.38}$$

$$\tag{4.39}$$

Here Γ_1 is the decay width of N_1, and can be calculated as

$$\Gamma_1 = \frac{M_1}{8\pi}\sum_\alpha h^{\nu *}_{\alpha 1}h_{\alpha 1} = \frac{M_1}{8\pi}\left((h^\nu)^\dagger h^\nu\right)_{11} \tag{4.40}$$

$$= \frac{M_1}{8\pi}\frac{\left(m_D^\dagger m_D\right)_{11}}{v^2/2} \tag{4.41}$$

Which let's us define the effective neutrino mass [15] $\widetilde{m} \equiv \widetilde{m}_1 = \frac{\left(m_D^\dagger m_D\right)_{11}}{M_1}$, and therefore leading to the total washout rate

$$\Gamma^W = \frac{6z^2 M_1^2\widetilde{m}}{8\pi^3 v^2/2}K_1(z) \tag{4.42}$$

$$\Rightarrow \frac{\Gamma^W}{zH} = \frac{6z^3\widetilde{m}}{\pi^2 m_*}K_1(z) \equiv W(\widetilde{m})\,, \qquad m_* = \frac{8\pi v^2/2}{M_*} \tag{4.43}$$

And in a similar manner for the right handed electron BE, we can collect all the terms and express them as a function only depending on $M_1 \equiv M_1$

$$\frac{\Gamma_e}{zH} = \frac{6CT}{zH} \tag{4.44}$$

$$= \frac{6CM_*}{M_1} = E(M_1) \tag{4.45}$$

With all this the only free parameters left in the BEs are $p_e, p_\mu, \widetilde{m}, M_1$ with the equations now looking like:

$$\frac{d}{dz}\begin{pmatrix} Q_{\Delta_e} \\ Q_{\Delta_\mu} \\ Q_{\Delta_\tau} \end{pmatrix} = W(\widetilde{m}) \begin{pmatrix} p_e & 0 & 0 \\ 0 & p_\mu & 0 \\ 0 & 0 & p_\tau \end{pmatrix} \left[\begin{pmatrix} -\frac{5}{13} \\ \frac{4}{37} \\ \frac{4}{37} \end{pmatrix} Q_e - \begin{pmatrix} \frac{6}{13} & 0 & 0 \\ 0 & \frac{41}{111} & \frac{4}{111} \\ 0 & \frac{4}{111} & \frac{41}{111} \end{pmatrix} \begin{pmatrix} Q_{\Delta_e} \\ Q_{\Delta_\mu} \\ Q_{\Delta_\tau} \end{pmatrix} \right] \tag{4.46}$$

$$\frac{dQ_e}{dz} = E(M_1) \left[-\frac{711}{481} Q_e - \frac{5}{13} Q_{\Delta_e} + \frac{4}{37} \left(Q_{\Delta_\mu} + Q_{\Delta_\tau} \right) \right] \tag{4.47}$$

To evaluate the efficiency we want to compare how much of the primordial right handed electron charge can be converted into the lepton flavour asymmetries. As we already normalised to the initial electron charge it is therefore sufficient to just add up the resulting lepton flavour asymmetries:

$$\kappa = \frac{10}{3} \left[Q_{\Delta_e}(z \to \infty) + Q_{\Delta_\mu}(z \to \infty) + Q_{\Delta_\tau}(z \to \infty) \right] \tag{4.48}$$

The factor $\frac{10}{3}$ here comes from the optimal conversion factor that could be achieved with the non dynamic right handed electron potential, as discussed in Section 3.3. As of now even low conversion factors would be just fine if we had a large enough primordial asymmetry to compensate and still produce the observed baryon asymmetry we see today, but as it turns out one cannot just have an arbitrarily large primordial right handed electron charge, as I will discuss in the next section.

4.3 Constraints on the conversion efficiency and the Chiral Plasma instability

The main constraint on the magnitude of the conversion efficiency is of course the observed size of the baryon asymmetry we want to explain through this mechanism $\eta_B^0 = 6.12 \times 10^{-10}$. Under the assumption that wash-in leptogenesis is the only mechanism that produces a $B - L$ asymmetry and is therefore fully responsible for the resulting baryon asymmetry through sphaleron conversion. The baryon asymmetry can then be expressed as

$$\eta_B^0 = \left.\frac{q_B}{n_\gamma}\right|_0 = \frac{g_{*,s}^0}{g_{*,s}^{\mathrm{SM}}} \left.\frac{q_B}{n_\gamma}\right|_{\mathrm{fin}} = C_{\mathrm{sph}} \frac{g_{*,s}^0}{g_{*,s}^{\mathrm{SM}}} \left.\frac{q_{B-L}}{n_\gamma}\right|_{\mathrm{fin}} = C_{\mathrm{win}} C_{\mathrm{sph}} \frac{g_{*,s}^0}{g_{*,s}^{SM}} \kappa \left.\frac{q_e}{n_\gamma}\right|_{\mathrm{ini}} \tag{4.49}$$

Where $C_{\mathrm{sph}} = \frac{12}{37}$ [38, 39] is the efficiency factor that gives the resulting B asymmetry from a $B - L$ asymmetry, and $C_{\mathrm{win}} = \frac{3}{10}$ is the optimal conversion efficiency we determined previously for wash-in leptogenesis, to convert a right handed electron asymmetry into a $B - L$ asymmetry. $g_{*,s}^0 = \frac{43}{11}$ are the entropy degrees of freedom in the standard model in present day, and $g_{*.s}^{\mathrm{SM}} = 106.75$ at high temperatures.

Including the expressions for n_γ and writing $q_e = \frac{\mu_e}{6T^2}$ in the units of a chemical potential again,

the total baryon asymmetry can further be expressed as

$$\eta_B^0 = C_{win} C_{sph} \frac{g^0_{*,s}}{g^{SM}_{*,s}} \kappa \frac{\pi^2}{6\zeta(3) g_\gamma} \left.\frac{\mu_e}{T}\right|_{ini} \tag{4.50}$$

$$\simeq 2.44 \times 10^{-3} \kappa \left.\frac{\mu_e}{T}\right|_{ini} \tag{4.51}$$

$$= 6.12 \times 10^{-10} \cdot \frac{1}{2.51 \times 10^{-7}} \kappa \left.\frac{\mu_e}{T}\right|_{ini} \tag{4.52}$$

$$= \eta_B^{\text{obs}} \cdot \frac{\kappa}{2.51 \times 10^{-7}} \left.\frac{\mu_e}{T}\right|_{ini} \tag{4.53}$$

So far the observed baryon asymmetry can be achieved with any conversion efficiency κ as long as the initial charge stored in the right handed electrons is sufficiently large. There is however a upper bound on this charge, due to the so called chiral plasma instability. This instability arises through the chiral anomaly, which - as seen before - couples chiral fermion currents to gauge fields.

$$\partial_\mu j_e^\mu = -\frac{h_e^2 g'^2}{16\pi^2} F_{\mu\nu} \tilde{F}^{\mu\nu} \tag{4.54}$$

So a too large chiral electron asymmetry would lead to a too efficient conversion of the asymmetry into helical hypermagnetic fields, which curiously enough can lead to an *overproduction* of a baryon asymmetry [40], as I already discussed in the section of baryogenesis through axion inflation (see 2.1.1.4)

In order to avoid triggering the instability we should have [37]

$$\left|\frac{\mu_{Y,5}}{T}\right| \lesssim 1.4 \times 10^{-3} \tag{4.55}$$

Where $\mu_{Y,5} = \frac{711}{481}\mu_e$[41, 32] refers to the chiral chemical potential. This leads to the limit for the maximally allowed right handed electron asymmetry at the start onset of wash-in leptogenesis

$$\left|\frac{\mu_e}{T}\right|_{\text{ini}} \lesssim 9.6 \times 10^{-4} \tag{4.56}$$

For the constraints of the conversion efficiency that now means that

$$\eta_B^0 \simeq \frac{\kappa}{2.6 \times 10^{-4}} \left.\frac{\mu_e/T}{9.6 \times 10^{-4}}\right|_{\text{ini}} \tag{4.57}$$

As the chiral plasma instability is not too well understood yet and these limits are rather rough, I will set the benchmark for the minimally required conversion efficiency to

$$|\kappa| \overset{!}{\gtrsim} 3 \times 10^{-4} \tag{4.58}$$

As the sign of the primordial right handed electron charge is not fixed both negative and positive values for κ are possible.

4.4 Solutions of the Boltzmann equations

Before starting out with scans of the entire 4-dimensional parameters space let us look at some individual solutions of the Boltzmann equations.

To start we can see how much the inclusion of the right handed electron charge influences the evolution of the charges. For this I pick some benchmark values to test the behaviour with. For the branching ratios I take $p_e = 0.6\,, p_\mu = 0.3\,, p_\tau = 0.1$ which fulfil the criterion of being rather "generic", while still inducing strong enough differences between the individual flavours (to distinguish the lines in the solution). Also to distinguish between the scenario of strong wash-in and weak wash-in, which can be parametrised through the effective neutrino mass $\widetilde{m}_1$, I pick once for strong wash-in $\widetilde{m}_1 = 100\,\text{meV}$,

while for weak wash-in $\widetilde{m}_1 = 0.1\,\text{meV}$. As initial conditions I always set $Q_{\Delta_\alpha} = 0, Q_e = 1$, so we start out with no primordial $B - L$ asymmetry.

At a RHN mass of $M_1 = 300\,\text{TeV}$ the previous description of a constant right handed electron charge (at the relevant times for leptogenesis) should still hold. In Figure 4.6 we see the evolution in the case of weak wash-in, and can see that qualitatively little changes whether we include the evolution of Q_e or keep it constant, though the total washed in asymmetry turns out to only be about half as big when including the evolution of Q_e, which makes makes sense as the washed-in asymmetry is depended on the size of the size of the electron asymmetry and if that gets washed out, less of the Δ_α asymmetries can be washed-in any more. And for the case of weak wash-in this effect is still rather small.

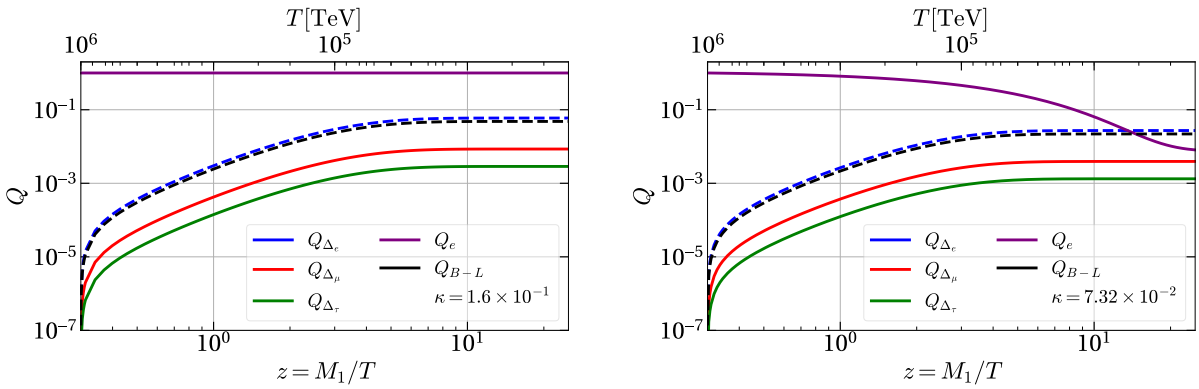

(a) Without BE for Q_e (b) Including the BE for Q_e

Figure 4.6: Evolution of the flavour asymmetries in the described benchmark scenario in the case of weak wash-in. The black line shows the total $B - L$ asymmetry created. Dashed lines indicate a negative sign for the respective charge

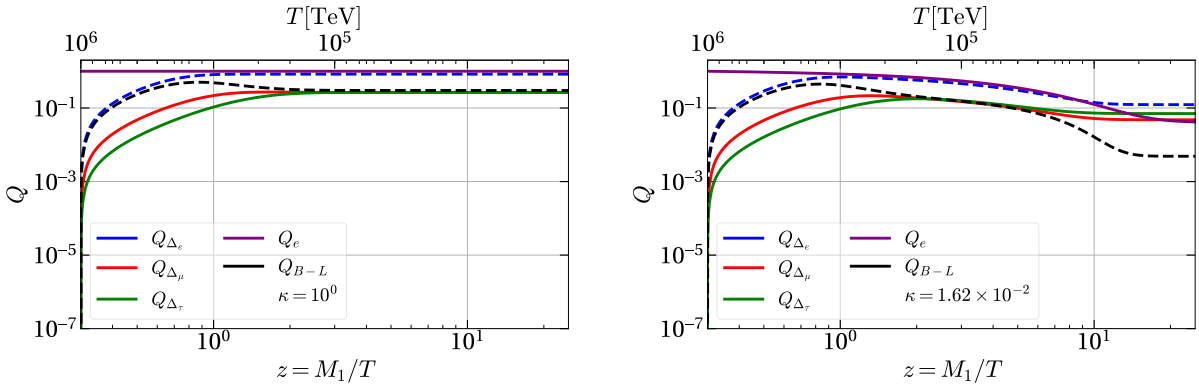

(a) Without BE for Q_e (b) Including the BE for Q_e

Figure 4.7: Evolution of the flavour asymmetries in the described benchmark scenario ($p_e = 0.6\,, p_\mu = 0.3, M_1 = 300\,\text{TeV}$ in the case of strong wash-in ($\widetilde{m} = 100\,\text{meV}$).

If we now look at the case of strong wash-in in shown in Figure 4.7 we can see a significant qualitative difference when we include the evolution of Q_e versus when we keep it constant, as the washed out right handed electron asymmetry is able to affect the flavour asymmetries up to later times due to the stronger wash-in strength, so instead of already plateauing for $z \ll 10$ the asymmetries still experience some washout around $z \sim 10$ before then assuming their final values. While for the old scenario in which Q_e is assumed to be constant we can indeed see that $\kappa = 1$ is achieved as the analytical considerations in 3.3 predicted, while when we include the according BE for Q_e the achieved

conversion efficiency is significantly smaller, even smaller than we saw before for a weak wash-in.

Also we can see a different flavour structure in the final asymmetry, which in the simplified case leads to $Q_{\Delta_\mu} \simeq Q_{\Delta_\tau}$ the now refined calculation results in more of a hierarchy between them, along with Q_{Δ_e} being less dominant.

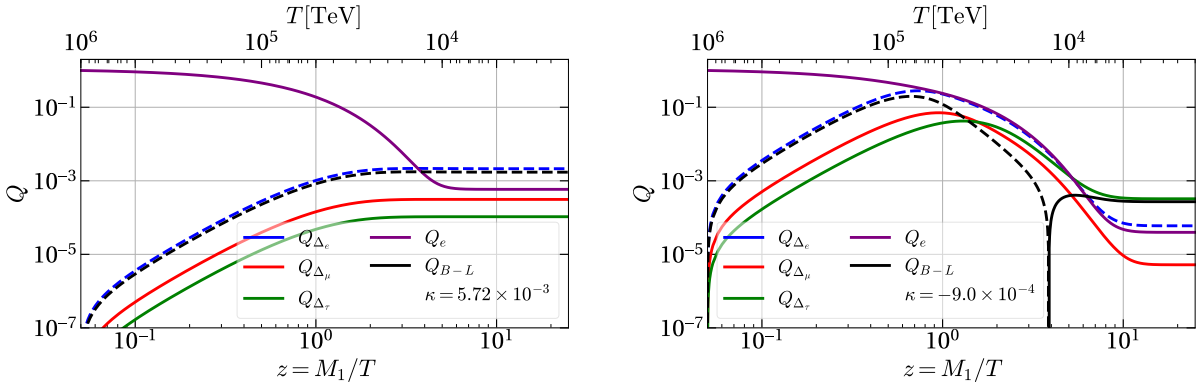

(a) Weak wash-in (0.1 meV)

(b) Strong wash-in (100 meV)

Figure 4.8: Evolution of the flavour asymmetries in the described benchmark scenario ($p_e = 0.6\,, p_\mu = 0.3$) but for a lower mass $M_1 = 50\,\text{TeV}$ both for the cases of strong and weak wash-in.
Due to the low RHN mass the BE for Q_e is now always included

With the inclusion of the Boltzmann equation for Q_e masses below 100 TeV can now also be considered, so taking the same benchmark scenario as before now with a RHN mass of $M_1 = 50\,\text{TeV}$ leads to the results shown in Figure 4.8. For weak wash-in strength it is a qualitatively similar picture to before, with the main difference being that Q_e is more strongly washed out, as the wash-in process takes place at lower temperatures now, at which Y_e is more equilibrated.

For strong wash-in though the picture changes more, in that one can now clearly see the strong washing in of the lepton asymmetries as first, which then experience wash-out again, as Q_e gets also washed out. Notably the sign of the total $B - L$ asymmetry produced here switches compared to the weak wash-in case.

4.4.1 Exploring the parameter space

Next I want to look at the parameter space of the branching ratios. For that I now take a few points in $M_1 - \widetilde{m}$ space and look at the conversion efficiency κ in $p_e - p_\mu$ space, which as we are talking about branching ratios that have to sum up to 1: $p_e + p_\mu + p_\tau = 1$ can be visualised in a triangular plot. [42] The way I calculate κ is by solving the Boltzmann equations from $z = M_1/10^6\,\text{GeV}$, so starting at a temperature of $T = 10^6\,\text{GeV}$, which is the upper limit where we (for now) assume the effects of other interactions can still be ignored, so the Boltzmann equations as stated still hold true. As an endpoint to evaluate the washed in Charge asymmetries I take the cut-off to be at $z = 25$ as at this point the entire process is mostly over, as we can see in the BE solutions in the previous section.

To start out before looking into the region of low RHN masses ($M_1 < 100\,\text{TeV}$) I want to explore again the previously considered case with a constant Q_e for RHN masses $100\,\text{TeV} < M_1 < 1000\,\text{TeV}$ for strong washout, as we already saw the conversion efficiency in this case through the analytical calculation, though which required a "generic" flavour structure. To visualise the need for these conditions we can now see Figure 4.9a that indeed a large part of parameter space is made up of $\kappa = (-)1$, at least in the centre containing the region of "generic" branching ratios, in which no single branching ratio clearly dominates over the others.

And we can also see in the more "extreme" regions that the conversion efficiency indeed deviates form the optimal case, and even is able to surpass it ($|\kappa| > 1$) in the specific edge cases of at least one branching ratio being zero or being very close to vanishing.

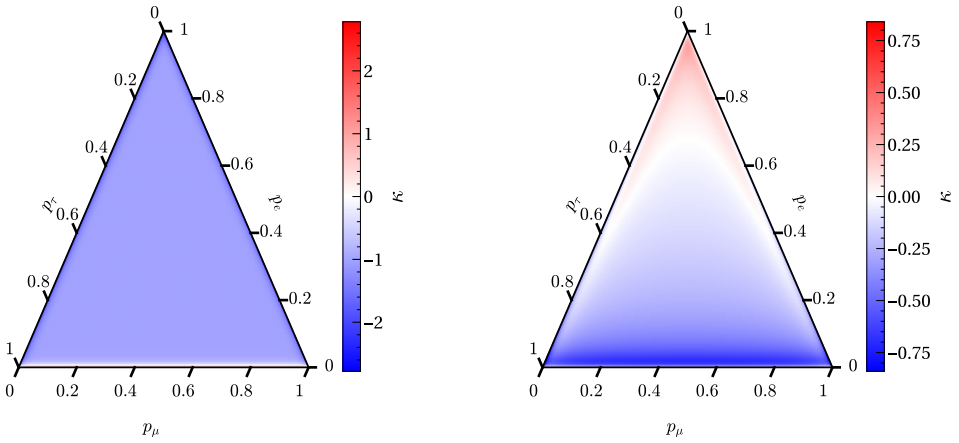

(a) Without the BE for Q_e (b) Including the BE for Q_e

Figure 4.9: Conversion efficiency κ in $p_e - p_\mu$ space for strong wash-in at $\widetilde{m} = 10\,\text{meV}$ with fixed RHN mass $M_1 = 300\,\text{TeV}$, once including the BE for the right handed electrons and once without.

Meanwhile 4.9b shows the same scenario including the dynamic modelling of Q_e and it can be clearly seen that the conversion efficiency is far from homogenous in $p_e - p_\mu$ space, and is for the most part also significantly less efficient.

We can now also take a look at one of these extreme points by plotting the solutions for that specific point $p_e = 0\,, p_\mu = p_\tau = 0.5$ in Figure 4.10, again once with modelling Q_e and once without. We see explicitly that $|\kappa| > 1$ when taking $Q_e = \text{const}$ and in 4.10b we see that taking a dynamical Q_e into account has a notable effect on the flavour asymmetries as at later times the washout of Q_e also drags down Q_{Δ_α} leading to a conversion efficiency that is on order of magnitude smaller than in the simplified case.

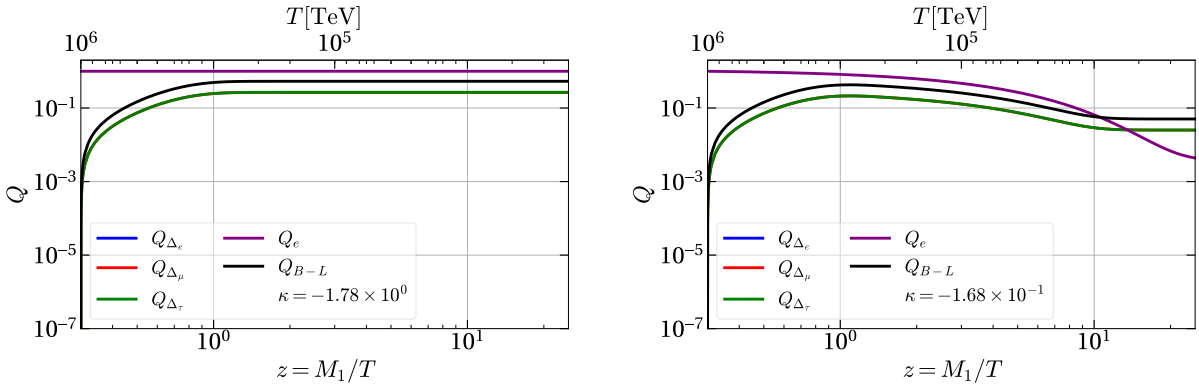

(a) Without BE for Q_e (b) Including BE for Q_e

Figure 4.10: Solution at one extreme point from Figure 4.9a ($M_1 = 300\,\text{TeV}\,, \widetilde{m} = 100\,\text{meV}$, at $p_e = 0$ and $p_\mu = p_\tau = 0.5$

Now we want to look into the actual mass range we are interested in by taking $M_1 = 100\,\text{TeV}$ and see how the branching ratio space looks like for different wash-in strengths in Figure 4.11. I consider four different strengths of wash-in. First weak wash-in 4.11a at an effective neutrino mass of $\widetilde{m} = 10^{-3}\,\text{meV}$ for which we can see that the conversion efficiency is rather low - with the highest value to be achieved at $\kappa \sim -4 \times 10^{-4}$ - and seems to be mostly independent of the choice of p_μ/p_τ but effected by p_e.

A higher wash-in strength at $\widetilde{m} = 1\,\text{meV}$ can be seen in 4.11b. In comparison to the weak wash-in we can observe significantly higher conversion efficiencies, along with some structure depending on p_μ (p_τ), though qualitatively still looking quite similar, with p_e dominantly contributing to the efficiency reached.

Going slightly higher in the strength of the wash-in to $\widetilde{m} = 10\,\text{meV}$ we can see in 4.11c a significant shift in the qualitative behaviour. While the conversion efficiency remains at the same order of magnitude now the lower values for p_e lead to a negative value and higher ones to a positive conversion efficiency, while in the previous cases this was flipped.

At the highest wash-in strength I now want to look at with $\widetilde{m} = 1\,\text{eV}$ we reach a quite extreme regime in which the wash-in of the asymmetry isn't the dominating effect anymore and we again reach a strong wash-*out*, except for very extreme values for the branching ratios. While for the case previously referred to as "generic" (i.e. the inner part of the triangle) any washed in asymmetry get's quickly washed out again.

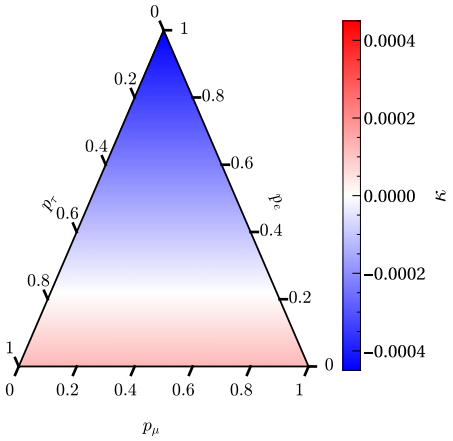

(a) Weak wash-in
($\widetilde{m} = 10^{-3}\,\text{meV}$)

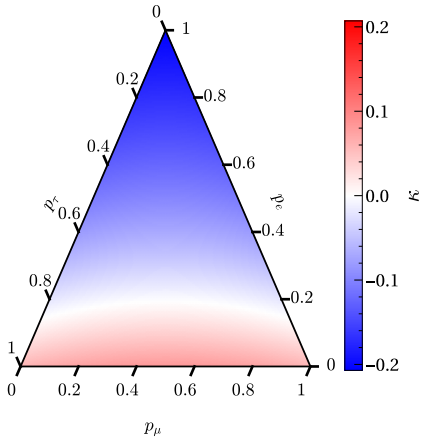

(b) Weak intermediate wash-in
($\widetilde{m} = 1\,\text{meV}$)

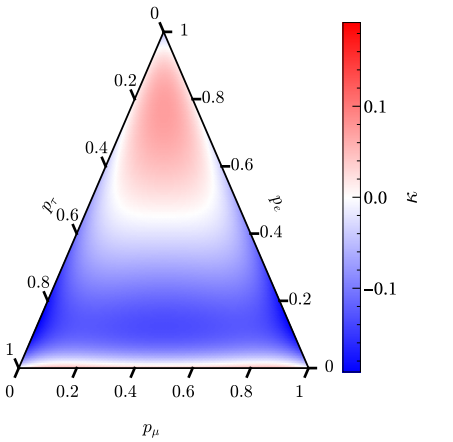

(c) strong intermediate wash-in
($\widetilde{m} = 10\,\text{meV}$)

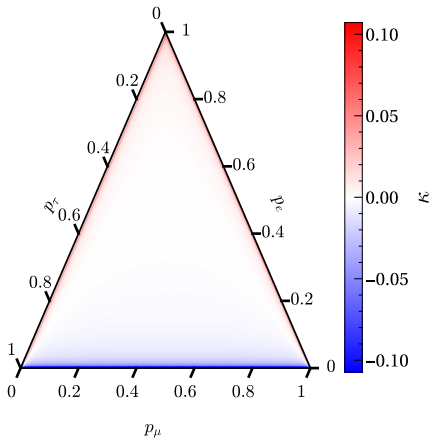

(d) strong wash-in
($\widetilde{m} = 1\,\text{eV}$)

Figure 4.11: Different scans in branching ratio for different wash-in strength for a RHN mass of $M_1 = 100\,\text{TeV}$

Doing the same for a lower RNH masses yields qualitatively only little difference. The conversion efficiency achieved ends up lower in total, and for strong wash-in the wash-out effect becomes a lot stronger, leaving only very slim regions that can still produce a significant asymmetry wash-in.

4.4.2 Full 4D scan

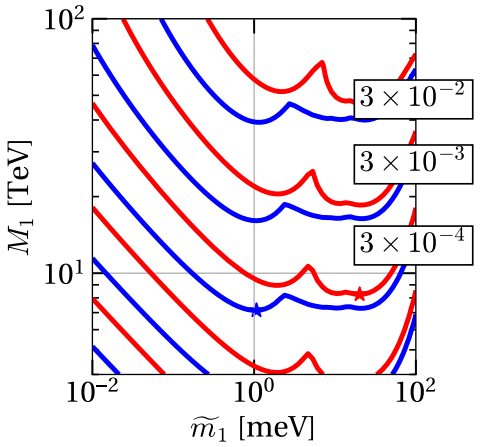

Figure 4.12: Contour plot showing the optimal conversion efficiency in $\widetilde{m} - M_1$ space, as discussed the lowest conversion efficiency possible is at $|\kappa| \approx 3 \times 10^{-4}$, so the lowest RHN masses reached on the according contour lines are indicated with a star

To produce a full scan over the entire 4-dimensional parameter space, I determine κ over a range for $p_e \in [0, 1]$ and accordingly $p_\mu \in [0, 1 - p_e]$. The mass ranges I want to look at is for the RHN mass of course bounded upwards at 100 TeV and as a lower limit I go down to 4 TeV, while I scan the effective neutrino mass over a range of $\widetilde{m} \in \left[10^{-2}, 10^2\right]$ meV. For the two neutrino mass parameters I use a logarithmic spacing on a grid of 71 points each. To keep computation time to a reasonable amount I choose a more coarse grid for the branching ratios, using a linear spacing for both and 21 points each.

In total I therefore calculate $\kappa(p_e, p_\mu, M_1, \widetilde{m})$ over a 4-dimensional grid of $21^2 \times 71^2 = 2\,223\,081$ points. To be able to visualise, I choose to reduce the dimensionality to show the dependence on M_1 and $\widetilde{m}$ while marginalising over the branching ratios. To do this I simply look what the highest and lowest (or highest negative) value of κ can be achieved for any pair of neutrino masses $(\widetilde{m}, M_1)$ and also take note of the required branching ratios for this optimal conversion efficiency. I then show the results in a contour plot, with one set of contour lines representing (shown in blue) corresponding to the highest value of $-\kappa$, i.e. for the case in which q_e is converted into a $B - L$ asymmetry with a negative sign, which I will further denote as κ^-, and in red a set of contour lines corresponding to the highest values of $+\kappa$, i.e. q_e is converted into a $B - L$ asymmetry of the same sign, which I will denote as κ^+.

The corresponding branching ratios at these optima I'll call $p_e^\pm, p_\mu^\pm$ respectively.

The results of this can be seen in Figure 4.12. The lowest values for M_1 on the $|\kappa| = 3 \times 10^{-4}$ contour end up at $(\widetilde{m}^-, M_1^-) = (1.07\,\text{meV}, 7.1\,\text{TeV})$ for κ^- and $(\widetilde{m}^+, M_1^+) = (\ldots\,\text{meV}, \ldots\,\text{TeV})$ for κ^+.

A major problem I encountered here is that comparisons with slightly closer spacing in branching ratios leads to significantly different results in the M_{min}^+, with p_e getting closer and closer 1. This is due to something we actually saw before in that for strong wash-in/out scenarios the inner parts of the parameter space of branching ratios lead to a vanishing conversion while for increasingly narrow parts of parameter space, close to $p_e = 0$ and $p_{\mu/\tau} = 0$. Thereby through the constant and linear spacing I start missing the optimal branching ratio which lies somewhere in between the last step in the interval $p_e^+ \in [0.95, 1]$, yet it falls off quickly around it.

The simplest solutions one could come up with is of course to just increase the resolution, though this would of course increase computation time immensely. Though as I can see now around what values the optimal branching ratios lie I can now exclude large part of parameter space and just scan around those values we have good reasons to believe the true optimum to lie in.

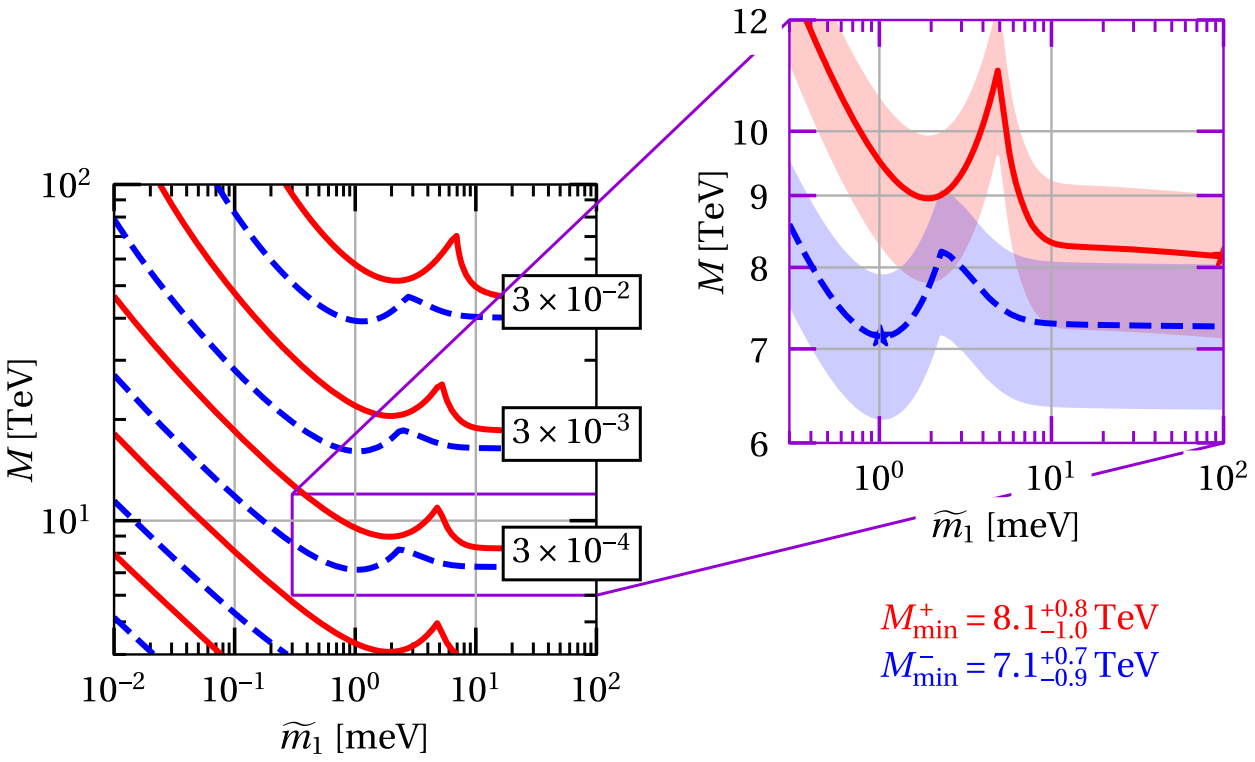

Figure 4.13: Contour plot showing the conversion efficiency κ achieved with a different spacing for the branching ratios. The inset shows the relevant $|\kappa| = 3 \times 10^{-4}$ contour line in more detail.
The lowest potential RHN masses are shown with a red and blue star respectively.

For this I started out by estimating the optimal value for $p_e^- \sim \frac{1\,\text{meV}}{\widetilde{m}}$ as well as $p_e^+ \sim 1 - \frac{1\,\text{meV}}{\widetilde{m}}$and use this as a centre point to place 10 logarithmically spaced points around it. The results from this improved scan are shown in Figure 4.13.

The lowest possible mass I achieve in the case of a negative conversion efficiency for which a clear minimum can be seen at $(\widetilde{m}^-, M^-_{\text{min}}) = (1.02\,\text{meV}, 7.1\,\text{TeV})$ with an optimal branching ratio of $p_e^- = 1$, and therefore $p_\mu^- = p_\tau^- = 0$.

We can now see that even for large wash-out strengths the minimal possible RHN mass can still be relatively low, or even drop further as in the case for M^+_{min} which arrives at its lowest value only at the end of the parameter range and only seems to drop further.

Problem with the positive conversion efficiency is that - as seen before - to achieve a good conversion efficiency in this very strong wash-out regime one needs to get the right branching ratios and cannot deviate to much from then, making the theoretically reached lower limits here quite unstable and in the need of a lot of fine tuning. The lowest value we get in this way is at $(\widetilde{m}^+, M^+_{\text{min}}) = (100\,\text{meV}, 8.1\,\text{TeV})$, which could be pushed down even further by going to higher $\widetilde{m}$.

In comparison if we look at the conversion efficiency in the branching ratio space, at $(\widetilde{m}^-, M^-_{\text{min}})$ we can check how fine tuned these branching ratios have to be. I show the results in 4.14a and it can be seen that the drop off in conversion efficiency isn't nearly as strong as in the strong wash-out regime, leading to a in total far bigger possible parameter space in this region.

A better value for the positive conversion efficiency could be achieved by taking the values at the first local minimum of the contour line instead of trying to find a global minimum. This first dip that can be seen in both contour lines, is for the κ^+ located at $(\widetilde{m}^+, M^+_{\text{min}}) = (1.93\,\text{meV}, 8.96\,\text{TeV})$. Performing a scan in branching ratio space here leads to 4.14b, where we can also see that the situation now needs a lot less fine tuning now.

Closer investigation reveals that the shape of these contour lines with the sharp peak - which for

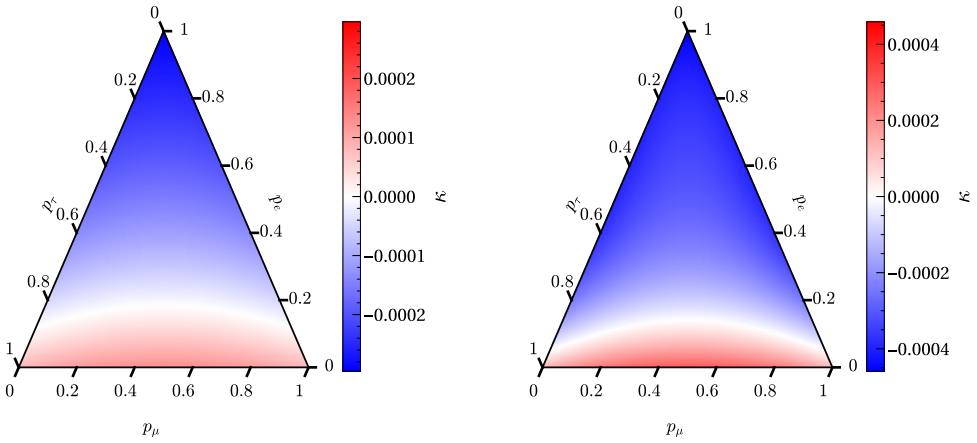

(a) At the position of M^-_{min} (b) At the position of M^+_{min}

Figure 4.14: The conversion efficiency in branching ratio space at the previously determined lowest potential masses in for positive and negative conversion efficiency respectively. In both cases it can be seen that a slight deviation in branching ratios would still lead to a comparable efficiency, unlike in the presence of strong wash-out.
It has to be noted that parameter space allowing for a positive conversion efficiency is markedly smaller

the $\kappa^+ = 3 \times 10^{-4}$ line is located at $\widetilde{m} = 5.2\,\text{meV}$ while for the κ^- line it is located at $\widetilde{m} = 2.29\,\text{meV}$ - arises from the fact that for low wash-in strengths, below that critical $\widetilde{m}_c$, the optimal conversion efficiency is always reached for $p_e^- = 1$ and $p_e^+ = 0$. For $\widetilde{m} > \widetilde{m}_c$ the situation changes and instead the optimal solutions are reached for $p_e^- \approx \frac{1.1\,\text{meV}}{\widetilde{m}}$ and $p_e^+ \approx 1 - \frac{2\,\text{meV}}{\widetilde{m}}$, indeed close to my initial guesses.

For the branching ratio into the μ (and τ) flavour I find $p_\mu^- = 0$ and $p_\mu^+ = \frac{1-p_e^+}{2}$ regardless of the wash-in strength. As the solutions are also symmetric between $\mu \leftrightarrow \tau$ as can be easily seen from the BEs, as well as from the 2D scans before, $p_\mu^- = 1$ gives the same result.

The sharp peaks in the contour lines now simply shows the transition between the two regimes of wash-in/out strength.

Chapter 5

Conclusions

5.1 Summary

So what I did in this work is expanding the framework of wash-in leptogenesis into temperatures below 100 TeV, which require the inclusion of an additional Boltzmann equation for the primordial charge stored in right handed electrons.

In this work, I have expanded the framework of wash-in leptogenesis below a temperature of 100 TeV by incorporating an additional Boltzmann equation for right-handed electrons. This extension let me analyse the lower bound on the mass of right-handed neutrinos required to maintain a sufficiently large conversion efficiency of the generated lepton flavor asymmetry into the observed baryon asymmetry of the Universe. The results indicate that the lowest viable mass for the lightest right-handed neutrino is $M_1 = 7.1\,\text{TeV}$. However, given the uncertainties surrounding the precise amount of baryon asymmetry needed and the fine-tuning required for specific branching ratios, it is reasonable to conclude that heavy neutrino masses below 10 TeV remain a viable possibility within this framework.

Furthermore, I could find that even at temperatures well above 100 TeV, the effects of a dynamically evolving right-handed electron asymmetry cannot be neglected. This challenges the assumption that a quasi conserved charge it would be irrelevant at higher energy scales, highlighting the need for a more comprehensive treatment of the conserved charges.

Wash-in leptogenesis thus continues to offer a versatile mechanism for generating a $B - L$ asymmetry without necessitating strong CP violation in the heavy neutrino sector. Instead, it provides a pathway in which a variety of primordial asymmetries - arising from primordial CP-violating processes - can be efficiently converted into a lepton asymmetry via right-handed neutrinos. This asymmetry is subsequently transformed into a baryon asymmetry through sphaleron processes, much like in classical leptogenesis. The results presented in this thesis reinforce the robustness of the wash-in mechanism and underscore its potential to accommodate a range of model parameters while remaining consistent with observational constraints.

I also examine the specific branching ratios that must be realized for successful wash-in leptogenesis at the lowest possible right-handed neutrino mass. The analysis shows that for large wash-in/wash-out strengths $\widetilde{m}$, the viable parameter space for the branching ratios becomes extremely narrow, requiring significant fine-tuning to maintain the lowest possible M_1. More generally, the results indicate that high values of $\widetilde{m}$ lead to a strong wash-out effect, which can severely limit the efficiency of lepton asymmetry generation and preservation.

5.2 Future steps

A natural next step in this line of research would be to extend the analysis to higher temperature regimes. While this work has already demonstrated that the effects of a dynamically evolving right-handed electron asymmetry remain relevant well above 100 TeV, a more systematic study at higher temperatures could provide deeper insights into the interplay of the different conserved charges and what happens when the corresponding interaction partially equilibrates.

Another important direction would be to include the effects of all right-handed neutrino species and investigate how different mass hierarchies influence the generation and evolution of the lepton asymmetry. In this work, the focus has been on only the contribution of the lightest right-handed neutrino, but incorporating the full right-handed neutrino sector could reveal additional effects that modify the efficiency of asymmetry conversion, especially in absence of a strong mass hierarchy.

Lastly, it could be interesting to explore whether the critical wash-in strength $\widetilde{m}$, which determines the transition between efficient and inefficient wash-in leptogenesis, can be determined analytically. While the numerical results provide valuable insights, an analytical expression for $\widetilde{m}_c$ would offer a clearer theoretical understanding of the wash-in mechanism and its dependence on key model parameters. Such a result could serve as a useful benchmark for future studies and further constrain the viable parameter space.

Acknowledgements

First and foremost, I would like to express my sincere gratitude to my advisor, Junior-Prof. Dr. Kai Schmitz, for giving me the opportunity to work on this thesis within his group. I deeply appreciate his guidance and support, as well as the chance to actively contribute to the research. I am especially grateful for the opportunity to present parts of my results at the DESY Theory Workshop 2024 in Hamburg.

I would also like to thank Martin Mojahed for his invaluable support, particularly for providing helpful cross-checks between numerical calculations in `Python` and `Mathematica`.

The plots shown in this work have been created using the python packages `matplotlib`[43], the `feynman`[44] to produce Feynman diagrams and `python-ternay`[42] for the triangle plots.

Bibliography

[1] W. Buchmüller, R. Peccei, and T. Yanagida, "Leptogenesis as the origin of matter," *Annual Review of Nuclear and Particle Science*, vol. 55, no. 1, p. 311–355, Dec. 2005. [Online]. Available: http://dx.doi.org/10.1146/annurev.nucl.55.090704.151558

[2] S. Navas *et al.*, "Review of particle physics," *Phys. Rev. D*, vol. 110, no. 3, p. 030001, 2024.

[3] C. Bambi and A. D. Dolgov, *Introduction to Particle Cosmology. The Standard Model of Cosmology and its Open Problems*, ser. UNITEXT for Physics. Springer, 2016.

[4] A. D. Sakharov, "Violation of CP Invariance, C asymmetry, and baryon asymmetry of the universe," *Pisma Zh. Eksp. Teor. Fiz.*, vol. 5, pp. 32–35, 1967.

[5] D. E. Morrissey and M. J. Ramsey-Musolf, "Electroweak baryogenesis," *New Journal of Physics*, vol. 14, no. 12, p. 125003, Dec. 2012. [Online]. Available: http://dx.doi.org/10.1088/1367-2630/14/12/125003

[6] G. R. Farrar and M. E. Shaposhnikov, "Baryon asymmetry of the universe in the minimal standard model," *Physical Review Letters*, vol. 70, no. 19, p. 2833–2836, May 1993. [Online]. Available: http://dx.doi.org/10.1103/PhysRevLett.70.2833

[7] T. Schröder and R. Brandenberger, "Embedded domain walls and electroweak baryogenesis," *Physical Review D*, vol. 110, no. 4, Aug. 2024. [Online]. Available: http://dx.doi.org/10.1103/PhysRevD.110.043516

[8] D. Hooper and G. Krnjaic, "Gut baryogenesis with primordial black holes," *Physical Review D*, vol. 103, no. 4, Feb. 2021. [Online]. Available: http://dx.doi.org/10.1103/PhysRevD.103.043504

[9] V. Domcke and K. Mukaida, "Gauge field and fermion production during axion inflation," *Journal of Cosmology and Astroparticle Physics*, vol. 2018, no. 11, p. 020–020, Nov. 2018. [Online]. Available: http://dx.doi.org/10.1088/1475-7516/2018/11/020

[10] E. W. Kolb and M. S. Turner, *The Early Universe*, 1990, vol. 69.

[11] R. D. Peccei and H. R. Quinn, "CP conservation in the presence of pseudoparticles," *Phys. Rev. Lett.*, vol. 38, pp. 1440–1443, Jun 1977. [Online]. Available: https://link.aps.org/doi/10.1103/PhysRevLett.38.1440

[12] R. T. Co, V. Domcke, and K. Harigaya, "Baryogenesis from decaying magnetic helicity in axiogenesis," *Journal of High Energy Physics*, vol. 2023, no. 7, Jul. 2023. [Online]. Available: http://dx.doi.org/10.1007/JHEP07(2023)179

[13] V. Domcke, B. v. Harling, E. Morgante, and K. Mukaida, "Baryogenesis from axion inflation," *Journal of Cosmology and Astroparticle Physics*, vol. 2019, no. 10, p. 032–032, Oct. 2019. [Online]. Available: http://dx.doi.org/10.1088/1475-7516/2019/10/032

[14] P. Di Bari, "An introduction to leptogenesis and neutrino properties," *Contemporary Physics*, vol. 53, no. 4, p. 315–338, Jul. 2012. [Online]. Available: http://dx.doi.org/10.1080/00107514.2012.701096

[15] W. Buchmüller, P. Di Bari, and M. Plümacher, "Leptogenesis for pedestrians," *Annals of Physics*, vol. 315, no. 2, p. 305–351, Feb. 2005. [Online]. Available: http://dx.doi.org/10.1016/j.aop.2004.02.003

[16] M. Fukugita and T. Yanagida, "Baryogenesis Without Grand Unification," *Phys. Lett. B*, vol. 174, pp. 45–47, 1986.

[17] DESI Collaboration, "Desi 2024 vi: Cosmological constraints from the measurements of baryon acoustic oscillations," 2024. [Online]. Available: https://arxiv.org/abs/2404.03002

[18] Katrin Collaboration, "Direct neutrino-mass measurement based on 259 days of katrin data," 2024. [Online]. Available: https://arxiv.org/abs/2406.13516

[19] J. Casas and A. Ibarra, "Oscillating neutrinos and $\mu \to e\gamma$," *Nuclear Physics B*, vol. 618, no. 1–2, p. 171–204, Dec. 2001. [Online]. Available: http://dx.doi.org/10.1016/S0550-3213(01)00475-8

[20] V. Brdar, A. J. Helmboldt, S. Iwamoto, and K. Schmitz, "Type i seesaw mechanism as the common origin of neutrino mass, baryon asymmetry, and the electroweak scale," *Physical Review D*, vol. 100, no. 7, Oct. 2019. [Online]. Available: http://dx.doi.org/10.1103/PhysRevD.100.075029

[21] I. Esteban, M. C. Gonzalez-Garcia, M. Maltoni, I. Martinez-Soler, J. P. Pinheiro, and T. Schwetz, "Nufit-6.0: updated global analysis of three-flavor neutrino oscillations," *Journal of High Energy Physics*, vol. 2024, no. 12, Dec. 2024. [Online]. Available: http://dx.doi.org/10.1007/JHEP12(2024)216

[22] S. Davidson and A. Ibarra, "A lower bound on the right-handed neutrino mass from leptogenesis," *Physics Letters B*, vol. 535, no. 1–4, p. 25–32, May 2002. [Online]. Available: http://dx.doi.org/10.1016/S0370-2693(02)01735-5

[23] W. Buchmüller, P. Di Bari, and M. Plümacher, "Cosmic microwave background, matter–antimatter asymmetry and neutrino masses," *Nuclear Physics B*, vol. 643, no. 1–3, p. 367–390, Nov. 2002. [Online]. Available: http://dx.doi.org/10.1016/S0550-3213(02)00737-X

[24] A. Pilaftsis and T. E. J. Underwood, "Resonant leptogenesis," *Nucl. Phys. B*, vol. 692, pp. 303–345, 2004. [Online]. Available: https://doi.org/10.1016/j.nuclphysb.2004.05.029

[25] ——, "Electroweak-scale resonant leptogenesis," *Phys. Rev. D*, vol. 72, p. 113001, 2005. [Online]. Available: https://doi.org/10.48550/arXiv.hep-ph/0506107

[26] A. Pilaftsis, P. Candia da Silva, D. Karamitros, and T. McKelvey, "Tri-Resonant Leptogenesis," *PoS*, vol. CORFU2022, p. 036, 2023. [Online]. Available: https://doi.org/10.48550/arXiv.2303.15227

[27] E. K. Akhmedov, V. A. Rubakov, and A. Y. Smirnov, "Baryogenesis via neutrino oscillations," *Physical Review Letters*, vol. 81, no. 7, p. 1359–1362, Aug. 1998. [Online]. Available: http://dx.doi.org/10.1103/PhysRevLett.81.1359

[28] K. Dick, M. Lindner, M. Ratz, and D. Wright, "Leptogenesis with dirac neutrinos," *Physical Review Letters*, vol. 84, no. 18, p. 4039–4042, May 2000. [Online]. Available: http://dx.doi.org/10.1103/PhysRevLett.84.4039

[29] K. Huang, *Statistical Mechanics*, 2nd ed. John Wiley & Sons, 1987.

[30] G. F. Giudice, A. Notari, M. Raidal, A. Riotto, and A. Strumia, "Towards a complete theory of thermal leptogenesis in the SM and MSSM," *Nucl. Phys. B*, vol. 685, pp. 89–149, 2004.

[31] V. Domcke, K. Kamada, K. Mukaida, K. Schmitz, and M. Yamada, "Wash-In Leptogenesis," *Phys. Rev. Lett.*, vol. 126, no. 20, p. 201802, 2021. [Online]. Available: https://arxiv.org/abs/2011.09347

[32] V. Domcke, Y. Ema, K. Mukaida, and M. Yamada, "Spontaneous baryogenesis from axions with generic couplings," 2023. [Online]. Available: https://arxiv.org/abs/2006.03148

[33] V. Domcke, K. Kamada, K. Mukaida, K. Schmitz, and M. Yamada, "Wash-in leptogenesis after axion inflation," *Journal of High Energy Physics*, vol. 2023, no. 1, Jan. 2023. [Online]. Available: http://dx.doi.org/10.1007/JHEP01(2023)053

[34] K. Schmitz and X.-J. Xu, "Wash-in leptogenesis after the evaporation of primordial black holes," *Phys. Lett. B*, vol. 849, p. 138473, 2024.

[35] M. A. Mojahed, K. Schmitz, and X.-J. Xu, "Gravitational chargegenesis," 9 2024.

[36] K. Mukaida, H. Watanabe, and M. Yamada, "Thermal wash-in leptogenesis via heavy Higgs decay," *JCAP*, vol. 09, p. 063, 2024.

[37] D. Bödeker and D. Schröder, "Equilibration of right-handed electrons," *JCAP*, vol. 05, p. 010, 2019. [Online]. Available: https://arxiv.org/abs/1902.07220

[38] J. A. Harvey and M. S. Turner, "Cosmological baryon and lepton number in the presence of electroweak fermion-number violation," *Phys. Rev. D*, vol. 42, pp. 3344–3349, Nov 1990. [Online]. Available: https://link.aps.org/doi/10.1103/PhysRevD.42.3344

[39] M. Laine and M. Shaposhnikov, "Remark on sphaleron erasure of baryon asymmetry," *Phys. Rev. D*, vol. 61, p. 117302, May 2000. [Online]. Available: https://link.aps.org/doi/10.1103/PhysRevD.61.117302

[40] V. Domcke, K. Kamada, K. Mukaida, K. Schmitz, and M. Yamada, "New constraint on primordial lepton flavor asymmetries," *Physical Review Letters*, vol. 130, no. 26, Jun. 2023. [Online]. Available: http://dx.doi.org/10.1103/PhysRevLett.130.261803

[41] M. A. Mojahed, K. Schmitz, and D. Wilken, "A lower bound on the right-handed neutrino mass from wash-in leptogenesis," 2025. [Online]. Available: https://arxiv.org/abs/2501.07634

[42] M. H. et al, "python-ternary: Ternary plots in python," *Zenodo 10.5281/zenodo.594435*. [Online]. Available: https://github.com/marcharper/python-ternary

[43] J. D. Hunter, "Matplotlib: A 2d graphics environment," *Computing in Science & Engineering*, vol. 9, no. 3, pp. 90–95, 2007.

[44] G. Antonius, "feynman," https://github.com/GkAntonius/feynman, 2018.

Appendices

Appendix A

Asymptotics of the form factors

A.1 The Propagator

It is helpful to have a look at the asymptotic behaviour of the functions that contribute to the effective cross sections and therefore the reaction rates of the scattering processes in order identify the scaling at high and low energies.

I start out with the propagator:

$$P_i^{-1} = \frac{1}{x - a_i + i\sqrt{a_i c_i}}$$
$$\left(P_i^{-1}\right)^* = \frac{1}{x - a_i - i\sqrt{a_i c_i}}$$

At low energies it is quite straight forward to see that energy dependence becomes irrelevant, so the propagator can be seen as constant:

$$P_i^{-1} \overset{x \ll a_i}{\approx} \frac{1}{i\sqrt{a_i c_i} - a_i} \qquad = \text{const}$$
$$\left(P_i^{-1}\right)^* \overset{x \ll a_i}{\approx} -\frac{1}{i\sqrt{a_i c_i} + a_i} \qquad = \text{const}$$

This then also translates to the squared propagator

$$\left(P_i^{-1}\right)^* P_j^{-1} \overset{x \ll a_i}{\approx} \frac{1}{a_i a_j + \sqrt{a_i a_j c_i c_j} + i a_i \sqrt{a_j c_j} - i a_j \sqrt{a_i c_i}} \qquad = \text{const}$$

At high energies on he other hand the energy dependence play of course a bigger role, and one also has to treat the real and imaginary contributions seperately, leading to

$$\left(P_i^{-1}\right)^* \overset{x \gg a_i}{\approx} \frac{1}{x - i\sqrt{a_i c_i}}$$
$$\rightarrow \Re\Big(\left(P_i^{-1}\right)^*\Big) \approx \frac{x}{x^2 + \sqrt{a_i c_i}} \qquad \sim \mathcal{O}\left(\frac{1}{x}\right)$$
$$\Im\Big(\left(P_i^{-1}\right)^*\Big) \approx \frac{\sqrt{a_i c_i}}{x^2 + \sqrt{a_i c_i}} \qquad \sim \mathcal{O}\left(\frac{1}{x^2}\right)$$

This differentiation between real and imaginary part also needs to applied for the propagatpor squared, leading to.

$$
\begin{aligned}
(P_i^{-1})^* P_j^{-1} &= \frac{1}{(x-a_i)(x-a_j)+\sqrt{a_i a_j c_i c_j}+i(x-a_i)\sqrt{a_j c_j}-i(x-a_j)\sqrt{a_i c_i}} \\
&\overset{x\gg a_i,a_j}{\approx} \frac{1}{x^2+ix\left(\sqrt{a_j c_j}-a_i c_i\right)} \\
\to \Re\Big((P_i^{-1})^* P_j^{-1}\Big) &\approx \frac{x^2}{x^4-x^2\left(\sqrt{a_j c_j}-\sqrt{a_i c_i}\right)} \sim \mathcal{O}\left(\frac{1}{x^2}\right) \\
\Im\Big((P_i^{-1})^* P_j^{-1}\Big) &\approx \frac{x\left(\sqrt{a_j c_j}-\sqrt{a_i c_i}\right)}{x^4-x^2\left(\sqrt{a_j c_j}-\sqrt{a_i c_i}\right)} \sim \mathcal{O}\left(\frac{1}{x^3}\right)
\end{aligned}
$$

Note here that in case $i=j$ the imaginary part vanished.

A.2 The $\mathcal{A}$ functions

A.2.1 $\mathcal{A}^{(ss)}$

The s-channel function $\mathcal{A}^{(ss)}$ is mainly dependent on the propagator squared, so at low energies only the x dependence from the prefactor remains:

$$
\mathcal{A}_{ij}^{(ss)} \overset{x\ll a_i,a_j}{\sim} x(P_i^{-1})^* P_j^{-1} \sim \mathcal{O}(x)
$$

At high energies though due to the difference in real and imaginary part of the propagator the asymptotics for $\mathcal{A}^{(ss)}$ come out as

$$
\begin{aligned}
\Re\mathcal{A}_{ij}^{(ss)} &\sim x\,\Re(P_i^{-1})^* P_j^{-1} && \sim \mathcal{O}\left(\frac{1}{x}\right) \\
\Im\mathcal{A}_{ij}^{(ss)} &\sim x\,\Im(P_i^{-1})^* P_j^{-1} && \sim \begin{cases} \mathcal{O}\left(\frac{1}{x^2}\right) & ,\text{if } i\neq j \\ 0 & ,\text{if } i=j \end{cases}
\end{aligned}
$$

A.2.2 $\mathcal{A}^{(st)}$

The interference contribution $\mathcal{A}^{(st)}$ depends in one part on the propagator again. The other factor scales at low energies like

$$
\begin{aligned}
\frac{x+a}{x}\ln\frac{x+a_j}{a_j} &= \left(1+\frac{a_j}{x}\right)(\ln x + a_j - \ln a_j) \\
&\overset{x\ll x_j}{\approx} \left(1+\frac{a_j}{x}\right)\left(\ln a_j - \ln a_j + \frac{x}{a_j}\right) \\
&= \frac{x}{a_j}+1 && \sim \mathcal{O}(x)
\end{aligned}
$$

Leading to in total a liner scaling at low energies

$$
\mathcal{A}^{(st)} \sim \mathcal{O}(x)
$$

At high energies the prefactor scales as

$$
\frac{x+a_j}{x}\ln\frac{x+a_j}{a_j} \overset{x\gg a_j}{\approx} \ln x \qquad \sim \mathcal{O}(\ln x)
$$

In total this leads to the overall scaling behaviour

$$
\begin{aligned}
\Re\Big(\mathcal{A}_{ij}^{(st)}\Big) &\sim \Re\big(P_i^{-1}\big)^*(1-\ln x) && \sim \mathcal{O}\left(\frac{\ln x}{x}\right) \\
\Im\Big(\mathcal{A}_{ij}^{(st)}\Big) &\sim \Im\big(P_i^{-1}\big)^*(1-\ln x) && \sim \mathcal{O}\left(\frac{\ln x}{x^2}\right)
\end{aligned}
$$

A.2.3 $\mathcal{A}^{(tt)}$

The t-channel contribution now does not depend on the propagator any more, so we just look at the individual terms.

At low energy for the case $i \neq j$

$$\begin{aligned}(x+a_j)\ln\frac{x+a_j}{a_j} &\approx (x+a_j)\left(\ln a_j - \ln a_j + \frac{x}{a_j}\right)\\ \to \mathcal{A}_{ij}^{(tt)} \sim \frac{1}{x}\left[(x+a_j)\frac{x}{a_j} - (x+a_i)\frac{x}{a_i}\right] &= x\left(\frac{1}{a_j}-\frac{1}{a_i}\right) \qquad \sim \mathcal{O}(x)\end{aligned}$$

And analogously for the case $i = j$, though we have to go to next to leading order in the expansion of the logarithm to obtain non vanishing contributions here

$$\begin{aligned}\ln\frac{x+a_i}{a_i} &= \frac{x}{a_i} - \frac{x^2}{a_i^2} + \mathcal{O}\left(x^3\right)\\ \mathcal{A}_{ii}^{(tt)} &\sim \frac{1}{x}\left[\frac{x}{a_i} - \frac{x}{a_i} + \frac{x^2}{a_i^2}\right] \qquad \sim \mathcal{O}(x)\end{aligned}$$

Again in both cases leading to linear scaling.

The high energy behaviour looks like

$$\begin{aligned}(x+a_j)\ln\frac{x+a_j}{a_j} &\overset{x\gg a_j}{\approx} x(\ln x - \ln a_j)\\ \to \mathcal{A}_{ij}^{(tt)} &\sim \frac{1}{x}\left[x\ln x - x\ln a_j - x\ln x + x\ln a_i\right] = \ln a_j - \ln a_i \qquad = \text{const}\end{aligned}$$

while for $i = j$

$$\ln\frac{x+a_i}{a_i} \approx \ln x - \ln a_i$$

In total therefore

$$\mathcal{A}_{ii}^{(tt)} \sim \frac{1}{2\pi} - \frac{\ln x}{x} + \frac{\ln a_i}{x} \qquad \approx \frac{1}{2\pi} = \text{const}$$

A.3 $\mathcal{B}$

The function for the next scattering at low energies is for $i \neq j$

$$\begin{aligned}\ln\frac{a_i(x+a_j)}{a_j(x+a_i)} &= \ln x + a_j - \ln x + a_i + \ln\frac{a_i}{a_j}\\ &\approx \ln a_j + \frac{x}{a_j} - \ln a_i - \frac{x}{a_i} + \ln\frac{a_i}{a_j} = x\left(\frac{1}{a_j}-\frac{1}{a_i}\right) \qquad \sim \mathcal{O}(x)\\ \ln\frac{(x+a_i)(x+a_j)}{a_i a_j} &= \ln x + a_i + \ln x + a_j - \ln a_i a_j\\ &\approx \ln a_i + \ln a_j - \ln a_i a_j + \frac{x}{a_i} + \frac{x}{a_j} = x\left(\frac{1}{a_i}+\frac{1}{a_j}\right) \qquad \sim \mathcal{O}(x)\\ \to \frac{1}{x+a_i+a_j}\ln\frac{(x+a_i)(x+a_j)}{a_i a_j} &\approx \frac{x}{a_i+a_j}\left(\frac{1}{a_i}+\frac{1}{a_j}\right) \qquad \sim \mathcal{O}(x)\end{aligned}$$

Very similarly for $i = j$

$$\begin{aligned}\frac{x}{x+a_i} &\approx \frac{x}{a_i} \qquad \sim \mathcal{O}(x)\\ \frac{2a_i}{x+2a_i}\ln\frac{x+a_i}{a_i} &\approx \frac{x}{a_i} \qquad \sim \mathcal{O}(x)\end{aligned}$$

Again one finds a linear dependence on energy, at low energies.

For high energies in the $i \neq j$ case:

$$\begin{aligned} \ln \frac{a_i\,(x+a_j)}{a_j\,(x+a_i)} &\approx \ln \frac{a_i x}{a_j x} = \ln \frac{a_i}{a_j} && \sim \mathcal{O}\,(1) \\ \frac{1}{x+a_i+a_j} \ln \frac{(x+a_i)(x+a_j)}{a_i a_j} &\approx \frac{1}{x} \ln \frac{x^2}{a_i a_j} && \sim \mathcal{O}\left(\frac{\ln x}{x}\right) \end{aligned}$$

So we see the dominant contribution in for large x is constant, while the $\frac{\ln(x)}{x}$ contribution vanishes here.

Very similarly we can see for the $i = j$ case

$$\begin{aligned} \frac{x}{x+a_i} &\approx \frac{x}{x} && = \text{const} \\ \frac{2a_i}{x+2a_i} \ln \frac{x+a_i}{a_i} &\approx \frac{2a_i}{x} \ln \frac{x}{a_i} && \sim \mathcal{O}\left(\frac{\ln x}{x}\right) \end{aligned}$$

As for $\mathcal{A}^{(tt)}$ one also gets a dominant constant contribution at large x in both cases for $\mathcal{B}$

A.4 $\mathcal{E}$

The last scattering that is not also covered by the considerations of a previous scattering process is the function $\mathcal{E}$ For low energies

$$\begin{aligned} \ln \frac{a_i\,(x+a_j)}{a_j\,(x+a_i)} &\approx \mathcal{O}\,(x)\ , && i \neq j \\ \frac{x}{\pi\,(x+a_i)} &\approx \mathcal{O}\,(x)\ , && i = j \end{aligned}$$

While for high energies

$$\begin{aligned} \ln \frac{a_i\,(x+a_j)}{a_j\,(x+a_i)} &\approx \text{const}\,, && i \neq j \\ \frac{x}{\pi\,(x+a_i)} &\approx \text{const}\,, && i = j \end{aligned}$$

Again resulting in a linear energy dependence at low energies, while at high energies becoming constant.

Declaration of Academic Integrity

I hereby confirm that this thesis, entitled *A lower limit for the lightest RHN mass from wash-in Leptogenesis* is solely my own work and that I have used no sources or aids other than the ones stated. All passages in my thesis for which other sources, including electronic media, have been used, be it direct quotes or content references, have been acknowledged as such and the sources cited. I am aware that plagiarism is considered an act of deception which can result in sanction in accordance with the examination regulations.

Münster, March 14, 2025, _____
(Signature of Student)

I agree to have my thesis checked in order to rule out potential similarities with other works and to have my thesis stored in a database for this purpose.

Münster, March 14, 2025, _____
(Signature of Student)